Universidade de Aveiro
2015
Secção Autónoma das Ciências da Saúde

Daniela Pais Ferreira

Sinergia entre terapia antiangiogénica e imunoterapia em cancro da mama

Synergy between antiangiogenic and immuno-therapies in breast cancer

Universidade de Aveiro Secção Autónoma das Ciências da Saúde
2015

Daniela Pais Ferreira

Sinergia entre terapia antiangiogénica e imunoterapia em cancro da mama

Synergy between antiangiogenic and immuno-therapies in breast cancer

Dissertação apresentada à Universidade de Aveiro para cumprimento dos requisitos necessários à obtenção do grau de Mestre em Biomedicina Molecular, realizada sob a orientação científica do Doutor Michele De Palma, Professor Assistente do Departamento das Ciências da Vida da Escola Politécnica Federal de Lausanne, e da Doutora Sandra Vieira, Professora Auxiliar Convidada da Secção Autónoma das Ciências da Saúde da Universidade de Aveiro.

o júri

Presidente

Doutora Ana Gabriela da Silva Cavaleiro Henriques
Professora Auxiliar Convidada, Universidade de Aveiro

Doutora Ana Sofia Pais Ribeiro
Investigadora, Ipatimup – Instituto de Patologia e Imunologia Molecular da Universidade do Porto

Doutora Sandra Isabel Moreira Pinto Vieira
Professora Auxiliar Convidada, Universidade de Aveiro

Agradecimentos
/
Acknowledgments

Foremost I would like to thank Dr. Michele De Palma for giving me the opportunity to perform my Master thesis in his Laboratory, which allowed me to acquire consistent knowledge in the tumor microenvironment field. I'll be forever grateful for his guidance, ideas and feedback, motivation, enthusiasm and immense knowledge.

I would also like to express my gratitude to my supervisor, Dr. Nicolò Rigamonti, for the continuous support and patience, and for the useful comments and remarks throughout this year, both during the research phase and the writing of this thesis.

I'm also grateful for the kind support and motivation from my co-coordinator, Dr. Sandra Vieira, as well as the remaining members of the thesis committee.

During this year I was lucky to have the support of a friendly and cheerful group of fellow colleagues, for which I'm also thankful. Particularly I would like to thank Céline, Ece and Caroline for the morning coffees and friendship; Nicolò, Mario and Cláudio for the after lunch coffees and for making me feel like I was home; Ioanna and Mario for their scientific expertise and insights, as well as their support; and Lucie for sharing the same feelings during our master projects. I would also like to thank all the other current and former members of the Angiogenesis and Tumor Microenvironment Laboratory who, in one way or another, made my abroad experiment easier and happier.

I would also like to thank the members of the Histology Facility and the Bioimaging and Optics Platform Facility of EPFL for their assistance and technical support in histochemistry stainings and FIJI analysis methodologies, respectively.

Furthermore, I'm also thankful to the Leenaards foundation, the San Salvatore foundation and to Roche for their financial support, necessary to perform this project.

I also would like to express my deepest gratitude to all my loved ones, for their kind support and encouragement, without which the completion of this thesis would not be possible. Therefore I would like to thank my parents for their unconditional love, education, unceasing encouragement and for supporting me throughout all my studies at the University; my boyfriend for the equally encouragement, support and attention during this year, and for always stand by my side since 2008; my beloved sister for the continuous support and motivation, although separated by distance she is always in my heart; and my uncles and aunt resident in Switzerland for their support this year, for all the Saturday dinners and Sunday lunches and all the laughs, which made this year more bearable. I would also like to thank my grandparents for their love and advices, as well as the rest of my family members, without exception.

Last, but not least, I would like to thank my best friend Cláudia for her enormous friendship since 2009, a friendship that not even time and distance can end. Thank you for all the Skype conversations and for always cheer me up.

This thesis was only possible with help and support of many others. Therefore I would like to extend my sincere thanks to all of them.

palavras-chave

Cancro da mama, angiogénese, VEGF-A, ANG-2, terapia anti-angiogénica, imunoterapia mediada por agonistas do recetor CD40

resumo

A angiogénese é um processo crucial para o crescimento, progressão e disseminação do cancro da mama, tornando-se assim um alvo terapêutico promissor. A maioria dos estudos clínicos de terapias anti-angiogénicas em cancro da mama baseiam-se na neutralização do fator de crescimento endotelial vascular (VEGF), uma vez que este apresenta um papel dominante na angiogénese tumoral. No entanto, todos os estudos clínicos baseados em terapias anti-angiogénicas têm-se revelado ineficazes no tratamento de pacientes com cancro da mama. Uma vez que a Angiopoietina 2 (ANG-2), outro fator de crescimento vascular, tem sido reportada como responsável pela resistência a terapias baseadas no bloqueio de função do VEGF, é possível que pacientes com cancro da mama beneficiem de uma estratégia terapêutica que neutralize simultaneamente ANG-2 e VEGF-A. De facto, através do uso de um anticorpo 'biespecífico', capaz de neutralizar tanto ANG-2 como VEGF-A e denominado A2V, observou-se uma forte inibição da progressão tumoral e aumento da sobrevivência num modelo pré-clínico de cancro da mama agressivo, baseado em ratinhos transgénicos e denominado MMTV-PyMT. Consistentemente, esta terapia levou ao aumento de necrose tumoral e a uma drástica redução na densidade vascular, sem evidência de revascularização ou resistência à terapia. A administração de A2V induziu ainda o aumento da associação entre células perivasculares (*'pericytes'*) e células endoteliais dos restantes vasos sanguíneos tumorais, favorecendo a maturação e normalização vascular, o que facilita o desenvolvimento de um microambiente que suporta respostas imunológicas. Estes resultados sugeriam assim que imunoterapia em cancro da mama poderia beneficiar da combinação com A2V, tendo-se por conseguinte combinado o anticorpo A2V com o anticorpo agonista de CD40 (FGK45), no modelo ortotópico de MMTV-PyMT. Esta terapia induziu uma notável inibição do crescimento tumoral, com obtenção de casos estáveis, e aumento adicional de necrose tumoral. Observou-se ainda o aumento de infiltração de células $CD8^+$ após terapia com FGK45, quer isoladamente ou em combinação com A2V, e uma correlação entre a extensão da inibição do tumor e o aumento da infiltração tumoral por células $CD8^+$. Isto sugere que o influxo de células $CD8^+$ nos tumores tratados com A2V e FGK45 foi o principal responsável pelas notáveis respostas anti-tumorais observadas. Em resumo, estes resultados apontam para uma sinergia entre a neutralização simultânea de ANG-2/VEGF-A e imunoterapia baseada em agonistas do recetor CD40, no modelo pré-clínico de cancro da mama MMTV-PyMT. Esta abordagem combinatória pode beneficiar pacientes com cancro da mama, por isso, mais estudos são necessários para explorar os mecanismos subjacentes à atividade cooperativa da terapia anti-angiogénica e a imunoterapia.

keywords

Breast cancer, angiogenesis, VEGF-A, ANG-2, anti-angiogenic therapy, cancer immunoediting, CD40 agonistic-mediated immunotherapy.

abstract

Angiogenesis is crucial for breast cancer growth, progression and dissemination, making it a promising therapeutic target. Given the dominant role of Vascular Endothelial Growth Factor (VEGF) signaling in tumor angiogenesis, the majority of clinical studies with anti-angiogenic therapies in breast cancer were based on VEGF blockade. However, lack of clinical efficacy was observed in all clinical studies with antiangiogenic therapies for breast cancer. Since angiopoietin 2 (ANG-2) has been reported to induce therapeutic resistance after VEGF-targeted therapies, breast cancer patients may benefit from a therapeutic strategy that simultaneously blocks ANG-2 and VEGF-A. Indeed, using the bispecific ANG-2/VEGF-A targeting antibody (A2V), durable inhibition of tumor progression, as well as increased survival, could be observed after dual ANG-2/VEGF-A blockade in the aggressive mouse model of breast cancer, the MMTV-PyMT transgenic mouse. Consistent with tumor inhibition, increased tumor necrosis and a drastic reduction of vascular density was observed after A2V therapy, with little evidence of tumor revascularization or resistance to therapy. Moreover, A2V led to increased perivascular coverage of the remaining tumor blood vessels, favoring vascular normalization, which is known to facilitate the development of an immunosupportive microenvironment. These findings suggested that breast cancer immunotherapy may benefit from the combination with A2V. Therefore the A2V mAb was combined with a CD40 agonistic antibody (FGK45). The combined therapeutic approach led to remarkable tumor growth inhibition in an orthotopic MMTV-PyMT model, with the achievement of cases of stable disease and further increase in tumor necrosis. Increased infiltration of $CD8^+$ cells after FGK45 therapy, either alone or in combination with A2V, could also be observed. Of note, a correlation between the extent of tumor inhibition and increased tumor infiltration by $CD8^+$ cells was detected, suggesting that the influx of $CD8^+$ cells in the combination therapy-treated tumors was responsible for the remarkable anti-tumor responses observed. In summary, these results point to a significant synergistic activity of anti-ANG-2/VEGF-A and CD40 agonistic therapy in the MMTV-PyMT model of breast carcinoma. This combinatorial approach may benefit breast cancer patients, so further studies that explore the mechanistic bases of the cooperative activity of antiangiogenic and immunostimulatory therapy are warranted.

Acronyms

Ab: Antibody

AI: Aromatase Inhibitor

ANG: Angiopoietins

APC: Antigen Presenting Cell

Bad: Bcl-2-associated death promoter

BMDC: Bone Marrow Derived Cell

BRCA: Breast Cancer gene

CD: Cluster of Differentiation

CLEVER1: Common Lymphatic Endothelial and Vascular Endothelial Receptor 1

CSC: Cancer Stem Cell

CSF-1: Colony-Stimulating Factor 1

CTL: Cytotoxic T Lymphocyte

CTLA-4: Cytotoxic T Lymphocyte Associate Antigen 4

CXCL14: Chemokine (C-X-C motif) ligand 14

DAAP: Double AntiAngiogenic Protein

DC: Dendritic Cell

DNA: DeoxyriboNucleic Acid

EC: Endothelial Cell

ECM: ExtraCellular Matrix

EGFR: Epidermal Growth Factor Receptor

ER: Estrogen Receptor

FAK: Focal Adhesion Kinase

FDA: Food and Drug Administration

FGF: Fibroblast Growth Factor

FKHR: Forkhead Homologue in Rhabdomyosarcoma

Flk-1: Fetal Liver Kinase 1

Flt: Fms-like tyrosine kinase

GIMAP5: GTPase of immunity-associated protein 5

HER: Human Epidermal growth factor Receptor

HIF-1: Hypoxia-Inducible Factor 1

HR: Hormone Receptor

HSC: Hematopoietic Stem Cell

ICAM1: InterCellular Adhesion Molecule 1

IDO: Indolamine-2,3-Dioxygenase

IFN: Interferon

IL: Interleukin

JNK: c-Jun-NH2-kinase

mAb: Monoclonal Antibody

MAPK: Mitogen-Activated Protein Kinase

MDSC: Myeloid-Derived Suppressor Cell

MHC: Major Histocompatibility Complex

MIN: Mammary Intraepithelial Neoplasia

MMP: Matrix MetalloProteinases

MMTV: Mammary Mouse Tumor Virus

mTOR: mammalian Target Of Rapamycin

NF-κB: Nuclear Factor-κB

NG-2: Neural-Glial 2

NK: Natural killer

OR: Overall Responses

ORR: Overall Response Rate

OS: Overall Survival

PARP: Poly ADP Ribose Polymerase

PD-1: Programmed cell Death protein 1

PDGF: Platelet-Derived Growth Factor

PDGFR: Platelet-Derived Growth Factor Receptor

PFS: Progression Free Survival

PI3K: PhosphatIdylinositol 3-Kinase

PIMO: Pimonidazole

PLGF: Placenta Growth Factor

PR: Progesterone Receptor

PTEN: Phosphatase and Tensin homolog

PyMT: Polyomavirus Middle T antigen

RAF: Rapidly Accelerated Fibrosarcoma protein kinase

RET: Rearranged During Transfection proto-oncogene

RR: Response Rate

RTK: Receptor Tyrosine Kinase

SMA: Smooth Muscle Actin

TAM: Tumor-Associated Macrophage

TCR: T Cell Receptor

TEM: TIE-2-Expressing Monocytes/Macrophages

TGF: Transforming Growth Factor

TKI: Tyrosine Kinase Inhibitor

TNBC: Triple Negative Breast Cancer

TNF: Tumor Necrosis Factor

TRAF: TNF Receptor Associated Factor

Treg: Regulatory T Cell

TSP1: Thrombospondin 1

VCAM1: Vascular Cell Adhesion Molecule 1

VEGF: Vascular Endothelial Growth Factor

VEGFR: Vascular Endothelial Growth Factor Receptor

Index

1. Introduction

Cancer is a complex disease whose development occurs in a multistep manner, each step reflecting a genetic alteration, driving the progressive transformation of normal cells into highly malignant derivatives (1). Throughout these transformations the cells acquire cancer hallmark capabilities that enable them to survive, proliferate and disseminate. Cancer is a dynamic system that continuously evolves by altering and recruiting the surrounding host non-cancer cells (endothelial cells, pericytes, cancer-associated fibroblasts and bone marrow-derived stromal cells) in order to create a more permissive milieu for its growth and progression, named tumor microenvironment (2). Indeed, it is known that the composition of the tumor stroma influences the prognosis of several forms of cancer, including breast cancer (3), and the clinical outcome of cancer treatments. Thus, therapies targeting these cells can impair the tumor growth and dissemination, prolonging the survival of cancer patients.

In this project, an innovative therapeutic approach, aiming to simultaneously target tumor angiogenesis and the tumor immune response, is discussed in mouse models of breast cancer.

1.1. Breast cancer

Breast cancer can be described as a heterogeneous disease encompassing multiple subgroups with differing molecular signatures, prognoses, and responses to therapies (4). Despite the scientific advances in the past several decades, breast cancer is the second leading cause of cancer related death in women (5). Among european women, the breast cancer alone accounts for 28,8% of all cancer cases, with a total of 464 000 incidence cases in 2012, of which 131 000 cases resulted in death, corresponding to 16,8% of the cancer-related deaths in women (6).

The mammary gland can undergo multiples cycles of proliferation, lactation and involution, due to the presence of a population of mammary stem cells, capable of self-renewal, lineage commitment and epithelial differentiation in both luminal or myoepithelial/basal cells (5). The breast cancer driven mutations can either occur in mammary stem cells, leading to the establishment of cancer-stem cells (CSCs), in lineage committed progenitor cells or even in differentiated cells, giving rise to different breast cancer subtypes (7).

Perou *et al*. were the firsts to describe the distinct molecular subtypes of breast cancer using microarray-based gene expression analysis (8). Six molecular subtypes of breast

cancer are known: luminal A, luminal B, HER2-enriched, basal-like, normal breast and claudin-low. Each subtype exhibits distinct cell signatures (with mesenchymal, luminal or basal signatures), with the expression of different proliferation-related genes and steroid and/or growth factor receptors, accordingly to the specific mutation occurring in each subtype (9, 10). More importantly, each subtype reveals different responses to therapy and distinct prognoses, with the basal-like/triple-negative subtype having the shortest survival (9).

For many years, the medical treatment of breast cancer relied solely on chemotherapy, where the combined action of paclitaxel and doxorubicin had the best responses (30%-50%) (10, 11). However, the different subtypes of breast cancer respond differently to chemotherapy, with the basal-like and HER2-enriched subtypes being more sensitive to paclitaxel and doxorubicin, in a neoadjuvant setting, than the luminal cancers (12). Therefore over the past twenty years, treatment has evolved to a more target-directed approach. From a clinical/therapeutic point of view, breast cancer can be subdivided into 3 major subtypes: (a) tumors expressing Hormone Receptors (HR), namely the Estrogen (ER) and Progesterone (PR) nuclear receptors, known as HR^+ breast cancer (60%); (b) tumors with overexpression of the Human Epidermal growth factor Receptor 2 (HER2), a tyrosine kinase receptor, $HER2^+$ breast cancer (20%); and (c) the triple negative tumors, that lack the expression of ER, PR and HER2 (20%) (13).

The estrogen receptor antagonist tamoxifen (Nolvadex®), as a single agent, has been the gold standard treatment for HR^+ breast cancers, achieving a 26% mortality reduction in patients treated with tamoxifen for 5 years (14). Other estrogen-focused therapies, based on the administration of aromatase inhibitors (AIs) that prevent the synthesis of estrogen, or the ER-degrading agent Fulvestran (Faslodex®), are able to extend the survival in breast cancer patients (15). Nonetheless, up to 50% of patients with HR^+ cancer develops resistance to HR-therapies, as a result of a cross talk between ER and HER2, leading to HER2 overexpression or the alternative activation of its downstream pathway, the PI3K/Akt/mTOR pathway (4). This resistance can be partially overcome by combining anti-estrogen and anti-HER2 therapies, as showed by the significant increased progression free survival when combining anastrazole (Arimidex®), an aromatase inhibitor, plus the anti-HER2 monoclonal antibody (mAb) trastuzumab in such cases (progression free survival (PFS) of 4.8 months vs. 2.4 with anastrazole alone) (16).

The first commercially available HER2 targeting agent was the mAb trastuzumab (Herceptin®), approved by the US Food and Drug Administration (FDA) in 1998 for the treatment of $HER2^+$ breast cancer (17). Trastuzumab established a new treatment paradigm for $HER2^+$ breast cancer and it is still the standard first line treatment for this subtype of breast cancer, in combination with chemotherapy or as a single agent (18). When combined with chemotherapy, trastuzumab increases the overall response rate and

improves the median survival time by approximately 25%, compared with chemotherapy alone (19). Other anti-HER2 therapeutic strategies include the dual HER1/HER2 tyrosine kinase inhibitor (TKI) lapatinib (Tyverb®), or pertuzumab (Perjeta®), an mAb that binds to a different domain of the extracellular portion of the HER2 than trastuzumab, inhibiting HER2 dimerization (13). However, just like the HR^+ cancer subtype, resistance to anti-HER2 agents may occur as a result of activating PIK3CA mutations or loss of function of the phosphatase PTEN, leading to aberrant activation of the PI3K/Akt/mTOR downstream pathway (20). PI3K/Akt/mTOR target approaches may improve the responses of these patients, and indeed everolimus (Afinitor®), an mTOR inhibitor, seems to restore the sensitivity to anti-HER2 agents: a phase I study combining everolimus, trastuzumab and paclitaxel in trastuzumab-pretreated patients with HER2-overexpressing breast cancer, showed an overall response rate (ORR) of 44%, with controlled disease for six months in 74% of the patients (21).

The Triple Negative Breast Cancer (TNBC), due to the lack of expression of the 3 key receptors in breast cancer (ER, PR and HER2), cannot be target with the therapies mentioned above (22). Instead TNBC, with high incidence of BRCA mutations, can be target using PARP (Poly ADP Ribose Polymerase) inhibitors. Impairing the remaining DNA repair machinery within BRCA-deficient cancer cells using PARP inhibition results in synthetic lethality, due to chromosomal instability, cell-cycle arrest and apoptosis. In fact, a study with the PARP1 inhibitor olaparib (AstraZeneca®), as a single agent, led to ORR of 41% in BRCA mutated breast cancer patients, without significant toxicity (23). EGFR or HER1, also expressed in this type of breast cancer, can be target by using the anti-EGFR monoclonal antibody cetuximab (Erbitux®), which has a limited activity as a single agent, but can double the antitumor activity of platinum salts, like cisplatin (24).

As a result of these novel target therapies, over the past two decades breast cancer mortality rates have decline by approximately 30% (25). Nevertheless, the development of resistance to all these therapies is an ongoing challenge, where the development of new, non-toxic therapies are greatly needed. A study developed by Finak *et al.* (2008) (26) disclosed that distinct gene expression signatures in breast tumor stroma reflected different clinical outcomes independently of the tumor subtype. They revealed that tumor stroma samples with overexpression of cytotoxic T cell and natural killer (NK) cell markers displayed a good clinical outcome, while samples with increased hypoxic and angiogenic responses, as well as a decrease in chemokines that stimulate NK cell migration (CXCL14) and mediate prosurvival signals in T lymphocytes (GIMAP5), displayed a poor outcome. This study strongly suggests that breast tumor stroma has a crucial role in disease progression and clinical outcome. Therefore anti-angiogenic and immune therapies, addressed hereafter, appear to be a promising approach for the treatment of breast cancer.

1.2. Angiogenesis and anti-angiogenic therapy

Blood vessels supply the normal tissues with oxygen and nutrients, while disposing of metabolic waste and carbon dioxide (27). Although the formation of blood vessels is required for physiological processes, such as pre/postnatal development and tissue repair, they are also required by tumors to allow their survival and proliferation (28).

Angiogenesis, the sprouting of new blood vessels from preexisting ones, plays a rate limiting role in tumor growth. Although cancer cells can recruit bone marrow derived cells (BMDCs), which include endothelial progenitor cells capable of inducing vasculogenesis (*de novo* formation of blood vessels) (29), without angiogenesis the rate of tumor cell proliferation reaches the equilibrium with the rate of cell death, and the tumor enters in a 'dormant phenotype' (30).

In adult tissues the vasculature becomes quiescent, as a result of a balance between pro- and anti-angiogenic factors. The most relevant pro-angiogenic factors are the Vascular Endothelial Growth Factor (VEGF), Fibroblast Growth Factor (FGF), Angiopoietins (ANG-1 and ANG-2), Platelet-Derived Growth Factor (PDGF) and IL-8. Conversely, Thrombospondin 1 (TSP1), Endostatin and Angiostatin are some of the factors that negatively regulate angiogenesis (31). In quiescent tissues angiogenesis is only turned on, transiently, to allow certain physiological processes such as wound repair. However, during tumorigenesis, both the tumor and its stroma cells secret an excess of pro-angiogenic factors tipping the balance in favor of angiogenesis. This process known as the 'Angiogenic Switch', where angiogenesis is persistently activated, allows continuous sprouting of new blood vessels. Induced early during tumorigenesis, the angiogenic switch is required for tumor progression to malignancy, allowing the tumor to growth and become more likely to metastasize (2, 32).

1.2.1. Angiogenesis regulation

The sprouting and maintenance of blood vessels is a complex process, tightly regulated by multiple pathways. Given the ancestral function of vessels to supply oxygen, endothelial cells (ECs) are equipped with oxygen sensors and hypoxia-inducible factors, allowing the vessels to readjust their shape and blood flow according to the oxygen levels (33). Quiescent mature ECs form a monolayer of cells, interconnected by V-cadherin and claudin molecules, and covered by pericytes, a contact stabilized by N-cadherin molecules. In this quiescent context, the ECs and the pericytes share a common basement membrane (27). When the levels of oxygen drop, hypoxic or inflammatory cells release VEGF and other angiogenic signals, creating a gradient of pro-angiogenic factors and chemotactic signals that promote angiogenic sprouting by guiding filopodial extension from specialized

endothelial cells located at the tips of the vascular sprouts, named 'tip cells', ensuring branch formation. This process requires proteolytic degradation of the basement membrane (mediated by matrix metalloproteinases (MMPs)), pericyte detachment (in response to ANG-2) and loosening of endothelial cell junctions. The 'tip cell' is then followed by the less mobile proliferating 'stalk cells', allowing elongation and lumen formation (34). Ultimately neighboring branches fuse and a perfused blood vessel is formed. However, for the vessel to become functional, it must become mature and stable. For this purpose signals such as PDGF, ANG-1 and NOTCH support pericyte coverage; protease inhibitors cause the deposition of the basement membrane, and junctions are re-established (35).

The constitutive activated angiogenesis and overexpression of different VEGF isoforms by the tumor cells leads to an aberrant and dysregulated tumor vascularity, characterized by a variable diameter, irregular shapes and chaotic blood flow (2, 32). Tumor vessels also fail to mature, due to persistent angiogenic stimulus, presenting scarce and loosely associated pericytes with incomplete basement membranes, which increases vessel leakiness (36). All together, these features lead to poor blood perfusion and high interstitial fluid pressure. Consequently, in spite of the tumor vasculature development, tumors retain a certain level of hypoxia, resulting in the continuous overproduction of VEGF and persistent aggravation of the abnormal tumor vessel phenotype (37).

Although regulated by multiple pathways, there is a strong dominancy of the VEGF pathway in angiogenesis, as shown by the embryonic lethality in mice with loss of a single *Vegf* allele (38, 39). There is also an important role played by the Angiopoetin-Tie signaling pathway in vessel maturation and quiescence, verified by the embryonic lethality in ANG-1 or TIE-2 knockout mice (40, 41). Since both of these pathways can regulate different aspects of blood vessel growth they are briefly explained below.

1.2.1.1. The VEGF pathway

The VEGF, also known as VEGF-A, is an endothelial cell-specific mitogen, first isolated from the supernatant of bovine pituitary cells by Ferrara and Henzel in 1989 (42). The VEGF family includes the VEGF-A, the Placenta Growth Factor (PLGF), the VEGF-B, C and D (43).

The human VEGF-A, known to remarkably regulate angiogenesis in a predominant fashion, is encoded by the VEGF-A gene, organized in eight exons. Alternative exon splicing generates several isoforms of the VEGF-A, differing in their ability to bind heparin (44). The VEGF 165, an heparin binding homodimeric glycoprotein, is the most physiologically relevant isoform (45). After secretion, a significant fraction of this molecule remains bound to the extracellular matrix (ECM), through the heparin-binding sites. Therefore, ECM

proteolysis by MMPs plays a key role in regulating vascular patterning *in vivo* by increasing the release, and consequently the bioavailability, of VEGF from the ECM (46). This process is thought to be responsible for the angiogenic switch in some tumors (47).

Besides the well-documented action in promoting the growth of ECs, the VEGF-A is also a homeostatic survival factor for these cells, an activity mediated by the phosphatidylinositol 3-kinase (PI3K)/Akt pathway (48). Akt activation in ECs is dependent on matrix attachment: integrin molecules when attached to the ECM can activate PI3K through the focal adhesion kinase (FAK). This leads to Akt activation and its downstream targets involved in apoptosis regulation, such as Bad and FKHR family of forkhead transcription factors, resulting in EC survival (49).

Although ECs are the primary targets of VEGF-A, BMDCs can also respond to its mitogenic/survival effects, including monocytes and their precursors (Hematopoietic Stem Cells – HSCs) (45). Furthermore the VEGF-A is also known as a vascular permeability factor and potential pro-metastatic factor, based on its ability to induce the loosening of the cell-cell contacts, facilitating the intravasion/extravasion of tumor cells (50).

Hypoxia is known to be a major inducer of VEGF-A gene transcription, a process mediated by the hypoxia-inducible factor 1 (HIF-1) (51). However VEGF-A gene expression can also be upregulated by oncogene signaling (52), and by the expression of several growth factors and inflammatory cytokines (43).

The VEGF-A effects are mediated by two receptor tyrosine kinases (RTKs): the VEGFR-1, also known as Flt-1, and the VEGFR-2, also known as Flk-1 (Figure 1) (53, 54). In addition VEGF-A can also bind to its co-receptors neuropilins (55). Another member of the VEGFR family is the VEGFR-3 (Flt-4), however it's not a receptor for the VEGF-A. Instead VEGFR-3 regulates lymphangiogenesis upon the binding to VEGF-C and D (56).

Although VEGFR-1 was the first RTK to be identified as a VEGF-A receptor, current data show that VEGFR-2 is the major mediator of the mitogenic, angiogenic and survival effects of VEGF-A (57). Unlike the binding of VEGF-A to VEGFR-2, the VEGFR-1 undergoes weak tyrosine autophosphorylation upon binding of VEGF-A, suggesting that this receptor acts as a 'decoy receptor' for the VEGF-A/VEGFR-2 signaling (58). In fact, at least during early development, the VEGFR-1 is a negative regulator of the VEGF-A activity, by preventing its interaction to VEGFR-2 (partially due to sequestering of VEGF-A by the soluble form of the VEGFR-1 (59)) (60). Nevertheless, the tyrosine kinase domain of VEGFR-1 is required for the migration of monocytes in response to VEGF-A (chemotaxis of monocytes) (61), and its activation by PLGF is able to reconstitute hematopoiesis by recruiting VEGFR-1 positive HSCs (62). Furthermore, VEGFR-1 can also induce the production of MMPs, which in a tumor context can facilitate metastasis (63).

VEGFR-2 undergoes dimerization and strong ligand-dependent tyrosine phosphorylation, leading to phosphorylation of several proteins involved in mitogenic and pro-survival pathways (64): VEGF-A/VEGFR-2 signaling leads to EC growth through activation of the Raf-Mek-Erk pathway (65), and induces their survival by activating the PI3K-Akt pathway (48).

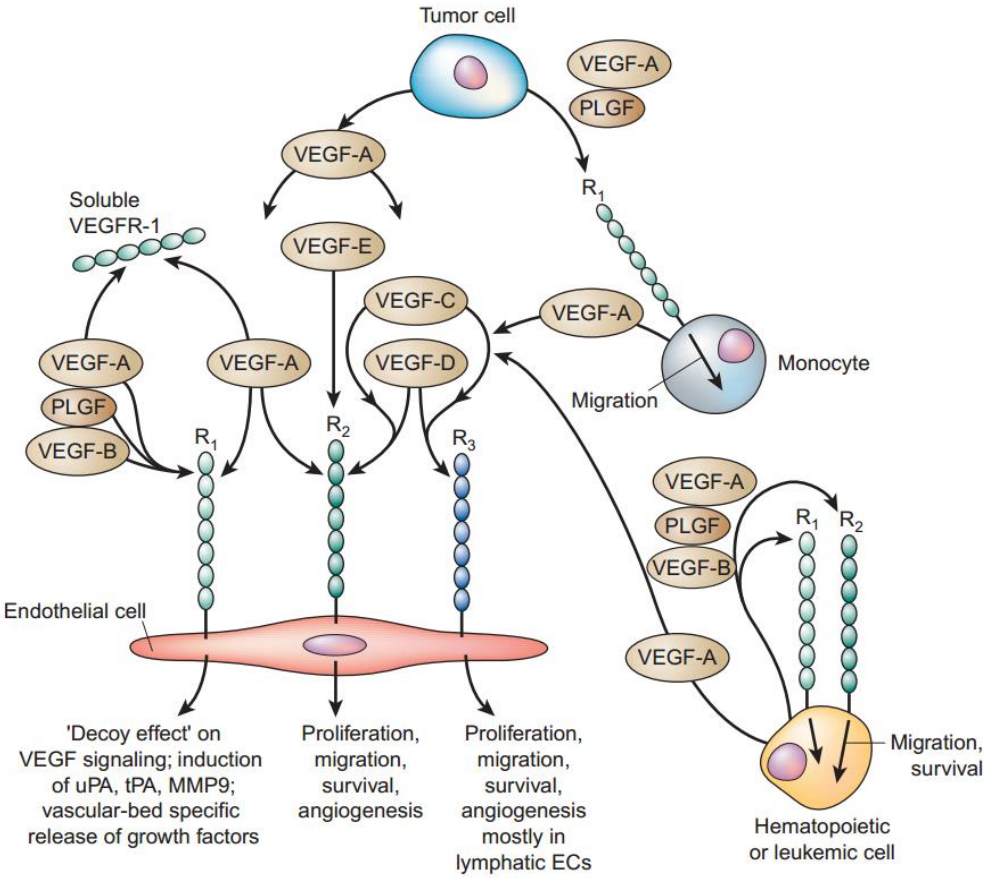

Figure 1. The VEGF pathway (Adapted from Ferrara *et al.*, Nature Medicine, 2003 (45))

Although essential for several physiologic processes, such as normal embryonic vasculogenesis/angiogenesis (39), endochondral bone formation (66) and the ovarian cycle (67), VEGF-A mRNA expression is present in many human tumors, allowing the formation of the tumor vasculature (68).

1.2.1.2. The Angiopoietin-TIE-2 pathway

The angiopoietin (ANG)-Tie system was the second endothelial-specific receptor tyrosine kinase signaling system identified (69). It regulates the later steps of the

angiogenic cascade, related to vessel maturation, and functions as a key regulator of adult vascular homeostasis (27, 70).

This system consists of two RTKs, TIE-1 and TIE-2, and three ligands, ANG-1, ANG-2 and ANG-3/4. TIE receptors are single transmembrane RTKs with an N-terminal ANG-binding domain and a C-terminal tyrosine kinase domain, mainly expressed on ECs and hematopoietic cells (70, 71). All angiopoietins bind to TIE-2, while TIE-1 is as an orphan receptor. However, TIE-1 interacts with TIE-2, and both can translocate to endothelial cell-cell contacts upon angiopoietins stimulation (mainly ANG-1), supporting EC junction (72). ANGs are cytokines consisting of an N-terminal coiled-coil domain and a C-terminal fibrinogen-like domain, responsible for the binding to TIE-2 receptor. Electron microscopy showed that both ANG-1 and ANG-2 bind to TIE-2 as multimers (70).

ANG-1 was initially identified as an agonistic TIE-2 ligand, maintaining the resting EC phenotype (71), while ANG-2 was identified as an antagonist of the ANG-1-TIE-2 signaling pathway (73), even though they bind with similar affinity and in the same domain (74). However, it is now known that ANG-2 can act as a partial TIE-2 agonist in a context-dependent manner (70). ANG-1 is mainly expressed by perivascular cells (pericytes and smooth muscle cells) acting on TIE-2 receptors of ECs through a paracrine manner, whereas ANG-2, produced by activated/sprouting ECs, acts in an autocrine manner (75). ANG-2 is stored by ECs in specialized endothelial storage granules, called Weibel-Palade bodies, and released upon vascular remodeling, promoting angiogenesis likely by antagonizing ANG-1-mediated EC quiescence (76).

The binding of ANG-1 to TIE-2 leads to strong phosphorylation of the tyrosine kinase domain, leading to the recruitment of adaptor proteins, such as PI3K, which results in the activation of the AKT pathway (77). In turn, AKT signaling modulates survival and apoptotic pathways, leading to EC survival and maintenance (Figure 2) (70). Furthermore, ANG-1-TIE-2 signaling results in a negative feedback loop on EC ANG-2 production, since AKT signaling inactivates the transcription factor FoXo1, which targets ANG-2 (78). Beside the well described effect on vascular homeostasis, the ANG-1-TIE-2 signaling in non-resting ECs can stimulate their migration, an effect mediated by phosphorylation of focal adhesion kinase (FAK) (70). ANG-1-activated TIE-2 can also decrease permeability and inflammation, by inhibiting the nuclear factor-κB (NF-κB) (79), and induce maturation of blood vessels, by stimulating the migration of pericytes towards ECs (thought to be mediated by heparin-binding epidermal growth factor, hepatocyte growth factor and serotonin) (70).

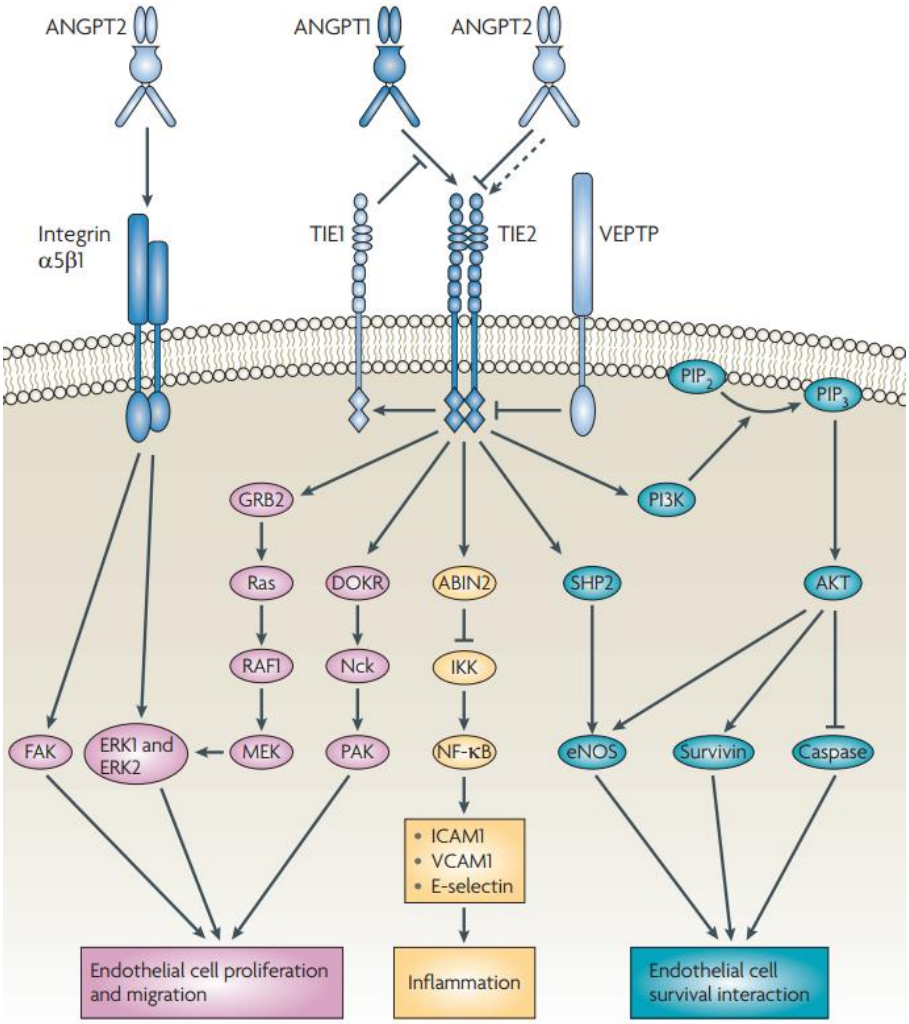

Figure 2. The ANG-TIE pathway (adapted from Huang *et al.*, Nat. Rev. Cancer, 2010 (75))

It is remarkable how ANG-1 and ANG-2 can induce opposite effects (vascular stabilization or angiogenesis, respectively) via the same TIE-2 receptor. Current studies suggest that ANGs can alter the subcellular localization of TIE-2 in a distinct manner, enabling different responses of the TIE-2 signaling: while ANG-1 leads to TIE-2 clustering and activation at inter-endothelial cell-cell junctions, mediating cell–cell adhesion, antipermeability and EC survival; ANG-2 binds to TIE-2 located at EC-ECM contact sites, antagonizing ANG-1 signaling and enhancing EC responsiveness to exogenous cytokines, such as VEGF (72). Furthermore, several reports suggest that ANGs can bind to integrins, which in turn can modulate ANG-1 and ANG-2 specific signals (75).

In quiescent tissues ANG-2 levels are low, favoring the ANG-1-TIE-2 signaling. However, during tumor angiogenesis ANG-2 expression is upregulated, favoring instead the ANG-2-TIE-2 signaling (70). In such cases the acute release of ANG-2 from activated ECs results in

pericyte detachment with consequent exposure of ECs to pro-angiogenic signals, favoring tumor angiogenesis (76). Tumor-associated ANG-2 can also promote angiogenesis by recruiting a population of hematopoietic TIE-2 expressing cells, first described by De Palma and co-workers: the TIE-2-Expressing Monocytes/Macrophages (TEMs) (80). Although weakly expressed by circulating resident monocytes, TIE-2 is upregulated in a subset of perivascular tumor-associated macrophages (TAMs), which display a distinct gene expression signature consistent with enhanced pro-angiogenic activity, when compared with TIE-2 negative TAMs (76, 81).

1.2.2. The angiogenic switch in breast cancer

In breast cancer, an increased infiltration of macrophages occurs in the nonmalignant adenoma stage, preceding the transition to the malignant stages of carcinoma associated with the angiogenic switch. This observation suggested that macrophages promote the angiogenic switch in breast cancer (82). Indeed, studies performed by Lin and co-workers reveled a dramatically delay of the angiogenic switch in mouse models of breast cancer upon macrophage depletion (83).

At a certain point, tumor cells start to produce monocyte chemokines, such as the Colony-Stimulating Factor 1 (CSF-1) (Figure 3), recruiting them into the tumor where they differentiate into TAMs, often with an alternative (also termed “M2”) polarization phenotype (84). These cells are then able to support the tumor progression through several mechanisms, including the induction of tumor angiogenesis (85), by producing angiogenic growth factors and proteinases, such as VEGF, ANG-2 and MMP-9 (82). Furthermore, vessel-associated TAMs, the TIE-2-Expressing Macrophages, can also promote the formation of the tumor vasculature, a process mediated by the ANG-2-TIE-2 signaling (80).

The tumor-promoting role of these cells in the progression of established tumors might explain the correlation between high density of macrophages and poor prognosis observed in human breast cancer (86).

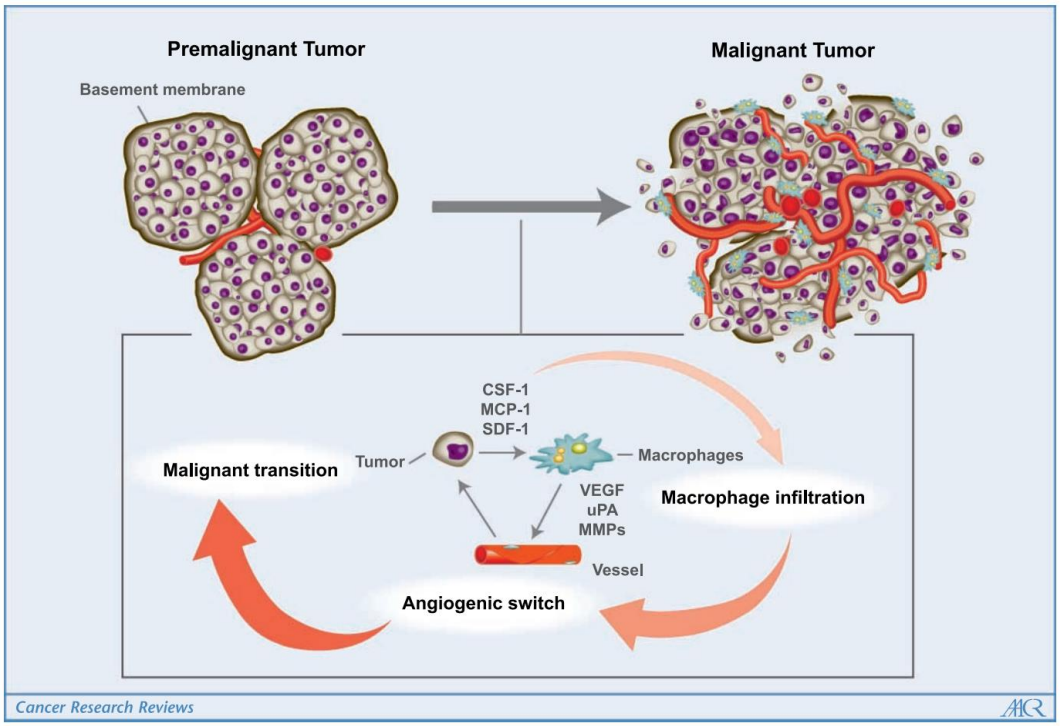

Figure 3. **TAMs as the drivers of breast cancer malignancy** (Adapted from Lin and Pollard, Cancer Res., 2006 (82))

1.2.3. Anti-angiogenic therapy

Decades ago Judah Folkman disclosed that without expanding the blood vasculature the tumor cannot exceed 2-3mm, and hypothesized that inhibition of angiogenesis would be an effective strategy to treat human cancer (87). Since then, an active search for angiogenesis inhibitors began and, despite some initial setbacks and negative clinical trial results, in 2004 the FDA approved the first anti-angiogenic drug for cancer therapy: the VEGF-A neutralizing mAb bevacizumab, as a first-line treatment for metastatic colorectal cancer (38).

1.2.3.1. Targeting the VEGF pathway

Because VEGF plays a central role in tumor angiogenesis, the first angiogenesis inhibitors aimed to impair the VEGF-A/VEGFR-2 signaling pathway, with several VEGF neutralizing mAbs, and multi-target TKIs already approved for clinical applications (32).

In 1993 Ferrara and co-workers developed the first anti VEGF-A mAb, a mouse anti-human antibody named A.4.6.1. They observed a potent inhibitory effect on tumor

angiogenesis and growth of several tumor cell lines in nude mice (70% to 90% of tumor growth inhibition) (88). Later on, they reported the humanized version of A.4.6.1, termed bevacizumab (Avastin©), which binds to and neutralizes all human VEGF-A isoforms and bioactive proteolytic fragments, but not to other VEGF ligands (VEGF-B, C or D) (38). Bevacizumab is currently approved for the treatment of advanced and metastatic colorectal cancer, renal cell cancer, non-small cell lung cancer and glioblastoma multiforme (89).

Besides targeting the VEGF-A, mAb targeting VEGFR-2 were also generated, as the DC101 murine antibody (ImClone Systems) (90) and the ramucirumab (Cyramza©) (91). The later was recently approved by the FDA for the treatment of gastric or gastroesophageal junction adenocarcinoma.

In addition, small molecule TKIs capable of inhibiting the activity of VEGFRs via ATP-competitive binding, have also been approved. Besides VEGFR, these TKIs also inhibit the Platelet-Derived Growth Factor Receptors (PDGFRs), Flt-3, c-Kit, RAF and RET, suggesting that they may have a direct antitumor effect (by inhibiting oncogenic and growth-promoting kinases) in addition to antiangiogenic functions. Sorafenib (Nexavar©), sunitinib (Sutent©) and pazopanib (Votrient©) are TKIs approved for the treatment of human cancers (92).

VEGF inhibitors have been approved by the FDA for the treatment of patients with highly advanced malignancies (metastatic setting) or in cases of inoperable diseases (43). Because one side effect of blocking VEGF is bleeding complications, anti-VEGF agents are not administered to patients before surgery (93).

However, like the majority of anticancer therapies, patients treated with anti-VEGF therapies develop resistance, and benefit from the therapy for only a few months (adaptive resistance) or don't benefit at all (intrinsic resistance) (29). Indeed, in several mouse tumor models, although VEGF inhibition results in reduced angiogenesis and tumor growth, tumors usually re-vascularize upon prolonged treatment (94). In 2008 Bergers and Hanahan reviewed the mechanisms of resistance to anti-VEGF therapy, which include the upregulation of alternative proangiogenic growth factors (as ANG-2), the increased coverage of blood vessels by perivascular cells, the increased recruitment of BMDCs and increased tumor cell invasiveness (29).

Compelling data have shown that ANG-2 is responsible for inducing tumor resistance to anti-VEGF therapy: upon VEGF blockade there is an overexpression of ANG-2, allowing the tumor vasculature to become VEGF independent. Preclinical studies, conducted by Rigamonti and co-workers, have shown an upregulation of ANG-2 at both transcript and protein levels upon prolonged VEGFR-2 blockade in the RIP1-Tag2 pancreatic tumor model

(95). They also demonstrated that the resistance to VEGF blockade could be reversed by ANG-2 neutralization. These results, as well as previous studies (96-98), suggest that targeting of ANG-2-TIE-2 and VEGF-VEGFR2 signaling pathways represent a promising therapeutic approach to avoid the induction of adaptive resistance and obtain a durable antiangiogenic effect.

1.2.3.2. Targeting the ANG-TIE pathway

Higher ANG-2/ANG-1 ratio, when compared with normal tissues, correlates with poor prognosis in many human cancers, including myeloid leukaemia (99), breast cancer (100), neuroendocrine cancers (101), prostate cancer (102), and many others (103-106). Although the effect of targeting ANGs is context dependent (107), higher ANG-2/ANG-1 ratio also correlates with increased angiogenesis, invasion and metastasis, making the antitumor and antiangiogenic benefits of targeting ANG-2 evident (75).

Several studies have demonstrated that specific inhibition of ANG-2 induces durable tumor growth inhibition, vascular regression with normalization of the remaining blood vessels, and suppression of metastatic spread (97, 98, 108). Furthermore, blocking ANG-2 also impedes TIE-2 upregulation by TAM/myeloid cells and their association with tumor blood vessels (98, 108), suggesting that targeting ANG-2-TIE-2 axis can also inhibit tumor angiogenesis indirectly, by impairing the pro-angiogenic functions of TEMs (besides directly targeting the autocrine signaling on ECs). According to these data, ANG-2 blockade represents a promising antiangiogenic therapy, capable not only of blocking angiogenesis and metastasis, but also impairing the recruitment of myeloid cells (109), known to allow tumor recovery after antiangiogenic therapy (29).

Specific inhibitors of ANG-2 have been developed over the past few years, including a human anti-ANG-2 mAb, termed MEDI-3617 (3.19.3) (97, 98), or a ANG-2 CovX-Body, composed of a peptide coupled to a monoclonal antibody via covalent linker, termed PF-4856884 (also known as CVX-060) (108). Recently the CVX-060 was evaluated, in combination with sunitinib, in a phase I/II trial in patients with metastatic renal cell cancer and solid tumors. Analysis demonstrated safety of CVX-060, however no increased overall survival (OS) was observed by combining CVX-060 with sunitinib (110). Additionally a peptibody targeting both ANG-1 and ANG-2, AMG-386, has been developed and tested in several clinical trials, with demonstrated tolerability but no clinical efficacy (111-113). The aforementioned molecules mediate their effects by preventing ANG-2 binding to TIE-2 receptor, however the TIE-2 receptor can also be targeted by kinase inhibitors, such as the CEP-11981 and the CE-245677 (75).

1.2.3.3. Co-targeting the VEGF and ANG-TIE pathways

High levels of VEGF-A and ANG-2 correlate with worse prognosis in several human cancers, including breast cancer, when compared with cancers expressing high levels of either alone (114). These results, together with the fact that ANG-2 might be a key player in the induction of adaptive resistance to anti-VEGF therapy, suggest that co-targeting ANG-2 and VEGF-A could provide a better antitumor effect, when compared to monotherapies.

In order to test that hypothesis several bi-specific drugs, targeting both VEGF-A and ANG-2, have been developed, such as the bi-functional CovX-Body CVX-241 (75), a chimeric decoy receptor DAAP (double antiangiogenic protein) (115), and the ANG-2-VEGF-A (A2V) CrossMab, a bispecific human IgG1 antibody capable of blocking VEGF-A and ANG-2 simultaneously (116).

A2V crossmab, produced by Kienast and co-workers, is composed of an arm based on bevacizumab (Avastin©), and another based on LCO6, an anti-ANG-2 human IgG1 antibody (117). The authors tested the A2V crossmab in a panel of orthotopic and subcutaneous mouse tumors and patients or cell line-derived human tumor xenografts, especially at later stages of tumor development, using LCO6 (117), bevacizumab (Avastin©) or B20-4.1 (an anti-VEGF-A mAb) (118) as monotherapies. They found that simultaneously blocking VEGF-A and ANG-2 had addictive effects on the inhibition of advanced tumor growth, angiogenesis and metastasis, when compared to the monotherapies. A2V crossmab was also able to target angiogenic escape pathways described in the clinic, upon anti-VEGF monotherapy, preventing tumor revascularization (116).

ANG-2 inhibition reduced tumor vessel sprouting, whereas VEGF-A inhibition induced vessel regression, significantly decreasing tumor vasculature (96). Furthermore, by blocking ANG-2, the effects mediated by ANG-1 are potentiated, inducing accumulation of adhesion molecules in cell–cell junctions and increasing pericyte coverage (107). As a result the remaining abnormal tumor blood vessels become normalized, slowing down tumor invasiveness and dissemination/metastasis and increasing the tumor responses to other therapies, such as chemotherapy (due to decrease leakage) (119).

1.2.4. Antiangiogenic therapy in breast cancer

Bevacizumab was the first antiangiogenic therapy to be evaluated in breast cancer (4). In a randomized phase III clinical trial (E2100) including mainly HER-2 negative patients, the efficacy of paclitaxel alone vs bevacizumab plus paclitaxel was evaluated. Analysis revealed an increased Response Rate (RR) (21 versus 37%, $P < 0.001$) and median PFS (25.2 versus 26.7 months, $P = 0.16$), with the addition of bevacizumab (120). These results led to the

approval of bevacizumab for HER2-negative metastatic breast cancer in combination with paclitaxel, in 2008 by the FDA (121). However, subsequent studies with bevacizumab and other chemotherapies demonstrated similar improvements in PFS but failed to show an OS advantage (122, 123), which led the FDA to recommend withdraw of bevacizumab for breast cancer in 2010 (27). Both the TKIs sunitinib and sorafenib have been evaluated in clinical trials (124, 125), but they didn't receive the approval for the treatment of breast cancer.

Because high levels of ANG-2 correlate with poor prognosis in breast cancer (100), agents that target ANG-2 were also evaluated, including a phase II placebo-controlled trial in HER2-negative metastatic breast cancer comparing the efficacy of paclitaxel plus AMG 386 versus paclitaxel plus bevacizumab versus paclitaxel in combination with both drugs. In this study, completed in January 2015, blocking ANG-2 showed no apparent prolongation of PFS, compared to the controls (126).

So far there is a lack of successful antiangiogenic therapies in breast cancer, with no prolonged OS in the clinical trials.

1.3. The tumor immune environment and immunotherapy

As previously stated, the host immune cells are also recruited to the tumor microenvironment, where they have the ability to recognize and destroy the cancer cells, a process known as "**cancer immunosurveillance**" (127-129). However, tumors can develop under the presence of a functional immune system, suggesting that cancer cells are able to edit the immune system, a process called "**cancer immunoediting**" (130).

1.3.1. Cancer immunoediting

According to Gavin P. Dunn and co-workers, cancer immunoediting better describes the dual role of the immune system in cancer ("host-protective" or "tumor-promoting"), and consists of 3 distinct phases: elimination, equilibrium and escape (Figure 4) (131).

Elimination: as described by the immunosurveillance theory, during the elimination phase the innate and adaptive immune system can detect and destroy the cancer cells, functioning as an extrinsic tumor suppressor (132). Several mechanisms can lead to activation of innate immune cells, including the tumor release of type I Interferon (IFN), which activates dendritic cells (DCs), or the binding of stress ligands expressed on the surface of tumor cells to receptors of antigen presenting cells (APCs), leading to release of pro-inflammatory cytokines (133).

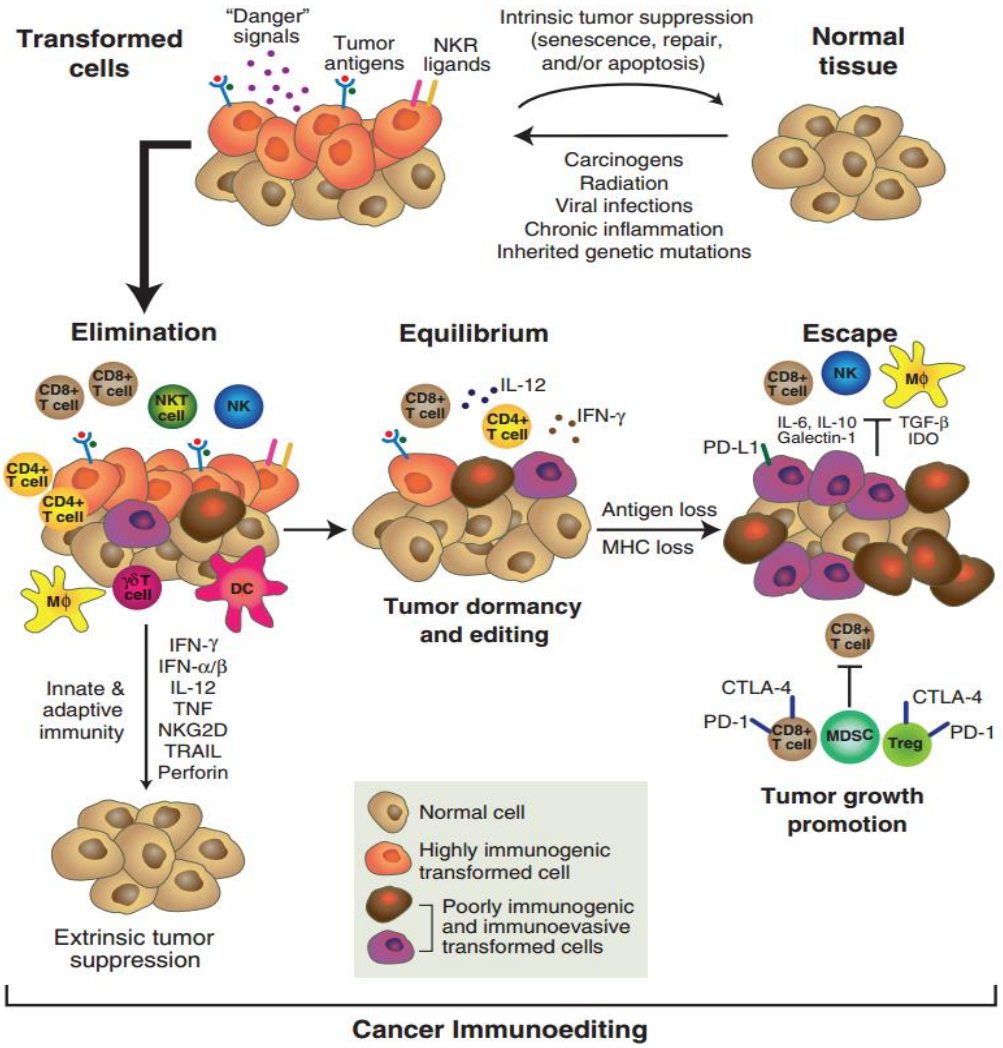

Figure 4. The three steps of tumor immunoediting (Adapted from Schreiber et al., Science, 2011 (133))

Besides the activation of the innate system, the adaptive system is also known to play a role in tumor surveillance. Malignant cells express cancer antigens – derived from oncogenic viruses, differentiation antigens, epigenetically regulated molecules or carcinogenic mutations (134) - which can differentiate them from normal cells (135, 136). These cancer antigens, associated with Major Histocompatibility Complex (MHC) class I molecules, can be recognized by the T Cell Receptor (TCR) of cytotoxic $CD8^+$ T cells, with subsequent activation of an anti-tumor adaptive immune response (137). If this phase is successful the tumor is suppressed and not clinically detected (130).

Equilibrium: this phase occurs when certain tumor cell variants survive the elimination phase. In such scenario the host immune system exerts selective pressure on the tumor, which is enough to contain it but not sufficient to eliminate it. Even though the adaptive

immune system is still able to maintain the tumor in a dormancy state, the tumor immune editing takes place in this phase: due to genetic instability new variants of tumor cells arise, carrying different mutations with reduced immunogenicity. The equilibrium phase is the longest, occurring over a period of many years in humans, and ends when the tumor is finally able to escape the immune system (131, 133).

Escape: due to selective immune pressure, tumor cells acquire the ability to evade immune recognition and/or destruction, entering in the escape phase, where the immune system is no longer capable of controlling tumor outgrowth (which becomes clinically visible) (131, 133).

1.3.1.1. Mechanisms of escape

Cancer cells can escape the immune system through a series of mechanisms, either by reducing immune recognition, or exploiting physiological mechanisms of immunosuppression, developed to prevent autoimmunity, in order to impair the host antitumor immune response (133). One of these mechanisms is the loss of tumor antigen expression by the tumor cells (reviewed in (138)), making them invisible to the immune system.

Tumor cells can also hijack the immune checkpoints for T cell activation (139). Naïve T cells require at least two signals to became fully activated (Figure 5): the interaction of antigen-MHC complexes with the TCR on the T cells, and the costimulatory signal mediated by the binding of B7 molecules (CD80 and CD86) on APCs to the CD28 receptor on the T cell surface (140).

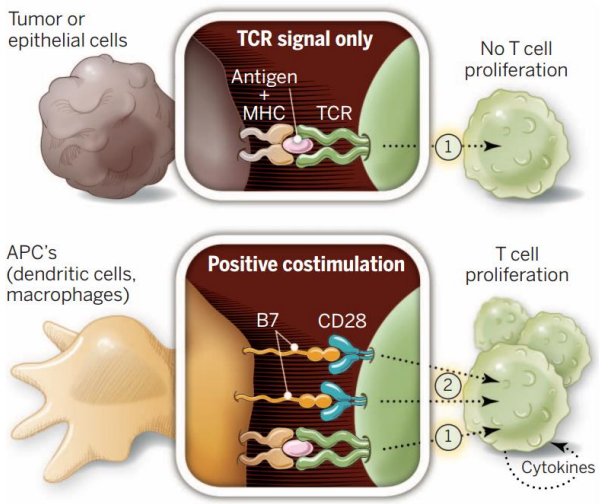

Figure 5. T cell activation signals. Inflammatory responses allows APCs to take up the cancer antigens, which can be presented to the T cells leading to their activation (Adapted from Sharma and Allison, Science, 2015 (141))

However, in order to regulate T cell responses, co-inhibitory molecules are also necessary (141). CTLA-4 (Cytotoxic T lymphocyte associate antigen 4) and PD-1 (Programmed cell death protein 1) are two well-known co-inhibitory molecules (termed immune checkpoint modulators) (142-144). Both CTLA-4 and PD-1 are present on the membrane of T cells, but while CTLA-4 competes with CD28 for the binding to CD80/86 (145), PD-1 binds to its ligands PD-L1 (B7-H1) and PD-L2 (146). The activation of a co-inhibitory pathway leads to attenuation/termination of T cell responses, necessary to maintain self-tolerance and modulating the duration and amplitude of T cell response. The tumor microenvironment can exploit this process, in order to suppress the antitumor immunity, by activating inhibitory receptors on T cells (147, 148).

Furthermore, cancer cells may evade the immune system by creating an immunosuppressive environment (133, 149). In order to do so they can produce immunosuppressive molecules, such as Transforming Growth Factor (TGF)-β (150), interleukin (IL)-10 or the enzyme indolamine-2,3-dioxygenase (IDO), a mediator of T cell activation and regulator of autoimmunity (151). Tumor cells can also recruit pro-tumoral infiltrating leukocytes - such as regulatory T cells (Treg), known to inhibit the function of cytotoxic T cells (152) -, myeloid-derived suppressor cells (MDSCs) and alternatively activated macrophages (M2), which can suppress effective immunity through secretion of immunosuppression cytokines, such as IL-10 and TGF-β (153-155).

All the mechanisms above described allow tumor cells to edit the host immune system in their favor, preventing immune responses that would lead to cancer cell dead.

1.3.2. Immunotherapy

The identification of the immunosuppressive mechanisms present in the tumor microenvironment opened the door for the use of immunotherapy for cancer patients. Immunotherapy aims to induce an effective immune anti-tumor response by re-editing the tumor immunosuppressive microenvironment to the immune surveillance/elimination phase (139). Immunotherapy strategies include, among others, vaccination with tumor antigens, to elicit strong specific lymphocyte responses, adoptive transfer of tumor-specific lymphocytes or inhibition of the mediators of cancer-induced immunosuppression (CTLA-4, PD-1, Treg, macrophages, etc) (133).

Special interest has been directed to the immune checkpoint blocking antibodies. Immune checkpoint blockade leads to an enhanced activation of cytotoxic T cells, thereby priming an anti-tumoral immune response and improving clinical outcomes (139). Indeed, ipilimunab (Yervoy©), a mAb against human CTLA-4 led to significant improvement of the OR in metastatic melanoma patients, leading to the FDA approval in 2001 (156). Following

ipilimunab, several immune checkpoint therapies were developed, including mAb targeting the PD-1/PD-L1 axis. The anti-PD-1 antibody MK-3475 (pembrolizumab) led to RR of 38% in patients with advanced melanoma in a phase I clinical trial (157), which led to its approval by the FDA in September 2014. Nivolumab, another anti-PD-1 antibody was also recently approved by the FDA (December 2014) for the treatment of metastatic melanoma, after showing an OR of 40% and OS of 73% in a phase III trial, compared with chemotherapy (158).

Besides immune checkpoint blockade, immunostimulatory antibodies, such as agonist CD40 mAb, are also in clinical development and show a potent anti-tumor effect (159). CD40 is a receptor of the Tumor Necrosis Factor (TNF) family and contributes to humoral immune responses (160). CD40 is expressed on the surface of several cells, including DCs, B lymphocytes, monocytes, ECs, and fibroblasts; while its ligand CD40L, also known as CD154, is manly expressed by T lymphocytes and platelets (161, 162).

The binding of CD40L (in a trimeric state) to CD40 causes a conformational change, allowing the recruitment of the TNF receptor associated factors (TRAFs) to the CD40 cytoplasmic tail. This in turn, recruits TRAF associated kinases leading to the activation of several signal transduction pathways, including the NF-κB, the p38/MAPK and the c-Jun-NH2-kinase (JNK) pathways. This allows CD40 to control essential processes such as apoptosis, cell cycle, cytokine production and expression of cell surface immune modulators (159).

Agonistic CD40 mAb can mount an anti-tumor response through the action of several mechanisms (Figure 6). Physiologically, the interaction between CD40L-expressing $CD4^+$ T cells and CD40-expressing DCs leads to maturation and activation of DCs. Activated DCs increase the expression of MHC and costimulatory molecules (CD80 and OX40L) and production of proinflammatory cytokines (163). This process, known as DC 'licensing', is required for cytotoxic T cell responses (164). However, agonistic CD40 mAbs can replace the activation signal delivered by the $CD4^+$ lymphocytes, allowing increased presentation of tumor antigens to CD8 T cells. This results in activation/expansion of cytotoxic T cells with subsequent anti-tumor adaptive immune response (165). T cell-independent mechanisms, mediating the therapeutic efficacy of agonistic CD40 mAb, have also been described. One of this mechanisms is the anti-tumor response achieved by the binding of CD40 mAb to CD40-expressing macrophages, which become tumoricidal (166). Some tumor cells can also express CD40 (167), including breast cancer cells (168), which upon binding to the CD40 mAb are destroyed, even in the absence of immune cells. The CD40-mediated tumor cell death is due to the activation of apoptotic pathways (169) and has been seen *in vivo* in breast carcinoma (170). Furthermore, cancer antigens released by the dying tumor cells, can enhance the activation of cytotoxic T cells, via APCs.

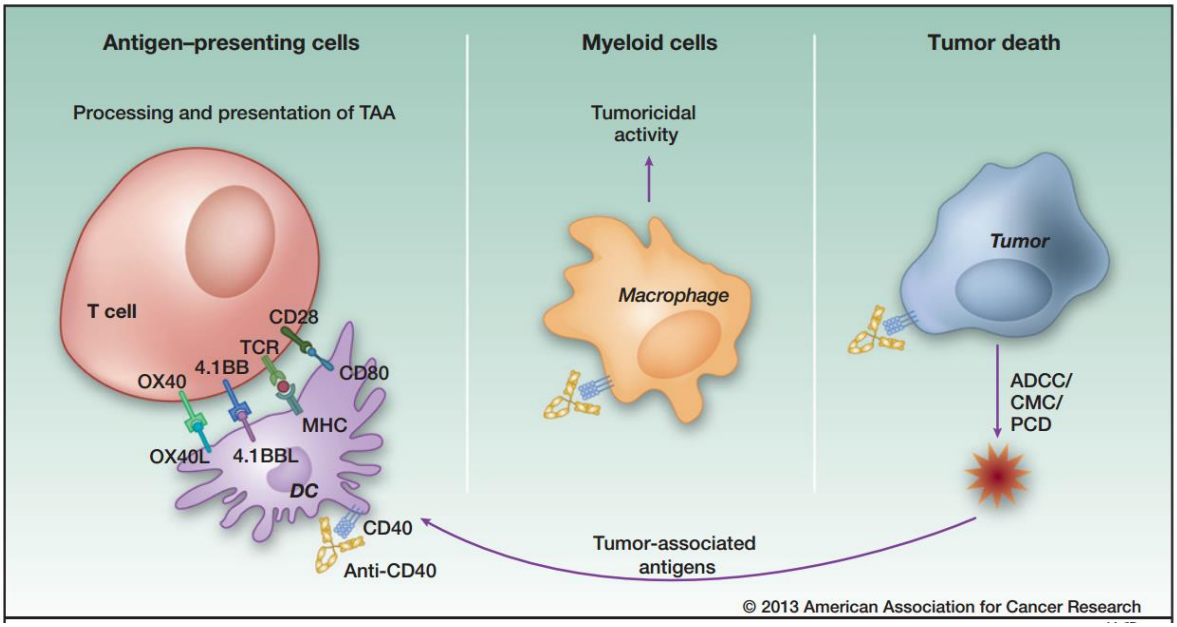

Figure 6. Immune dependent and independent mechanisms of action of agonistic CD40 mAb. (Adapted from Vonderheide and Glennie, Clin Cancer Res, 2013 (171))

Several CD40 mAbs have been tested in clinical trials, including the mAb CP-870,893 (Pfizer) (172), dacetuzumab (Seattle Genetics) (173) and lucatumumab (Novartis) (174). Of special interest is the CP-870,893, a fully human agonist CD40 mAb, which displays a clinical efficacy in both metastatic pancreatic cancer (175) and advanced solid tumors (176). Therefore, agonistic CD40 mAb should be considered for the treatment of cancer.

Other immunotherapy strategies include targeting the immunosuppressive cells recruited to the tumor, such as Treg and TAMs, by using anti-CD25 (177) and anti-CSF1R mAbs (178), respectively.

1.3.3. Immunotherapy in breast cancer

Increased numbers of infiltrating $CD8^+$ T cells have been associated with better clinical outcomes in patients with breast cancer (179), while worse clinical outcomes were observed in the presence of increased Treg (180) and macrophage (181) infiltration. Therefore, immune strategies that either increase the infiltration of cytotoxic T cells or decrease the infiltration of immunosuppressive cells have been tested in breast cancer.

Blockade of PD-1/PD-L1 pathway has been shown to enhance the response of radiotherapy in advanced breast cancer (182), and to be associated with anti-tumor activity in a phase I study, with an anti-PD-1 mAb (MDX-1106) as a single agent (183). Blockade of CTLA-4 (using tremelimumab and ipilimumab) was also evaluated in breast cancer, but with no significant clinical response (184).

Additionally, both anti-CD25 antibody-mediated Treg neutralization (185) and anti-CSF1R-mediated TAM depletion (83, 186) induced a strong anti-tumor immune responses in pre-clinical models of breast cancer, which encouraged their evaluation in clinical trials. The FDA approved daclizumab, an anti-CD25 mAb, was found to lead to prolonged elimination of Treg cells in the peripheral blood of metastatic breast cancer patients taking a cancer vaccine, who had a 30% increased survival, compared to those patients taking the cancer vaccine alone (187). RG7155 (Roche), a humanized mAb targeting CSF1R, is currently being evaluated in a phase I study as a monotherapy and in combination with paclitaxel in patients with advanced solid tumors, including an arm with metastatic breast cancer (NCT01494688).

All together, these results suggest that therapeutic approaches aiming to adequately stimulate a T cell response in breast cancer, through the mechanisms described above, can be a promising strategy to treat breast cancer patients.

1.3.4. Angiogenesis and Immunosuppression

A substantial number of cells have the ability to promote both immunosuppression and angiogenesis including, among others, MDSCs, macrophages and the ECs (reviewed in (188)). Of particular interest is the distinct role of the tumor vasculature in editing the tumor immunosuppressive microenvironment (188). To do so, tumor endothelial cells can either regulate the traffic of leukocytes or directly suppress immune responses (Figure 7).

During a normal inflammatory response, ECs can upregulate chemotactic factors and adhesion molecules, such as intercellular adhesion molecule 1 (ICAM1) and vascular cell adhesion molecule 1 (VCAM1), enable them to recruit leukocytes and mediate diapedesis/extravasation in the target tissue (Figure 7a) (189). However, in a tumor microenvironment context, the production of angiogenic factors decreases the expression of the adhesion molecules ICAM1 and VCAM 1, thereby decreasing leukocyte extravasation, and infiltration in the tumor (Figure 7b) (190, 191). Furthermore, the upregulation of certain molecules, such as common lymphatic endothelial and vascular endothelial receptor 1 (CLEVER1), can selectively allow the extravasation of Treg cells, known to have pro-tumor activity, into the tumor microenvironment (192).

Moreover, tumor ECs can express mediators capable of suppress adaptive immune responses (Figure 7c), including the expression of the T cell inhibitory ligands PD-L1 and PD-L2 (193), the enzyme IDO (194) or the EC marker CD31, also reported to inhibit T cell activation (195). Furthermore, ECs can also express immunosuppressive soluble mediators, such as IL-6, IL-10 or the TGF-β (196).

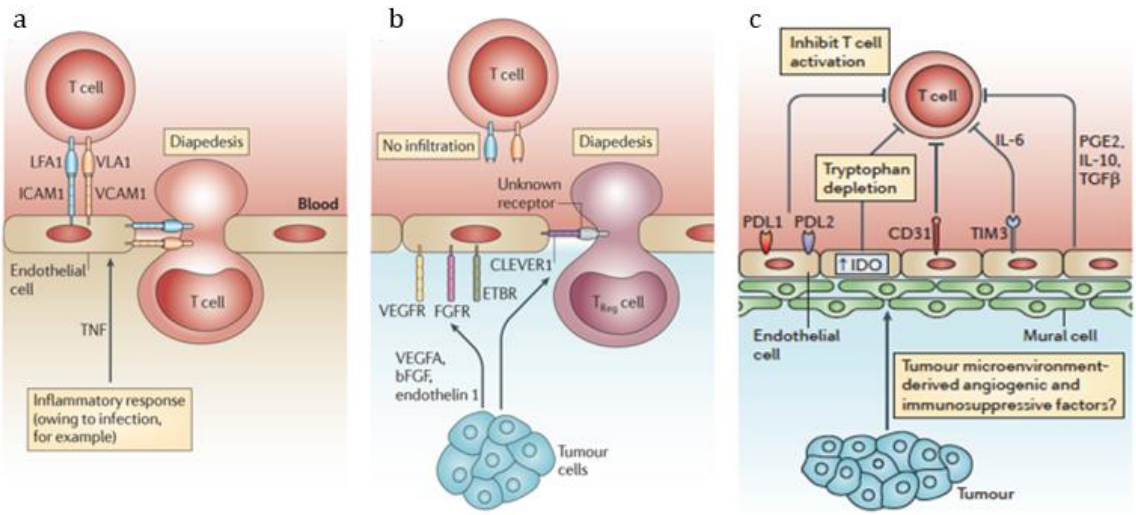

Figure 7. Vasculature regulation of immune responses: (a, b) the role in leukocyte trafficking and (c) direct immune regulation. (Adapted from Motz and Coukos, Nature, 2011 (188))

Given the strong immunosuppressive role of ECs in the tumor microenvironment, it is possible that immunotherapy might benefit from a co-targeting approach aiming to simultaneously target tumor angiogenesis and tumor immunity. Thus, a combined antiangiogenic and immunotherapy strategy for the treatment of breast cancer was pursued in this study, using the MMTV-PyMT mouse model of breast cancer.

1.4. MMTV-PyMT transgenic mouse model of breast cancer

The MMTV-PyMT mouse model is a well-established model to study breast cancer, where the Mammary Mouse Tumor Virus (MMTV) promoter drives the mammary gland-specific expression of the Polyomavirus Middle T antigen (PyMT), resulting in a spontaneous development of multifocal mammary tumors (197, 198). Carcinogenesis is driven by the activation of specific proto-oncogenes, such as the Shc and the PI3K, as a result of the phosphorylation of the membrane-anchored PyMT protein by the Src family of TK (198). This model, generated by Guy and colleagues in 1992, is characterized by high penetrance (with virtually 100% tumor incidence), short latency (1-6 months) and high metastasis incidence (>85%) in lungs and lymph nodes (199).

Tumorigenesis in this model occurs throughout four stages, with similarities to human breast cancer (Figure 8): hyperplasia (at 4-6 weeks of age), adenoma/mammary intraepithelial neoplasia (MIN) (8-9 weeks), early (8-12 weeks) and late carcinoma (>10 weeks) (197). Basement membrane disruption and myoepithelial cell loss, followed by

leukocyte and macrophage infiltration occurs even in pre-malignant stage (198). Like in human breast cancer, tumor progression to malignancy in the MMTV-PyMT model correlates with gradual loss of hormone receptors (ER and PR) and integrin-β1, and increased expression of cyclin D1 (197, 200), making it an ideal model to study human breast cancer.

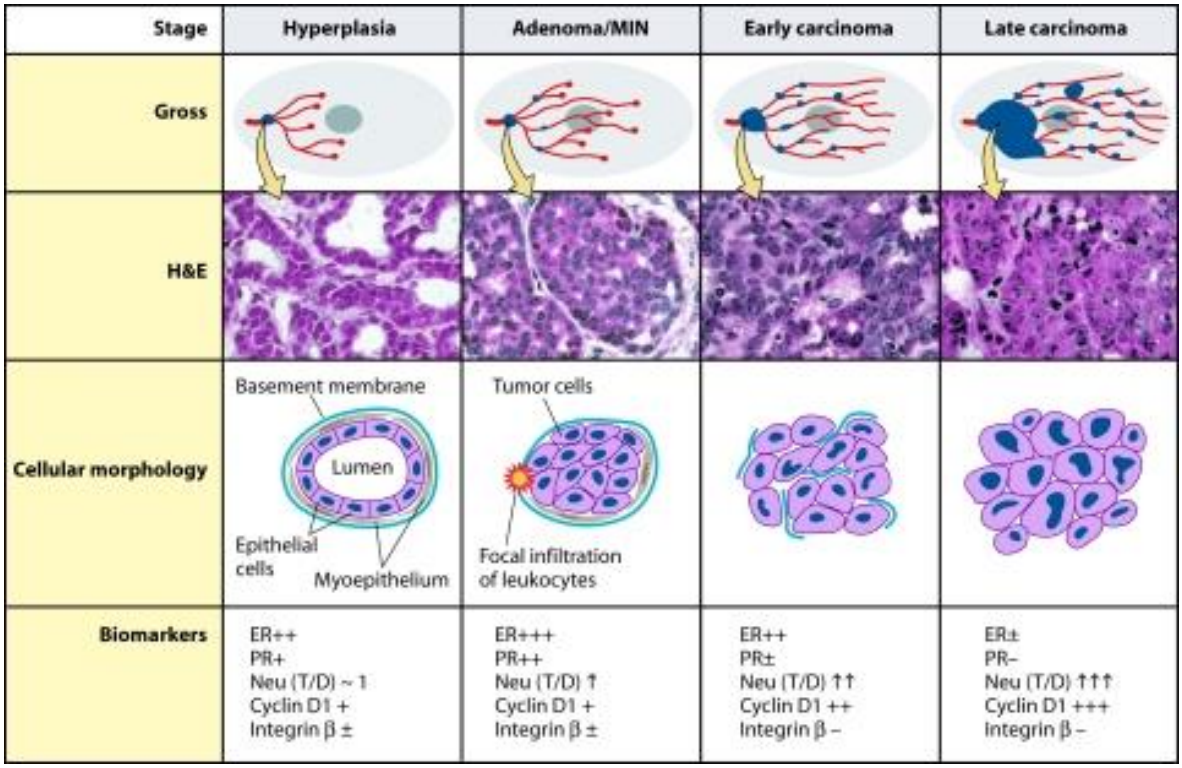

Figure 8. The 4 stages of tumor progression in the MMTV-PyMT model, with correspondent morphology and biomarkers (Adapted from Fluck and Schaffhausen, Microbiol Mol Biol, 2009 (198))

Besides the spontaneous model, orthotopic MMTV-PyMT model can also be generated by implanting MMTV-PyMT cells (retrieved from a spontaneous MMTV-PyMT tumor bearing mouse) into the mammary fat pad of syngeneic mouse (mouse with identical genetic background from the donor mice). This leads to formation of primary tumors with possible subsequent formation of metastases. By using syngeneic recipient mice the immunologic donor-versus-recipient reaction can be avoid, allowing to evaluate the contribution of the immune system to tumor development (201).

2. Aims of the Project

2.1. The first aim of the project was to evaluate the anti-tumor effect of dual ANG-2/VEGF-A blockade in the MMTV-PyMT mouse model of breast cancer. To do so, a novel bispecific Ab termed A2V, capable of neutralizing ANG-2 and VEGF-A simultaneously, was administered.

Responses to the therapy were evaluated based on:

- Tumor growth and survival of the mice;
- Tumor necrosis and fibrosis;
- Relative tumor vascular area;
- Perfusion of tumor blood vessels;
- Tumor hypoxia;
- Tumor blood vessel coverage.

2.2. The second goal was to assess the possible clinical benefit of co-targeting tumor angiogenesis and tumor immunity in the MMTV-PyMT mouse model. For this purpose the A2V-based therapy and a CD40-agonistic mAb, termed FGK45, were combined. Additionally to the parameters above described, tumor responses were also evaluated based on tumor infiltration of T lymphocytes, both by Immunofluorescence staining and flow cytometry analysis.

3. Materials and Methods

3.1. Mouse tumor models

FVB/N and transgenic FVB/MMTV-PyMT mice were purchased from Charles River Laboratories (L'Arbresle, France). The animals were accommodated in the Animal Facility of the *École Polytechnique Fédérale de Lausanne* (EPFL), under pathogen-free conditions with a 12h light/dark schedule, and provided with satisfactory amount of food and water. Ethical approval was obtained by the Veterinary Authorities of the Canton Vaud (license 2577), and all procedures were performed according to the Swiss law.

To obtain orthotopic MMTV-PyMT tumors, late-stage mammary tumors of a 16-week old tumor-bearing transgenic MMTV-PyMT female mouse were harvested and smashed in a petri dish containing a small volume of a enzymatic solution, prepared by diluting Liberase TH (75 µg/ml, Roche, REF: 05401151001) and Liberase TM (75 µg/ml, Roche, REF: 05401127001) in Hank's Balanced Salt Solution (HBSS) buffer (Life Technologies, REF: 14175053). The cells were then collected to a 50 mL polypropylene falcon tube (Falcon©, Corning Inc., REF: 352070), excluding membranous tissues, and incubated with 15 mL of the liberase enzymatic solution for 30 min at 37°C. After, the cell suspension was homogenized and passed through a cell strainer (70 µm nylon filter from Corning Inc., REF: 352350) to obtain a single cell suspension. Cell viability was determined using Tripan blue solution (1:2) (Sigma, REF: T8154) and cells were ressuspended in Dulbecco´s Phosphate buffered saline (PBS) w/o Ca^{++}/Mg^{++} (BioConcept, REF: 3-05F29-I) at a concentration of $2x10^7$ live cells/mL. Finally 100 µL of this dispersed cell solution, containing $2x10^6$ MMTV-PyMT tumor-derived cells, were injected in the third mammary fat pad of 9-10 week old syngeneic FVB female mice.

3.2. mAbs and experimental design

All the therapeutic mAbs used in this study were provided by Roche, including the bispecific mouse anti-ANG-2/VEGFA IgG1 (A2V) administered at 10-20 mg/kg; mouse IgG1 (A2V control) at 20-40 mg/kg; rat anti-mouse CD40 agonistic IgG2a (FGK45) at 4 mg/kg; and rat IgG2a (FGK45 control) at 4 mg/kg. Each drug was injected in 200 µL of Dulbecco's PBS w/o Ca^{++}/Mg^{++} (BioConcept, REF:3-05F29-I), were the amount of Ab per injection was 0,25-0,5 mg for A2V; 0,5-1 mg for mouse IgG1; 100 µg for FGK45; and 100 µg for rat IgG2a.

Both the spontaneous and orthotopic MMTV-PyMT tumor models were employed, using the experimental design displayed in Figure 9. For the spontaneous MMTV-PyMT model (Figure 9 A), female MMTV-PyMT transgenic mice of 8-9 weeks old, correspondent to the adenoma stage in cancer development, were randomized in order to obtain

systematically similar groups with an identical age average. The treatments started immediately after the randomization, and included one control group with mice that received mouse IgG1 (20 mg/kg) (number of mice (n) = 8) and another group with mice treated with A2V (20 mg/kg) (n=6). Each mAb was administered by intraperitoneal (i.p.) injection, with a weekly schedule, and the mammary tumors were monitored biweekly. Transgenic MMTV-PyMT mice were euthanized when the tumor burden reached a critical size, according to protocols approved by the veterinary authorities.

For orthotopic MMTV-PyMT tumors (Figure 9 B), following the transplantation of MMTV-PyMT derived-tumor cells (see previous section), the mice and tumor growth were monitored every other day, and the tumor size was measured using precision calipers. The tumor volume (mm^3) was calculated as [(length/2) x (width/2) x height x π x 4/3]. Then, when the tumors reached an average of 200-300 mm^3, the mice were randomized in order to have a similar tumor volume average (200-300 mm^3), with identical number of mice, in each group, avoiding biased results. Immediately after the randomization the treatments started (day 0), delivering every mAb by i.p. injection, and the mice were sacrificed either 9 days after the first injection (day 9 - Short-term treatment) or when the tumor burden reached the average of 1000 mm^3 (day X - Long-term treatment).

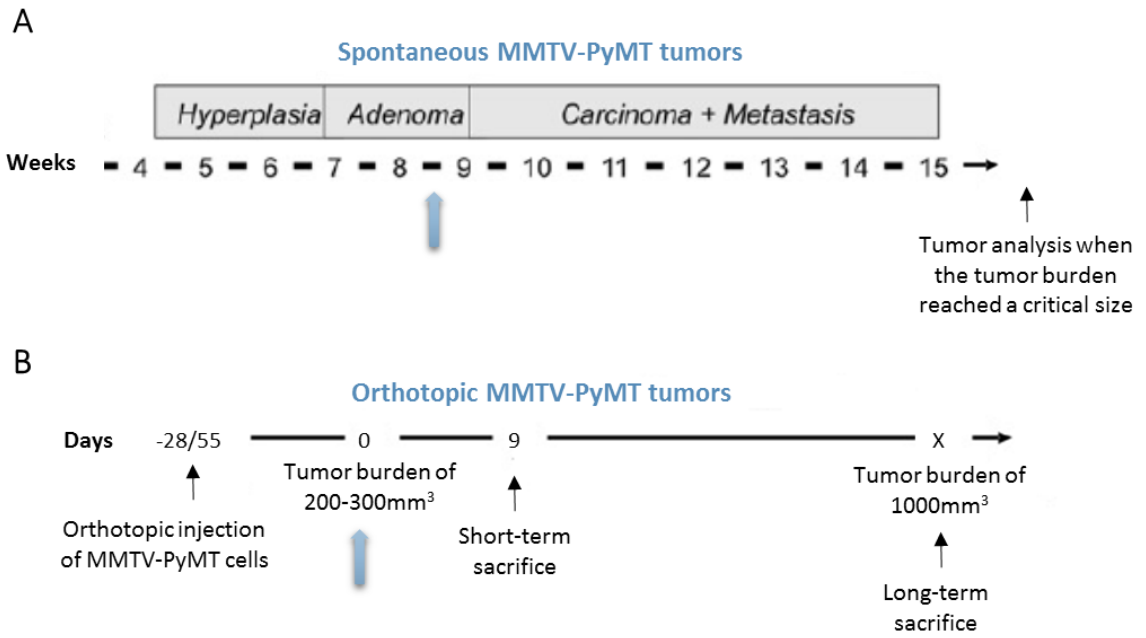

Figure 9. Schematics of the experimental design. *Treatment schedules for (A) spontaneous MMTV-PyMT tumors and for (B) orthotopic MMTV-PyMT tumors. Blue arrow indicates the start of the treatments.*

The treatments of orthotopic tumors included one control group that received mouse IgG1 and rat IgG2a (CTRL IgGs), one group treated with A2V (+ rat IgG2a), one group treated with FGK45 (+ mouse IgG1), and a group that received the combination of

the two therapeutic Abs (A2V + FGK45). Only one dose of FGK45 and its isotype control (rat IgG2a) were administered, during the first injection, while the remaining Ab were administered weekly. For the **short-term treatment**, the number of mice (n), as well as the concentration of the mAbs, were as following:

- **CTRL IgGs** (n=5): 20 mg/kg of mouse IgG1; 4 mg/kg of rat IgG2a
- **A2V + CTRL IgG** (n=4): 20 mg/kg of A2V; 4 mg/kg of rat IgG2a
- **FGK45 + CTRL IgG** (n=4): 4 mg/kg of FGK45; 20 mg/kg of mouse IgG1
- **A2V + FGK45** (n=4): 20 mg/kg of A2V; 4 mg/kg of FGK45

For the **long-treated tumors** the settings were those described below:

- **CTRL IgGs** (n=11): 40 mg/kg of mouse IgG1; 4 mg/kg of rat IgG2a
- **A2V + CTRL IgG** (n=10): 10 mg/kg of A2V; 4 mg/kg of rat IgG2a
- **FGK45 + CTRL IgG** (n=11): 4 mg/kg of FGK45; 40 mg/kg of mouse IgG1
- **A2V + FGK45** (n=10): 10 mg/kg of A2V; 4 mg/kg of FGK45

During necropsy, spontaneous and orthotopic tumors were harvested, using scissors and tweezers, and weighted using a precision balance. At this point the tumors were divided for posterior analysis, including histological analysis in stained tumor sections, flow cytometry analysis and gene expression analysis (not shown). In some cases, before euthanasia, the mice received intravenous (i.v.) injection of FITC-labeled lectin or i.p. injection of Pimonidazole (see perfusion and hypoxia studies).

3.3. Histology

For histology analysis the tumors were fixed for 4-6 hours in a 4% paraformaldehyde (PFA) solution, prepared by diluting a 32% PFA aqueous stock solution (Electron Microscopy Science, REF: 3291471) in Dulbecco's PBS w/o Ca^{++}/Mg^{++} (BioConcept, REF:3-05F29-I). Afterwards, the tumors were gradually transferred to sucrose (Sigma, REF: BCBN6225V) solutions (12-15-18-30%) in Dulbecco's PBS w/o Ca^{++}/Mg^{++} (BioConcept, REF:3-05F29-I). The samples were in each solution for approximately 24 hours at 4°C, allowing to remove the water from the tumors. Finally the samples were embedded in O.C.T. compound (Cryomatrix™ from Thermo Scientific, REF: 6769006) and snap-frozen by cold fumes generated by dry-ice in a close container. The tumors were then preserved and stored in -80°C. For all histology analysis the tumors were sectioned using a Leica Cryostat (CM1850 or CM1950), with a thickness of 8 µm. Sections were placed in Superfrost Plus microscope slides (Thermo Scientific, REF: J1800AMNZ) and stored at 4°C, protected from light, before being stained.

3.4. Necrosis analysis

To analyze the state of necrosis, Hematoxylin and Eosin staining (H&E) was performed in 8 µm frozen tumor sections (obtain as described above). To do so, the slides were hydrated with water and placed in Hematoxylin during 5 min for nuclear staining. This was followed by a wash and differentiation with 1% acid-alcohol for a few seconds. After washing in running water for 10 min, the slides were place in 0,25% Erythrosine (Eosin) solution during 1 min for cytoplasm staining. Finally, they were washed briefly in water, dehydrated and mounted using Eukitt (Sigma) mounting medium (Histology Core Facility, EPFL).

Whole tumor sections were then acquired with the motorized Olympus slide scanner VS120-L100, with a 20x objective in brightfield mode. This scanner uses OlyVIA software to visualize the images, which has a file format (.vsi) incompatible with FIJI software (202). Therefore, acquired images were opened using the BIOP VSI Reader tool in Fiji, a plugin developed by the Bioimaging Core Facility of EPFL that allows to open .vsi files and convert them in other file formats (203).

For this analysis necrotic tissue was assumed to be tissue where the Hematoxylin signal was absent, but where Eosin signal was present. Using the BIOP VSI reader the images were downscaled 16 times and converted in .tif format. In these pictures, displaying the entire tumor section, color deconvolution was applied, separating the Hematoxylin and Eosin channels, and the Huang threshold method was used to obtain binary masks for each channel. The eosin mask was cleaned using a closing operation (4 iterations, count=2) and was assumed to represent total tissue area. To detect the necrotic area, a binary XOR operation was applied between the two masks. To estimate the density of necrotic tissue, the number of neighbors of each pixel that are part of the necrotic area were calculated, by averaging the binary image with a kernel of radius 9 pixels. A threshold was applied to this "Necrosis Density Map" to keep only areas with >50% necrosis. Finally, the regions were filtered by size (>5000 pixels) and the total area remaining was measured, which was considered as the necrotic area. Artifacts such as connective tissues, with a positive signal for necrosis, were excluded using ROI sets. Besides, tumor holes left by intensive necrosis, not detected by this method, were also delimited manually, their area was measured and added to the necrotic area. The percentage of necrosis for every tumor section was calculated as (Necrotic area/Total Tissue area)*100.

3.5. Collagen analysis

To evaluate the tumor collagen^{+} area a Sirius Red staining, specific for collagen fibers, was done on 8 µm frozen sections. First the sections were hydrated and stained with Weigert's working Hematoxylin solution for 10 min. Then the slides were washed in

tap water for 10 min, and placed in the Sirius red solution during 60 min for collagen staining. After, the slides were washed in two changes of acidified water and dehydrated in three changes of 100% ethanol. Lastly they were cleaned with xylene and mounted using Eukitt (Sigma) mounting medium (Histology Core Facility, EPFL). The results in light microscopy are the collagen fibers stained in red and the cytoplasm stained in yellow.

Whole tumor sections were again acquired with the motorized Olympus slide scanner VS120-L100, with a 20x objective in brightfield mode. The images were then downscaled 8 times and converted in .tif format, using the BIOP VSI Reader. Afterwards, color deconvolution (FastRed FasBlue DAB) was used to separate the collagen fibers (red channel) from the cytoplasm (yellow-brown channel), on entire tumor sections. For both channels the ReniyEnropy threshold method was used to obtain binary masks, which were cleaned using the smooth operation (count =3), and the area limited to threshold was measured. The area measured in the red channel was assumed to be the Collagen^{+} area and the area measured in the yellow channel was assumed to be the Total tissue area. The percentage of the tumor Collagen^{+} area was calculated as (Collagen^{+} area/Total Tissue Area)*100.

3.6. Perfusion Studies

Perfusion studies were accomplished by *in vivo* labeling of perfused blood vessels with lectin from *Lycopersicon esculentum* (tomato). Lectin from tomato binds specifically to N-acetylglucosamine oligomers present on the luminal surface of the endothelium, therefore binding only to perfused and functional vessels (204). Before lectin injection, the mice were anaesthetized with 30 µL of Pentobarbital (150 mg/ml, from EPFL) intramuscular injection. When the mice were unresponsive, 100 µL of FITC-conjugated lectin from tomato (Sigma-Aldrich, REF: L0401-1MG, 2 mg/ml, diluted with Dulbecco's PBS w/o Ca^{++}/Mg^{++} (BioConcept, REF:3-05F29-I) to a final concentration of 1 mg/ml) was delivered into their bloodstream, by intraocular injection. After 10 min the mice were sacrificed by cervical dislocation, the tumors were excised and treated as describe in the Hystology section above. Direct visualization of FITC-conjugated lectin in tumor sections was possible, without secondary amplification, using a confocal microscope (see Immunofluorescence staining (IFS) and microscopy below).

3.7. Tumor hypoxia studies

In vivo labeling of tumor hypoxic regions was performed using Pimonidazole (PIMO), which at $pO_2 \leq 10$ mmHg forms covalent bonds with thiol proteins in hypoxic cells, forming intracellular clusters detectable through immunohistochemistry (205). Mice were

injected i.p. with 200 µL of PIMO HCl (10 mg/ml, from Hypoxyprobe, Inc., REF: HP-100mg) and euthanized after 30 min by cervical dislocation. Tumors were then dissected and treated as described in the histology section above. To visualize hypoxic areas, 8 µm tumor sections were stained with a monoclonal antibody conjugated to Dylight™549 (HP-Red549 from Hypoxyprobe, Inc., REF: HP7-x), that binds to PIMO clusters, and imaged using confocal microscopy (see IFS and microscopy below).

3.8. Immunofluorescence Staining (IFS) and Microscopy

For IFS, tumor sections (8 µm) were first hydrated and washed in PBS 1x solution for 10 min. This solution was prepared by dissolving PBS buffer 10x powder (Applichem, REF: 38210000) in ultrapure milli-Q water, obtaining a PBS 10x solution, which was then diluted to obtain 1x solution. Next, they were incubated with 0,3% Triton X-100 (Applichem, REF: 34021300) solution, prepared in Dulbecco's PBS w/o Ca^{++}/Mg^{++} (BioConcept, REF: 3-05F29-I), for 30 min at room temperature (RT). This step was followed by 3 times 10 min wash with PBS 1x solution. Following, the tumor sections were blocked for 60 min at RT with Blocking solution, which contained 10% Fetal Bovine Serum (FBS) (EuroClone, REF: ECS0180D), 3% Bovine Serum Albumin (BSA) (Sigma, REF: A7906) and 0,1% Triton X-100 (Applichem, REF: 34021300) in Dulbecco's PBS w/o Ca^{++}/Mg^{++} (BioConcept, REF: 3-05F29-I). After washing with PBS 1x solution 3 times for 10 min each, the sections were incubated with primary Abs diluted in blocking solution during 90 min in a dark and humid chamber at RT. Next, after 2 times 10 min wash with PBS 1x solution, the tumor sections were incubated with the secondary Abs diluted in blocking solution (if unconjugated primary Abs were used) for 60 min at 4°C. This step was followed by 2x10 min wash with PBS 1x and 10 min incubation with DAPI (1 mg/ml solution was diluted in Dulbecco's PBS w/o Ca^{++}/Mg^{++} (BioConcept, REF: 3-05F29-I) to a final concentration of 1 µg/ml, from Sigma, REF: D9542) for cell nuclei staining. Finally the sections were washed in PBS 1x solution for 5 min, mounted with DAKO™ fluorescence mounting medium (Agilent Technologies, REF: S3023) and covered with cover glass (Heathrow Scientific, REF: 10216). To avoid photobleaching the slides were preserved and stored at 4°C in the dark, before being imaged.

In every IFS, tumor sections were incubated with a purified rat anti-mouse FcγII/III receptor (CD32/16) monoclonal antibody (5 µg /ml, Mouse Fc Block™, BD Biosciences, REF: 553142) diluted in the blocking solution, to avoid high background staining.

All Abs used in IFS, as well as their concentrations, are listed below:

Marker	Fluorochrome conjugated	Host	Reactivity	Concentration used (µg/ml)	Supplier
CD31/PECAM-1 (Clone: MEC 13.3)	FITC	Rat	Mouse	10	BD Biosciences (553372)
α-SMA (Clone: 1A4)	Cy3™	Mouse	Mouse, rabbit, goat, Human, …	10-15	Sigma (C6198)
NG-2	Unconjugated	Rabbit	Mouse, Human and monkey	5	Millipore (AB5320)
Rabbit IgG F(ab')2	Alexa Fluor® 647	Goat	Rabbit	2-2,5	LifeTechnologies (A21246)
CD8a (Clone: 53-6.7)	Alexa Fluor® 647	Rat	Mouse	4	BD Biosciences (557682)
CD4 (Clone: RM4-5)	PE	Rat	Mouse	4	Biolegend (100512)
PIMO	Dylight™ 549	Mouse	All species	10	Hypoxyprobe, Inc. (HP7-x)

The majority of the Abs used were fluorochrome-conjugated, except for the primary rabbit anti-NG2 Ab, which was revealed by using the goat anti-rabbit Alexa Fluor-647 conjugated secondary antibody.

For imaging, the confocal microscope Zeiss LSM 700, with INVERT Zeiss AxioObserver Z1 stand was used. Both manual and motorized versions of this equipment were used, where the later was used to obtain tile scans. A 20x objective was used in all acquisitions, with a resulting 200x magnification of the tumor sections and a total sample image area of 409 600 μm^2. The software used in this microscope, the ZEN 2009, allowed sequential acquisition and pseudocoloration of fluorescent signals from individual fluorophores (single optical sections).

3.9. Quantification of confocal microscopy images

For all quantifications of images acquired with the confocal microscope, the FIJI open-source software was used. Multiple pictures (8-15) of each IF stained tumor section were randomly acquired and quantified. Following, the resulting values were averaged to obtain the mean values for each tumor/mouse.

a) Relative Vascular Area

To quantify the relative tumor vascular area, IFS with anti-CD31 Ab conjugated with FITC in tumor sections or in vivo FITC-conjugated lectin labeling was perform (as previously described). Acquired images were quantified as followed: manual threshold (B&W) for positive signal was applied in $CD31^+$ or $lectin^+$ single fluorescence channels to obtain binary masks. Next the area (in μm^2) limited to threshold was measured. The total imaged area was also measured to calculate the fraction area occupied by the $CD31^+$ or $lectin^+$ signal, which was defined by the $CD31^+$ or $lectin^+$ area divided by the total area. This values were then considered as the relative vascular area in each image.

b) Hypoxic Areas

Tumor hypoxic regions were quantified after *in vivo* injection of PIMO and *ex vivo* IFS with anti-PIMO Ab in tumor sections (previously described in 3.8). Manual threshold (B&W) for positive signal, in acquired pictures, was applied to the $PIMO^+$ single fluorescence channel. The area (in μm^2) limited to the threshold and the fraction area ($PIMO^+$ area/total imaged area) was calculated by the software, where the later was considered as the relative hypoxic area in each image.

c) Perivascular cell Coverage

The proportion of tumor blood vessels covered by perivascular cells was assessed by IFS in tumor sections with a triple staining using Abs against CD31, NG2 and αSMA (as previously described in 3.8). For every marker-positive signal a binary mask was created by applying a manual threshold (B&W). Next the area (in μm^2) limited to threshold as well as the faction area were measured in each image. Then, double positive $NG2^+CD31^+$ or αSMA^+CD31^+ and the triple positive $NG2^+\alpha SMA^+CD31^+$ fraction areas were calculated applying the binary AND operation (Image calculator) between the masks. This values, indicating marker-positive vascular area fraction, were considered representative of the degree of association between $NG2^+$, αSMA^+ or both cells and blood vessels, respectively. Finally the fraction (%) of blood vessels covered by $NG2^+$ and αSMA^+ cells or both ($NG2^+\alpha SMA^+$) was calculated by dividing double positive $NG2^+CD31^+$ or αSMA^+CD31^+ and the triple positive $NG2^+\alpha SMA^+CD31^+$ fraction areas by the $CD31^+$ fraction area, respectively.

d) Number of $CD8^+$ and $CD4^+$ cells

Anti-CD8 and anti-CD4 Abs were used to visualize $CD8^+$ and $CD4^+$ cells in IF stained tumor sections (previously described in 3.8). Single $CD8/4^+$ cells were counted in each picture, which corresponds to a microscopic field of 409 600 μm^2. Due to high background signal in the $CD8^+$ single fluorescence channel, the number of $CD8^+$ cells per microscope filed was obtained by manual counting using the Cell Counter plugin in FIJI (206). $CD4^+$ single fluorescence channel displayed low/inexistent background signal, allowing the use of the Analyze Particles FIJI tool to calculate the number of $CD4^+$ cells per microscope field. To do so, a manual threshold (B&W) was applied to the $CD4^+$ single fluorescence channel, since

automatic particle analysis requires a binary image. Then, overlapping cells were separated using the Watershed FIJI command. Finally, the Analyze Particles tool was used in these segmented binary images, with adjusted size and circularity to exclude non-specific objects (Size: 10-200 μm^2; circularity: 0,2-1,0), obtaining the number of $CD4^+$ cells.

3.10. Flow cytometry analysis

For flow cytometry analysis, half of each tumor harvested was processed to obtain a single cell suspension. For this purpose, following the excision during necropsy, the tumors were immediately placed in 15 mL falcon tubes (SPL Life Sciences, REF: 50015) at 4°C and chopped with scissors. Then, they were incubated (in a shaker) with 2-4 mL of liberase enzymatic solution (75 µg/ml Liberase TH (Roche, REF: 05401151001) and 75 µg/ml Liberase TM (Roche, REF: 05401127001) in HBSS buffer (Life Technologies, REF: 14175053)) for 30 min at 37°C. Next, the resulting cell suspension was filtered by passing it through two 70 µm nylon filters (Corning Inc., REF: 352350) and washed in cold Dulbecco's PBS w/o Ca^{++}/Mg^{++} (BioConcept, REF: 3-05F29-I), obtaining a single cell suspension. Afterwards, the cells were centrifuged at 1500 rpm, 4°C for 5 min, the supernatant discarded and the cells ressuspended in ~100 µl of the Dulbecco's PBS w/o Ca^{++}/Mg^{++} (BioConcept, REF: 3-05F29-I). Following a second centrifugation (1500 rpm, 4°C, 5 min) the supernatant was discarded and the cells were incubated in the dark during 30 min at 4°C with a viability staining solution (LIVE/DEAD® Fixable Dead Cell Stain Kit, with blue fluorescent reactive dye, from Life Technologies REF:L23105). This solution was prepare by adding 50 µl of Dimethyl sulfoxide (DMSO) to the vial of the reactive dye (both provided by the kit), and was used with a 1:1000 dilution. The samples were subsequently centrifuged (1500 rpm, 4°C, 5 min) and washed with Dulbecco's PBS w/o Ca^{++}/Mg^{++} (BioConcept, REF: 3-05F29-I). Following this step, the samples were incubated with a mix of Primary Abs, diluted in Dulbecco's PBS w/o Ca^{++}/Mg^{++} (BioConcept, REF: 3-05F29-I), for 15-30 min at 4°C, protected from the light. The Ab mix included Abs against the surface markers CD45 (0,7 µg/ml, APC-conjugated, from BD Biosciences, REF:559864), CD8a (0,5 µg/ml, Brilliant Violet™ 605-conjugated, from Biolegend, REF:100743) and CD4 (0,5 µg/ml, Brilliant Violet™ 785-conjugated, from Biolegend, REF:100551), as well as the rat anti-mouse FcγII/III receptor (CD32/16) antibody (5 µg/ml, Mouse Fc Block™, BD Biosciences, Cat: 553142). Finally the samples were centrifuged (1500 rpm, 4°C, 5 min) and washed 2 times with Dulbecco's PBS w/o Ca^{++}/Mg^{++} (BioConcept, REF: 3-05F29-I) to eliminate the excess of Ab.

Single cell suspensions were then analyzed using the BD Bioscience LSRII cytometer, a 5-laser and 18-detector analyzer. Antibody positive controls – a solution containing 0,5 µL of the Antibody linked to OneComp eBeads (eBioscience, REF: 01-1111) in 500 µL of Dulbecco's PBS w/o Ca^{++}/Mg^{++} (BioConcept, REF: 3-05F29-I) – and un-stained

(US) cell suspensions were used for compensation, with adjusted voltage to the beads or cell size. $CD8^+$ and $CD4^+$ cell subsets, gated on alive $CD45^+$ cells were analyzed. Negative controls - cell suspensions stained with Fluorescence Minus One (FMO) solution (Dulbecco's PBS w/o Ca^{++}/Mg^{++} (BioConcept, REF: 3-05F29-I) with mouse Fc Block and all antibodies except one) - were required to determine the proper position of each gate.

3.11. Statistical analysis

All statistical analysis and graphs presented were done using the GraphPad Prism 6© software. In all cases values were expressed as mean ± Standard error (SEM). Statistical analysis were performed using two-tailed unpaired Student's t test or ordinary one-way ANOVA with Tukey's multiple comparisons test, as indicated in each figure, with 95% confidence intervals. Differences were considered statistically significant when p values were inferior to 0,05 (*, $p < 0.05$; **, $0.001<p< 0.01$; ***, $p < 0.001$).

4. Results

4.1. Simultaneous blockade of ANG-2 and VEGF-A inhibits tumor growth and increases the survival in mammary tumor models

The therapeutic efficacy of double ANG-2/VEGF-A blockade was first evaluated in the MMTV-PyMT mouse model of breast cancer, one of the most aggressive pre-clinical models of mammary carcinoma, and poorly responsive to the current treatments. In parallel, the orthotopic MMTV-PyMT model, obtained by transplanting MMTV-PyMT tumor cells into the mammary gland of syngeneic wild type mice – FVB mice, was also employed.

In order to study the anti-tumor effects of blocking ANG-2 and VEGF-A, a bispecific mouse mAb that neutralizes both ANG-2 and VEGF-A, termed A2V, was administered (116). As isotype control the MOPC21 antibody, a mouse IgG1 mAb with irrelevant specificity, was used and termed CTRL IgG.

Established orthotopic tumors (tumor volume of 200-300 mm^3) were weekly treated with i.p. injections of either A2V or CTRL IgG. Mice were sacrificed either 9 days after the first injection (short-term treatment) (Figure 10 A), or when the tumor burden reached the average size of 1000 mm^3 (long-term treatment) (Figure 10 B). Female spontaneous MMTV-PyMT transgenic mice of 8-9 weeks of age (in adenoma stage) were also treated weekly with i.p. injections of either A2V or CTRL IgG, and euthanized when the tumor burden reached a critical size (in late carcinoma stage), according to protocols approved by the veterinary authorities ('survival' study) (Figure 10 C). Tumor analysis was performed at the endpoint.

A2V treatment led to a powerful inhibition of tumor growth in the orthotopic model (Figure 10 A and B). The mean tumor volume in orthotopic MMTV-PyMT mice, treated with A2V (Figure 10 A, left panel), showed a 70% tumor growth inhibition, when compared to mice treated with the CTRL IgG, during the short-term treatment. Respectively, the *ex vivo* tumor weight of A2V treated mice was reduce by ~50% (Figure 10 A, right panel). Fifty percent of tumor growth inhibition was also observed during the long-term treatment with A2V at day 42 (Figure 10 B), extending the survival by 2 weeks, comparing to control treated tumors.

Furthermore, A2V treatment also increased the survival in spontaneous MMTV-PyMT mice (Figure 10 C). According to the median survival, mice treated with A2V survived 40 days longer, when compared to mice treated with control IgG (105 days vs. 145 days), with some mice living up to 154 days (all mice in the control group died by 115 days).

Collectively, the aforementioned data indicate that A2V treatment effectively impairs the progression of established orthotopic MMTV-PyMT tumors, both during the short- and long treatment schedule, and extends the survival also in the more clinically relevant and aggressive spontaneous MMTV-PyMT model.

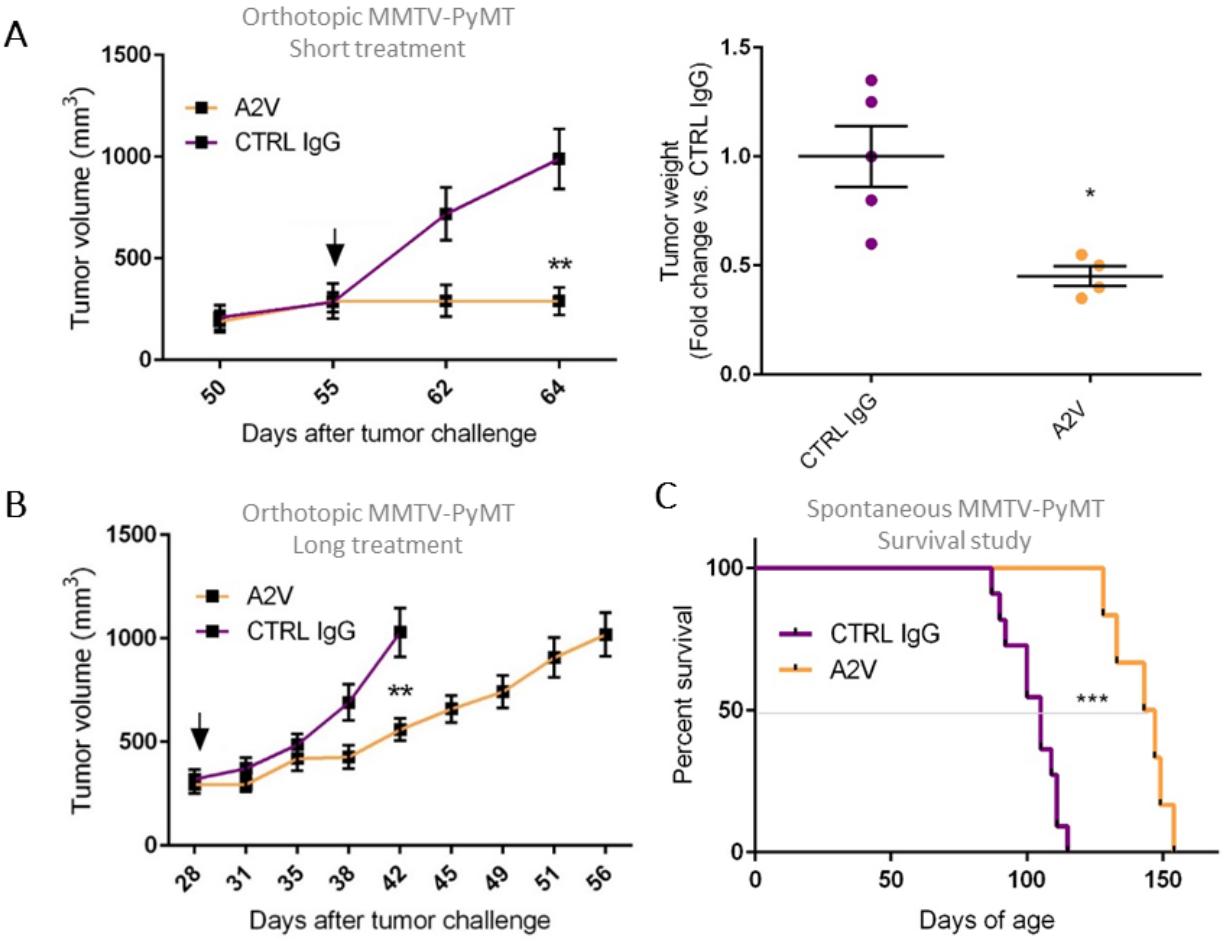

Figure 10. Dual ANG-2 and VEGF-A blockade inhibits tumor growth in both orthotopic and spontaneous MMTV-PyMT tumor models. (A) *Volume and weight of orthotopic MMTV-PyMT tumors with short-term treatment; left panels illustrate the tumor growth (mean tumor volume ± SEM) following the treatment with A2V or the CTRL IgG, arrow indicates the start of the treatments; right panels show the ex vivo tumor weight expressed as fold change vs. CTRL IgG (mean values ± SEM), where each dot represents one tumor, derived from one mouse. (B) Tumor growth (mean tumor volume ± SEM) of orthotopic MMTV-PyMT tumors with long-term treatment; arrow indicates the start of the treatments. Statistical analysis by unpaired Student's t test with 95% confidence interval. (C) Survival curve of spontaneous MMTV-PyMT mice, showing a median survival of 105 days for mice treated with the CTRL IgG and 145 days for mice treated with A2V. Statistical analysis by Log Rank (Mantel-Cox) test (* = p value < 0.05; *** = p value < 0.001).*

4.2. Dual blockade of ANG-2 and VEGF-A leads to increased necrosis in orthotopic MMTV-PyMT mammary tumors, during early stages of tumor development

The state of necrosis of MMTV-PyMT mammary tumors treated with A2V was assessed by performing Hematoxylin and Eosin staining (H&E) on tumor sections and measuring the percentage of the necrotic area (see materials and methods). Because spontaneous MMTV-PyMT mice at the endpoint have multiple aggressive tumors, with different stages of tumor progression – there is variability among the different individual tumors in each mouse – necrosis evaluation of these tumors may not reflect the real conditions. Conversely, progression of orthotopic tumors is synchronized, allowing to better evaluate the tumor response to therapy. Therefore, the state of necrosis was evaluated in orthotopic MMTV-PyMT tumors.

Following this analysis, a significant increase of the necrotic area in orthotopic MMTV-PyMT tumors could be observed after a short-term treatment with A2V, comparing with the control (Figure 11 A, left panel). Of note, A2V treated tumors were more necrotic even though they were smaller than the CTRL IgG treated tumors (see Figure 10 A). However, this difference was not observed in long treated tumors (Figure 11 A, right panel), where both treatments lead to the same extent of tumor necrosis (~50% of tumor necrotic area).

The ECM plays a key role in breast development and it is known to be involved in breast cancer progression: increased deposition of ECM, especially collagen fibers, leads to the formation of a fibrotic-like stroma that supports tumor progression and correlates with poor prognosis in breast cancer patients (207, 208). Therefore, the tumor collagen^{+} area was evaluated by performing a Sirius red staining (see materials and methods). For the same reasons mentioned above the orthotopic tumor model was used for this assessment.

Although no significant differences were found between tumors treated with A2V and tumors treated with the CTRL IgG, a trend for increased Collagen^{+} area was found in orthotopic MMTV-PyMT tumor after A2V treatment in both treatment schedules (Figure 11 B, left and right panels).

Generally, A2V treatment increases necrosis of MMTV-PyMT tumors during the early stages of tumor progression, an effect that seems to be partially lost at the later stages of tumorigenesis. A trend of increased collagen deposition was also found after A2V treatment, likely due to inflammation/tissue repair processes due to increased necrosis/tumor cell death.

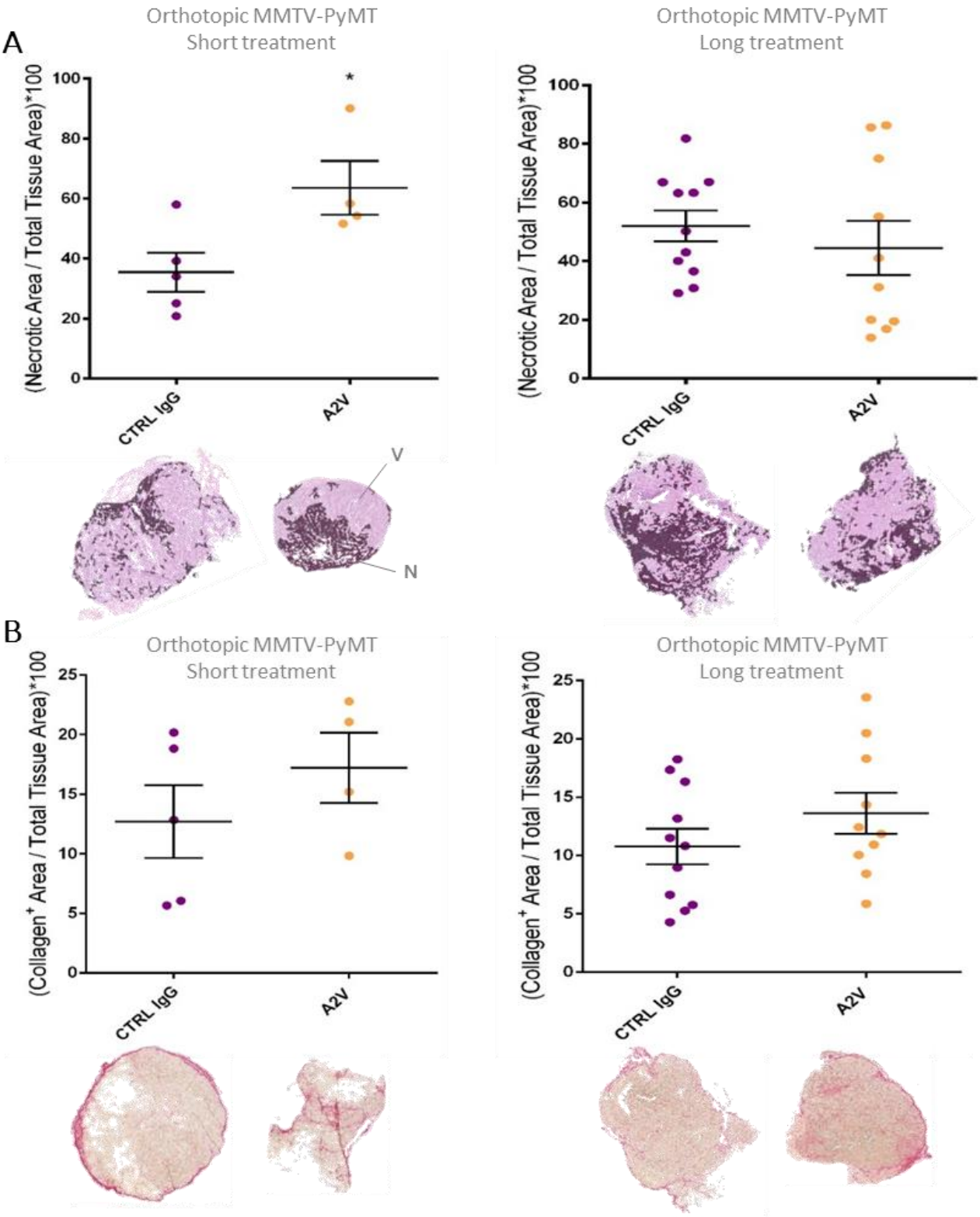

Figure 11. A2V leads to increased tumor necrosis during the early stages of orthotopic MMTV-PyMT tumor development, with a trend toward increased collage deposition. *(A) Percentage of the necrotic area in orthotopic MMTV-PyMT tumors upon short-term treatment (left panel) and long-term treatment (right panel) with either A2V or CTRL IgG; top panels show quantitative analysis of the necrotic areas (mean values ± SEM), bottom panels show representative*

pictures of the whole tumor sections, with necrotic areas highlighted in black (V=Viable area; N=Necrotic area). (B) Collagen positive area in orthotopic MMTV-PyMT tumors upon short-term treatment (left panel) and long-term treatment schedules (right panel); top panels represent quantitative analysis of collagen positive areas (mean values ± SEM), bottom panels show representative pictures of the whole tumor sections, with collagen fibers highlighted in pink-red. In all the graphs each dot represents one tumor, derived from one mouse. Statistical analysis by unpaired Student's t test with 95% confidence interval (= p value < 0.05).*

4.3. A2V treatment leads to tumor vasculature regression and angiogenesis inhibition in MMTV-PyMT mammary carcinomas

The antiangiogenic effect of ANG-2/VEGF-A blockade was then assessed in spontaneous and orthotopic MMTV-PyMT carcinomas. To do so, tumor blood vessels were analyzed on tumor sections stained with anti-CD31/PECAM Ab, to visualize the whole tumor vascular network, and/or after *in vivo* FITC-lectin perfusion to identify functional and perfused tumor blood vessels. Analysis of confocal microscope images revealed qualitative differences of the blood vessels between the 2 groups (Figure 12 A). While tumors treated with the CTRL IgG displayed a more dense and heterogeneous vascular network, A2V-treated tumors showed intermittent and short blood vessels with a smaller diameter and poorly branched. Remarkably, dual ANG-2/VEGF-A blockade produced ample avascular areas, especially localized in the inner part of the tumor (Figure 12 B), suggesting that both inhibition of angiogenesis and vascular regression had occurred. In these tumors, blood vessels were mainly localized at the tumor periphery (Figure 12 B), suggesting that they may exploit the preexisting mature blood vessels of the host organ (that are less sensitive to antiangiogenic treatments) to receive supplies and support their progression, a mechanism termed vessel co-option.

Furthermore, the relative tumor vascular area was measured on these immunofluorescence stained tumor sections, where a drastic reduction of the tumor vascular area could be observed in both models and schedules after the dual ANG-2/VEGF-A blockade (Figure 12 C, D and E). A consistent reduction in blood vessel density of ~50% could be found in every tumor analyzed, both in terms of lectin$^+$ area (Figure 12 C) and CD31$^+$ area (Figure 12 D and E).

Taken together, these data suggest that A2V is able to impair angiogenesis and leads to vascular regression, showing therefore a potent anti-angiogenic effect in these models of breast cancer.

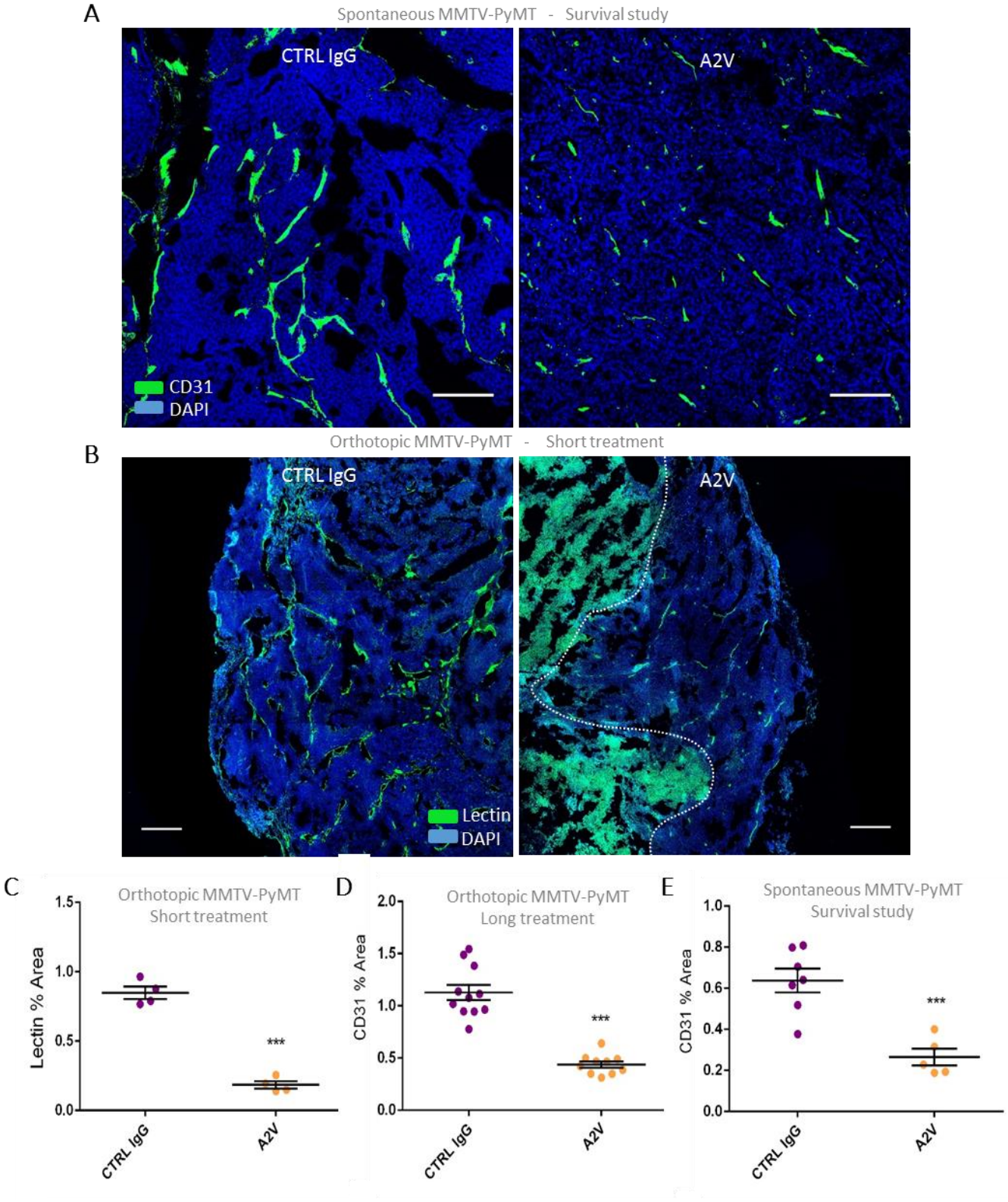

Figure 12. Co-targeting ANG-2 and VEGF-A remarkably decreases tumor vasculature and inhibits angiogenesis in the MMTV-PyMT tumor models. *(A) Representative pictures of the treated tumors, with CD31 (green) and DAPI (blue) immunofluorescence staining in spontaneous MMTV-PyMT tumor sections, analyzed immediately after discontinuation of therapy. The confocal*

*microscope magnification is 200x; scale bar, 100 µm. (B) Representative pictures with lectin (green) and DAPI (blue) showing avascular areas and the peripheral localization of tumor blood vessels (delimitated by the doted white line) in orthotopic tumors treated with A2V; tumors treated with CTRL IgG do not display this characteristic; the pictures are the result of tile scans (3x3) with a confocal microscope magnification of 200x; scale bar, 200 µm. Relative vascular area in orthotopic tumors, during short- (C) and long-term treatment (D), and in spontaneous tumors (E), is represented by the relative lectin⁺ area (C) or the relative CD31⁺ area (D and E). In every graph (mean values ± SEM) each dot corresponds to one tumor/mouse and displays the average of the analysis of 8-15 pictures per tumor. Statistical analysis by unpaired Student's t test with 95% confidence interval (*** = p value < 0.001).*

4.4. Consistent with angiogenesis inhibition, ANG-2/ VEGF-A blockade leads to increased tumor hypoxia

Antiangiogenic treatment and consequent vessel regression is known to increase tumor hypoxia (29), therefore tumor hypoxic areas were quantified using an anti-pimonidazole (PIMO) staining (see Material and Methods). In this analysis, fewer and smaller hypoxic areas were detected in CTRL IgG treated tumors when compared to the A2V treated tumors (Figure 13 A), associated with their high or poor vascularization status, respectively. Quantitative analyses of the relative PIMO⁺ area (Figure 13 B) corroborated these observations, with a significant increase in tumor hypoxic areas following the treatment with A2V.

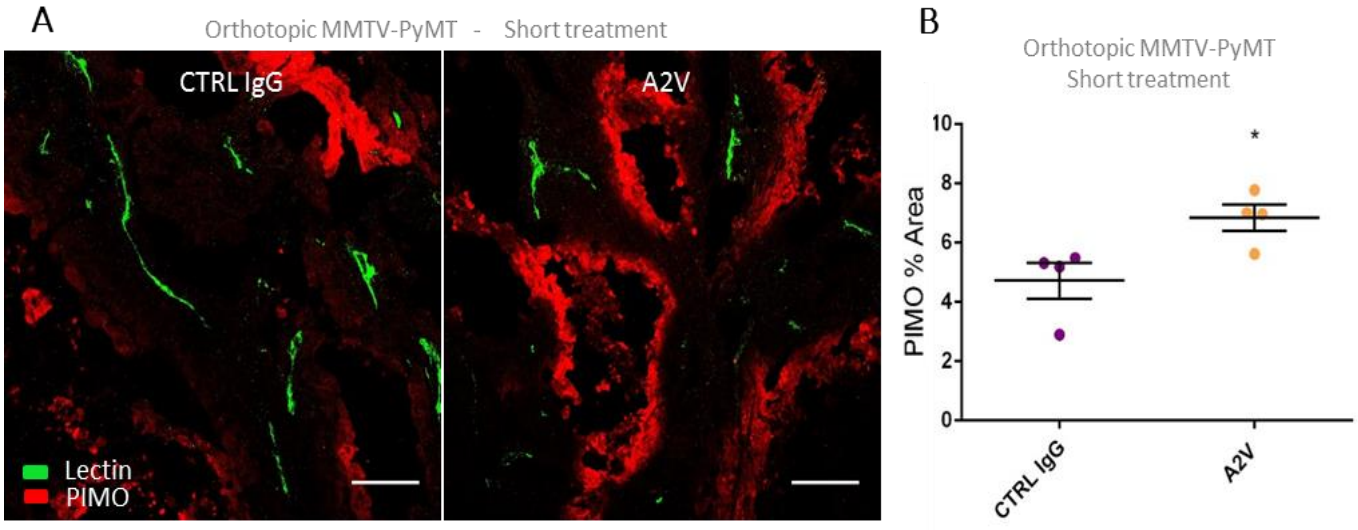

Figure 13. ANG-2/VEGF-A blockade increases tumor hypoxia in orthotopic MMTV-PyMT tumors. *(A) Representative pictures of lectin (green) and PIMO (red) immunofluorescence staining in orthotopic MMTV-PyMT tumor sections upon short-term treatment, analyzed immediately after discontinuation of therapy. The confocal microscope magnification is 200x; scale bar, 100 µm. (B)*

Quantitative analysis of relative PIMO⁺ area (mean values ± SEM) in orthotopic tumors. Each dot corresponds to one tumor/mouse and displays the average of the analysis of 8-15 pictures per tumor. Statistical analysis by unpaired Student's t test with 95% confidence interval (= p value < 0.05).*

4.5. ANG-2/VEGF-A blockade increases perivascular coverage of the remaining tumor blood vessels

It known that ANG-2 antagonism of ANG-1-mediated TIE-2 signaling causes detachment or loss of perivascular cells, such as pericytes, and consequent vessel destabilization (108). Therefore, the effect of A2V treatment on pericyte coverage of tumor blood vessels was also investigated is this study. For this purpose an immunofluorescence staining on spontaneous MMTV-PyMT tumor sections was performed, using an anti-NG2 (Neural-Glial 2) antibody, as a marker for pericytes; an anti-αSMA (Smooth Muscle Actin) antibody, a marker expressed by smooth muscle cells, but also expressed in a subset of mature pericytes; and the anti-CD31 antibody to stain ECs.

The confocal microscopy pictures reveled decreased presence of both NG2⁺ and αSMA⁺ cells in the control tumors, when compared to the tumors treated with A2V (Figure 14 A). Detail analyses of these pictures showed an increased NG2⁺ and αSMA⁺ cell coverage of blood vessels in tumors that received the A2V crossMab (Figure 14 B), while the majority of the blood vessels in the CTRL IgG treated tumors were poorly associated with these cells.

Quantitative analysis, showing the proportion of blood vessels covered by αSMA⁺ cells (Figure 14 C, left panel), NG2⁺ cells (Figure 14 C, middle panel) or double positive αSMA⁺NG2⁺ cells (Figure 14 C, right panel), confirmed the data above mentioned: the remaining tumor blood vessels after A2V treatment were significantly more coated with αSMA⁺ and NG2⁺ cells, when comparing to the tumor blood vessels of the control treated tumors.

Collectively, the aforementioned data indicate that A2V-mediated ANG-2/VEGF-A blockade increases mural cell coverage of tumor blood vessels, favoring vascular stability. In previous experiments (not reported), a similar phenomenon was observed using LC06 (a mAb that neutralizes only ANG-2, and not VEGF-A), suggesting that A2V increases perivascular coverage of tumor vasculature by enhancing the ANG-1/TIE-2 signaling, due to ANG-2 blockade, rather than the VEGF-A neutralization.

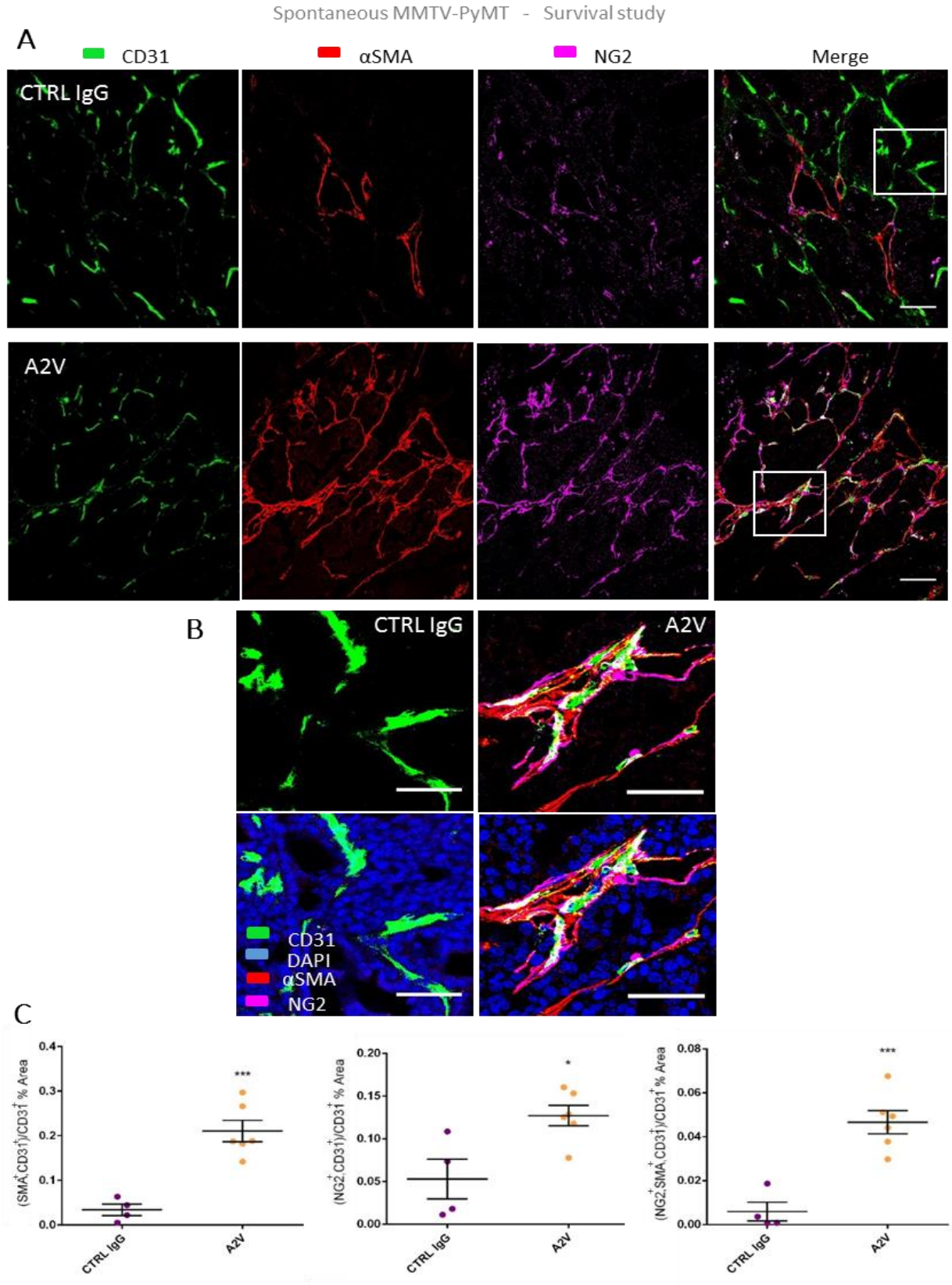

Figure 14. ANG-2/VEGF-A blockade increases the association between mural cells and ECs in the spontaneous MMTV-PyMT model. *(A) Representative pictures of the CTRL IgG and A2V treated tumors, with CD31 (green), αSMA (red) and NG2 (magenta) immunofluorescence staining in spontaneous MMTV-PyMT tumor sections, analyzed immediately after discontinuation of therapy.*

The confocal microscope magnification is 200x; scale bar, 100µm. (B) Enlargement of the insets in the pictures above, with additional nuclear staining (DAPI, blue) in the bottom panel. Scale bar, 50µm. (C) Quantitative analysis of the proportion of tumor blood vessels covered by perivascular cells (mean values ± SEM); left panel: the proportion of blood vessels covered by αSMA$^+$ cells is represented by the ratio between the CD31$^+$αSMA$^+$ area (degree of association between αSMA$^+$ cells and blood vessels) and the overall CD31$^+$ area; middle panel: proportion of blood vessels covered by NG2$^+$ cells represented by the ratio between the CD31$^+$NG2$^+$ area and the overall CD31$^+$ area; right panel: proportion of blood vessels covered by double positive αSMA$^+$NG2$^+$ cells represented by the ratio between the CD31$^+$αSMA$^+$NG2$^+$ area and the overall CD31$^+$ area. Each dot corresponds to one tumor/mouse and displays the average of the analysis of 8-10 pictures per tumor. Statistical analysis by unpaired Student's t test with 95% confidence interval (= p value < 0.05; *** = p value < 0.001).*

4.6. Combining A2V with agonistic anti-CD40 mAb further inhibits tumor growth in orthotopic MMTV-PyMT mammary mouse model, showing a synergistic anti-tumor effect

Because the tumor vasculature is known to directly suppress adaptive immune responses, the elimination of tumor blood vessels, through the use of antiangiogenic therapies, could, in theory, boost the efficacy of immunotherapeutic strategies (188). To test the veracity of this hypothesis, the A2V crossMab was combined with an anti-mouse CD40 agonistic mAb (clone FGK45, rat IgG2a).

The orthotopic MMTV-PyMT mouse model, obtained as previously described, was employed for this study, where the treatments started when the tumors were well established (about 300 mm^3). Orthotopic tumor-bearing mice received injections of A2V, FGK45, the combination of the two (A2V + FGK45) or the appropriate control [mouse IgG1 (MOPC21) + rat. IgG2A, termed CTRL IgGs], according to either a short- or long-treatment schedule, already described above. In order to balance the total amount of mouse and rat immunoglobulins injected in each mouse, among the different groups, FGK45 and A2V were administered with mouse IgG1 (FGK45 + MOPC21) and rat IgG2A (A2V + rat IgG2A), respectively. This setting allows to consider and rule out possible unspecific antibody-mediated effects, such as antibody-dependent cell-mediated cytotoxicity (ADCC) triggered by the binding of Fc receptors (FcR) to the Fc portion of our antibodies. Only one dose of the FGK45 mAb and its own control, rat IgG2A, was administered, in the beginning of the treatments, while the remaining Abs were injected (i.p.) weekly.

The mean growth of these orthotopic MMTV-PyMT tumors was then analyzed, where a similar effect in tumors treated with FGK45, as a monotherapy, and the control treated tumors could be perceived. This effect, observed both in short and long term treatment schedules (Figure 15 A and B, left panels), suggested that the FKG45-based

immunotherapy alone has no significant anti-tumor effect in this model. However, following the combination of FGK45 with A2V, a potent anti-tumor effect was observed.

In the short-term setting, no additive antitumor effect in combining A2V with FGK45 was detected. Indeed the volume of A2V + FGK45-treated tumors was reduced, compared to the control groups, at the same extent as the A2V monotherapy-treated tumors (Figure 15 A, left panel). In agreement with the mean tumor growth, *ex vivo* tumor weight was significantly reduced by 50% in tumors treated with A2V alone or the combination therapy, comparing to the FGK45 or control treated tumors (Figure 15 A, right panel).

In tumors treated with a long-term schedule, a comparable tumor inhibition effect between the A2V monotherapy and the combination therapy was observed during the initial phase of tumor progression (Figure 15 B, left panel), reproducing the data obtained in the short-term schedule. However, in the late stage of tumor progression, a more pronounced tumor inhibition in the combination therapy treated mice could be observed, compared to the A2V treated mice. Importantly, A2V + FGK45 treatment remarkably prolonged the survival by 31 days when compared to the CTRL IgGs group, showing a strong therapeutic potential of combining CD40 agonists and tumor vascular disruption. As expected, no significant difference in *ex vivo* tumor weight was found (Figure 15 B, right panel), since the mice were sacrificed when the tumors reached the same volume (about 1000 mm^3). Next, the individual growth curves of tumors treated during a long term schedule were assessed (Figure 15 C). It could be observed that in both FGK45 and CTRL IgGs treated groups the tumor progression was aggressive, reaching the tumor volume average of 1000 mm^3 in just 14 days after the beginning of the treatments (Figure 15 C, top panels). Tumors treated with A2V monotherapy reached the same volume average only 28 days after the start of the treatment (Figure 15 C, left bottom panel), demonstrating that A2V alone was able to delay tumor progression (A2V doubled the survival of the mice, compared to FGK45 and CTRL IgGs). Moreover, A2V + FGK45 led to additional tumor progression delay, compared to the A2V monotherapy, since the tumor volume average of 1000mm^3 was only reached 51 days after the beginning of the treatment. More importantly, the combination therapy was capable to achieve three cases of stable disease (Figure 15 C, right bottom panel, grey rectangle), where the tumors kept nearly the same volume throughout the treatments.

Taken together, these data suggest a strong anti-tumor effect mediated by the combination therapy with A2V and FGK45, suggesting a synergistic effect between A2V and the agonistic CD40 mAb FGK45.

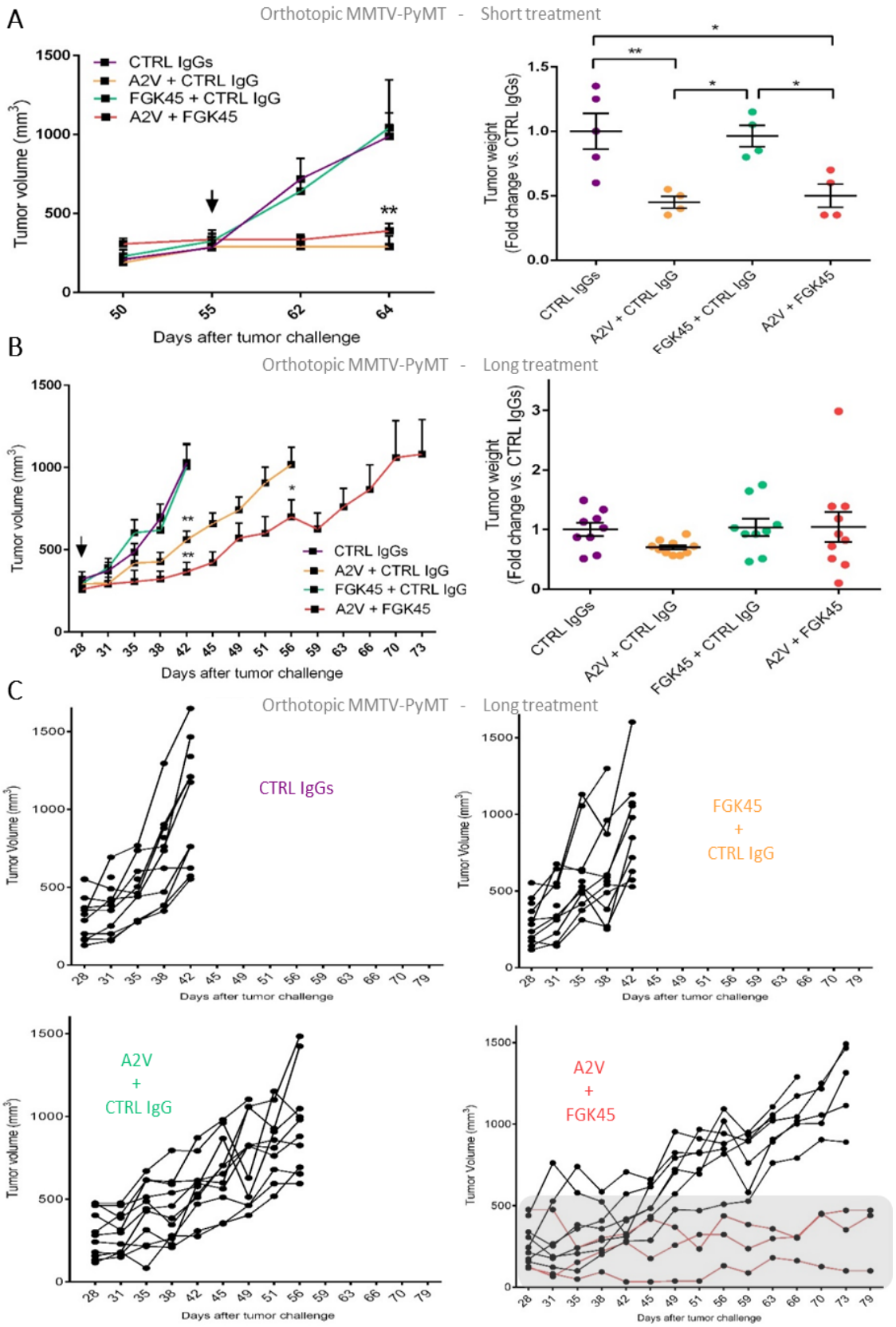

Figure 15. Combining A2V with agonistic anti-CD40 mAb further inhibits tumor growth in the orthotopic MMTV-PyMT mouse model. *Growth and weight of orthotopic MMTV-PyMT tumors*

after short term treatment (A) or long term treatment (B): left panels illustrate the tumor growth (mean tumor volume ± SEM) where the arrow indicates start of the treatments; right panels show the ex vivo tumor weight expressed as fold change vs. CTRL IgGs (mean values ± SEM), where each dot represents one tumor, derived from one mouse. Statistical analysis by ordinary one-way ANOVA with Tukey's multiple comparisons test (= p < 0.05; ** = 0.001<p< 0.01); (C) individual tumor growth curves, following a long term treatment schedule with control IgGs (top left panel), FGK45 monotherapy (top right panel), A2V monotherapy (bottom left panel) or the combination therapy (bottom right panel) with cases of stable disease highlighted inside the grey rectangle.*

4.7. The combination therapy with A2V and FGK45 increases necrosis of orthotopic MMTV-PyMT tumors in the early stages of tumor progression, and enhances tumor fibrosis

The state of tumor necrosis was subsequently evaluated as previously described, after the short-term treatment with FGK45 or the combination therapy. While FGK45 alone did not augment tumor necrosis, compared to the control group (Figure 16 A left panel, and 16 B), in combination with A2V led to a remarkable increase of the tumor necrotic area, compared to the monotherapies and the control group (Figure 16 A left panel, and 16B). These tumors, almost completely necrotic (~90% of necrosis), were significantly more necrotic than the FGK45 or the control treated tumors, even though they were half of their size (see Figure 15 A). Furthermore, the combination therapy was able to further increase the tumor necrosis, when compared to the A2V monotherapy (~65% necrosis). These statistical differences could not be observed in the long-term treated tumors, where all treatments displayed a similar percentage of necrosis. However a trend for increased tumor necrosis still remained after the combination therapy (Figure 16 A, right panel).

Administration of agonistic CD40 mAb in pre-clinical studies was shown to shift the phenotype of TAMs from pro- to anti-fibrotic, facilitating the depletion of collagen, which leads to tumor regression (209). However, after analyzing the collagen$^+$ area of these orthotopic MMTV-PyMT tumors (as previously described), an opposite effect could be observed. While the collagen$^+$ area of FGK45-treated tumors was similar to those treated with the CTRL IgGs and the A2V monotherapy, tumors treated with both A2V and FGK45 displayed a significant increase of the collagen$^+$ area, suggesting an enhancement of fibrosis, during the short-term treatment (Figure 16 C, left panel, and 16 D). Furthermore, a trend for increased fibrosis following the combination therapy could also be observed during the long-term treatment (Figure 16 C, right panel).

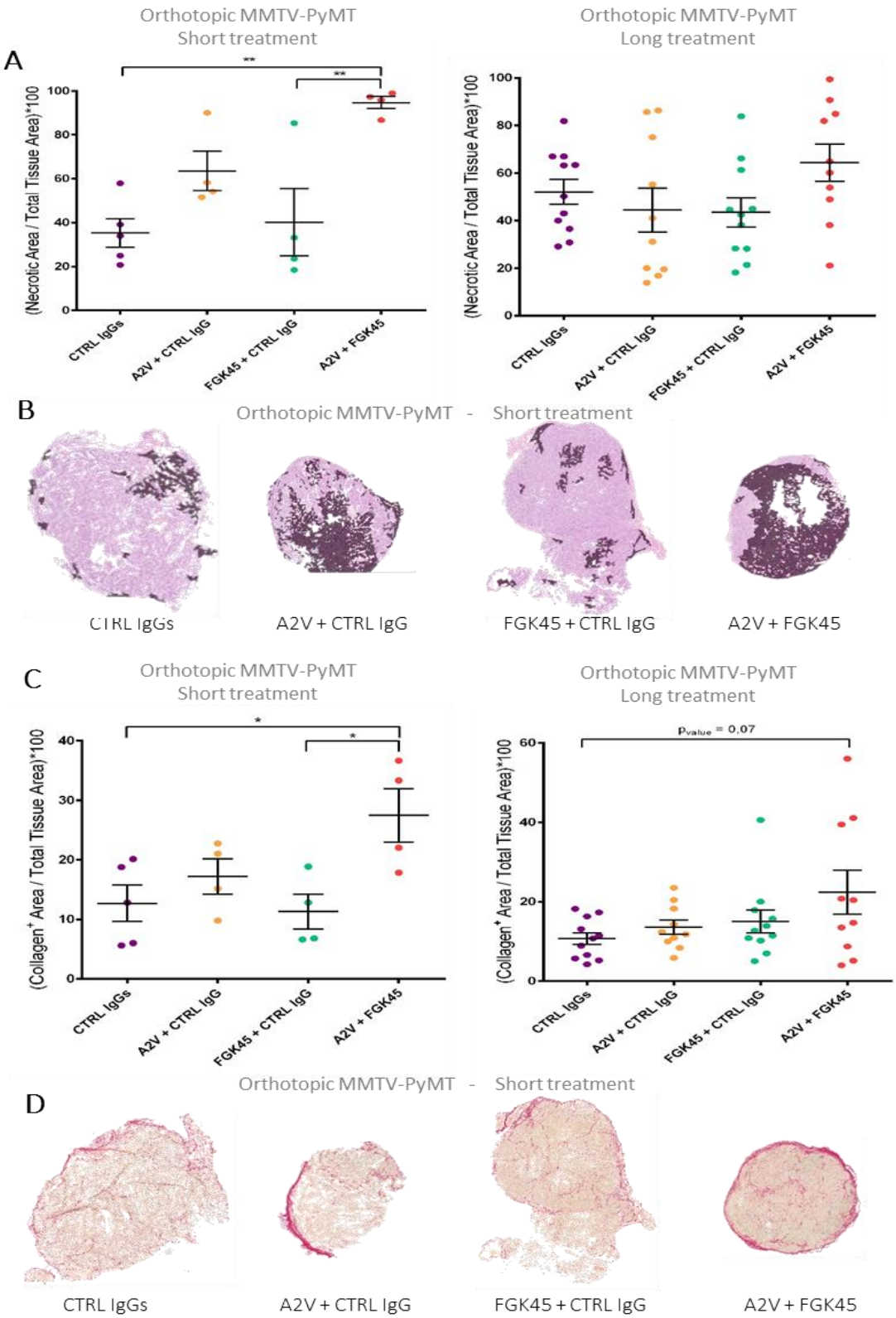

Figure 16. Combining A2V with FGK45 further increases tumor necrosis in the orthotopic MMTV-PyMT model, and enhances fibrosis. *(A) quantitative analysis of the necrotic percentage*

area (mean values ± SEM) in orthotopic MMTV-PyMT tumors with short-term treatment (left panel) and long-term treatment schedules (right panel); (B) representative pictures of the whole tumor sections, with necrotic areas highlighted in black; (C) quantitative analysis of collagen$^+$ percentage area (mean values ± SEM) in orthotopic MMTV-PyMT tumors with short-term treatment (left panel) and long-term treatment schedules (right panel); (D) representative pictures of the whole tumor sections, with collagen fibers highlighted in pink-red. In all the graphs each dot represents one tumor, derived from one mouse. Statistical analysis by ordinary one-way ANOVA with Tukey's multiple comparisons test (= $p < 0.05$; * = $0.001<p< 0.01$).*

Taken together, these findings indicate that FGK45 with A2V-mediated antiangiogenic therapy leads to a potent anti-tumor effect that results in intensive tumor necrosis. This effect was stronger in the combination therapy than in either of the therapies alone, suggesting that these therapeutic mAbs act cooperatively to induce this response. It is possible that tumor cell death accomplished by A2V (by blocking oxygen and nutrient supply to tumor cells) enhances the effect of the FGK45 mAb: increased tumor antigens, released from dying tumor cells, can be presented by FGK45-activated APCs to cytotoxic T cells, leading to adaptive anti-tumor immune responses, further increasing tumor cell death. In this study, different from what has been reported in literature, the combination therapy induced an increase of fibrosis in orthotopic MMTV-PyMT tumors, an effect likely due to tissue repair processes, following the powerful necrotic-inducing effect of this treatment.

4.8. FGK45 does not impair the anti-angiogenic effect of A2V in the orthotopic MMTV-PyMT mouse model

It has been reported that the binding of CD40L to CD40 expressed on ECs activates the PI3K pathway, leading to the expression of angiogenic factors, such as VEGF-A, promoting angiogenesis (210-212). This led to the evaluation of angiogenesis, as previously decribed, in orthotopic MMTV-PyMT tumors treated with FGK45, either as a monotherapy or in combination with A2V. Following this analysis, a similar blood vessel morphology could be observed in tumors treated with FGK45 and those treated with the CTRL IgGs (Figure 17 A), which display a heterogeneous and dense vascular network. Quantitative analysis, with both relative lectin$^+$ and CD31$^+$ area (Figure 17 B and C, respectively), demonstrated comparable relative blood vessel area between the two groups, showing that FGK45 treatment did not influence tumor angiogenesis.

Moreover, dual A2V + FGK45 therapy led to the same extent of angiogenesis inhibition as the A2V monotherapy (~50% ihnibition) in both short- and long-term

treatment (Figure 17 B and C). Besides, an intermittent and short morphology of the tumor blood vessels after the dual treatment was also detected, similarly to previously observed data in A2V treated tumors (Figure 17 A).

In agreement with these results, an increase of the relative PIMO$^+$ area (Figure 17 D), and therefore tumor hypoxic areas (Figure 17 A), was also found after the treatment with A2V + FGK45, compared to the FGK45 monotherapy or the control treated tumors. Again this effect was similar to previously observations with A2V monotherapy.

All together, these informations demonstrate that, opposite to data previously reported, FGK45 does not increase angiogenesis and does not impair the anti-angiogenic effect of the A2V crossMab.

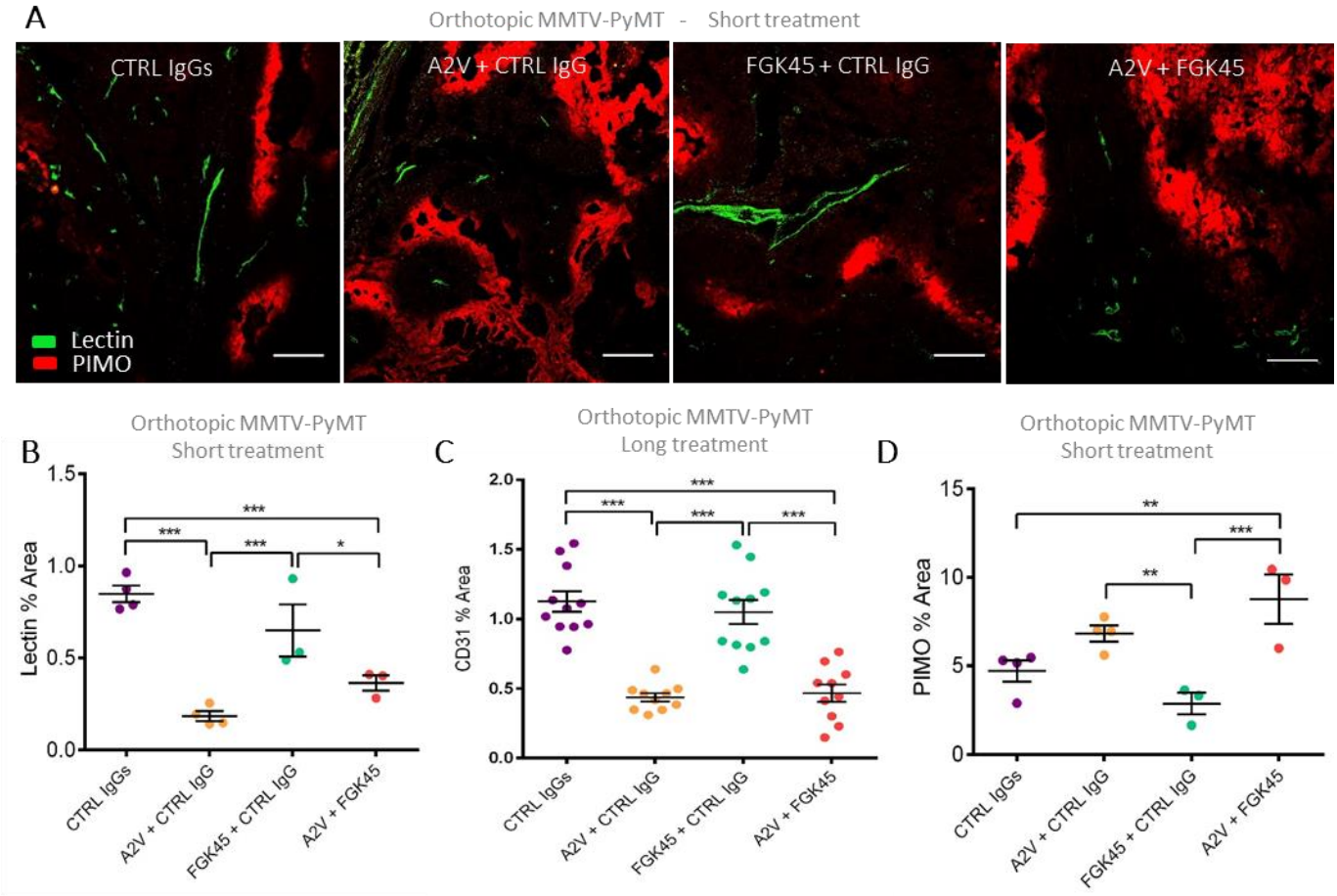

Figure 17. FGK45 does not impair the anti-angiogenic effect of A2V in orthotopic MMTV-PyMT tumors *(A) Representative pictures of tumor sections with lectin (green) and PIMO (red) immunofluorescence staining in the orthotopic MMTV-PyMT model, after a short-term treatment schedule. The confocal microscope magnification is 200x; scale bar, 100 µm. Quantitative analysis of the relative tumor vascular area (mean values ± SEM), showing the relative lectin$^+$ area in short treated tumors (B) or the relative CD31$^+$ area in long-treated tumors (C); (D) quantitative analysis of*

relative PIMO⁺ area (mean values ± SEM) in short-term treated tumors. For every graph each dot corresponds to one tumor/mouse, and displays the average of the analysis of 8-15 pictures per tumor. Statistical analysis by ordinary one-way ANOVA with Tukey's multiple comparisons test (= p < 0.05; ** = 0.001<p< 0.01; *** = p < 0.001).*

4.9. FGK45 increases the tumor infiltration of CD8⁺ T lymphocytes, potentiating an adaptive anti-tumor immune response

In order to assess the adaptive immune response triggered by FGK45 treatment, the pool of T lymphocytes within the tumor microenvironment was evaluated. To do so, both immunofluorescence staining on tumor sections (Figure 18) and flow cytometry analysis of single tumor cell suspension (Figure 19) were performed.

To identify potential cytotoxic T lymphocytes, the CD8 surface marker was used in immunofluorescence staining of orthotopic MMTV-PyMT tumor sections, treated with a short-term schedule. CD4⁺ T lymphocytes were identified by their expression of CD4 marker. Following, the number of CD8⁺ and CD4⁺ cells on these IF stained tumor sections were quantified, by counting individual cells present in each confocal microscope field (640x640µm) (see material and methods). This quantitative analysis exposed a statistic significant increase of the number of CD8⁺ cells per field in FGK45 treated tumors, alone or in combination, compared to the A2V monotherapy or control treated tumors (Figure 18 A and D). This suggests that FGK45 helps the recruitment and/or the activation/proliferation of effector T cells, supporting the mounting of an anti-tumor immune response. Moreover, even if not statistic, a trend for further increase of the CD8⁺ cell numbers after dual FGK45 and A2V therapy was detected, when compared to FGK45 monotherapy. The amount of CD4⁺ cells within the tumor microenvironment was similar for all groups, with a slender increase in the combination therapy (Figure 18 B and E). The ratio between CD8⁺ and CD4⁺ cells was significantly raised after the treatment with FGK45, comparing to the A2V monotherapy and control treated tumors (Figure 18 C). Although no statistical differences were found, the CD8⁺/CD4⁺ cell ratio was also increased after the combination therapy.

However, not only the amount of tumor infiltrating T cells can influence an immune response, their localization within the tumor is also important. For instance, the presence of CD8⁺ effector T cells in the tumor core correlates with better prognosis in cancer patients, than their presence in the invasive margin of the tumor (213). In this study, while the presence of CD4⁺ cells was restricted to the blood vessel surrounding areas (Figure 18 E) at the margin of the tumor, CD8⁺ cells could extravasate (Figure 18 F, left image) and spread more within the tumor tissue (Figure 18 D). Nonetheless, a limiting effect driven by hypoxia for the CD8⁺ cell proliferation was observed, since these cells were rarely seen overlapping with hypoxic areas (Figure 18 F, right image).

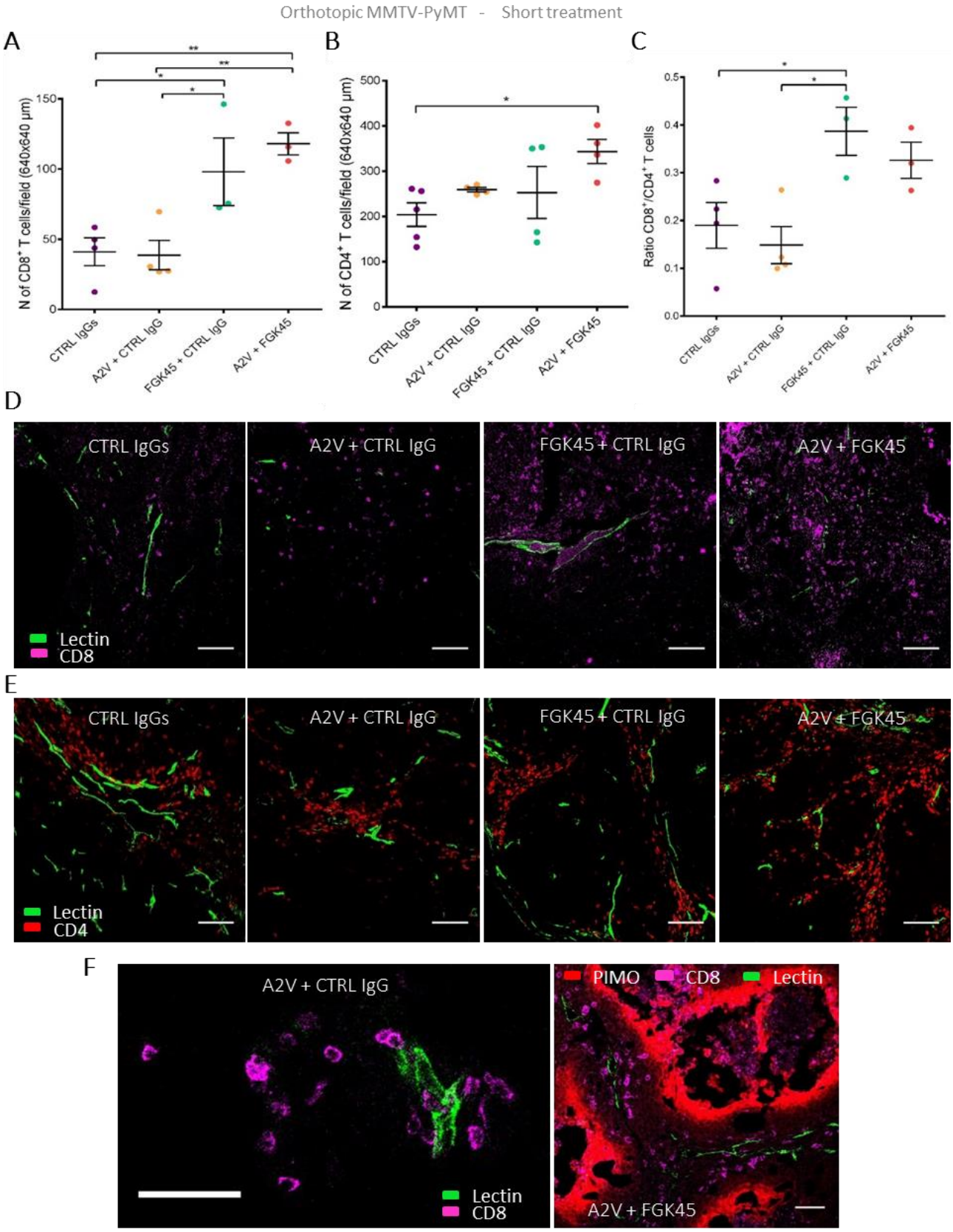

Figure 18. FGK45 increases the tumor infiltration of CD8⁺ T lymphocytes in orthotopic MMTV-PyMT tumors after the short-term schedule. *Quantitative analysis of the number of*

$CD8^+$ T cells (A) or $CD4^+$ T cells (B) per microscope filed, and the ratio of $CD8^+/CD4^+$ cells (C) (mean values ± SEM). For every graph each dot corresponds to one tumor/mouse, and displays the average of the analysis of 8-15 pictures per tumor. Statistical analysis by ordinary one-way ANOVA with Tukey's multiple comparisons test (= p < 0.05; ** = 0.001<p< 0.01). (D) Representative pictures with lectin (green) and CD8 (magenta) or (E) lectin (green) and CD4 (red) immunofluorescence staining in orthotopic MMTV-PyMT tumor sections. Microscope magnification is 200x; scale bar, 100 µm. (F) left image illustrates $CD8^+$ cells extravasation into the tumor, with lectin (green) and CD8 (magenta) immunofluorescence staining; right image illustrates the relative localization of $CD8^+$ cells in concern to the blood vessels and hypoxic areas, with lectin (green), CD8 (magenta) and PIMO (red) immunofluorescence staining. Microscope magnification is 200x; scale bar, 50 µm.*

For the long-term treated tumors, the tumor infiltrating T cells were analyzed using flow cytometry analysis. To do so, whole tumors were processed in order to obtain single tumor cell suspensions (see materials and methods for detailed description). Single cells were then incubated with a viability staining, allowing to differentiate alive from dead cells, since only cells with disrupted membrane, therefore dead cells, are stained. Finally the tumor cell suspension was stained with 3 surface markers, CD45, CD8 and CD4 for the flow cytometry analysis. The gating strategy used is represented in Figure 19 A: after excluding debris (1^{st} gate – SSC x FSC) and doublets (2^{nd} gate - FSC-H x FSC-A and 3^{rd} gate - SSC-H x SSC-A), cells were gated with the viability staining and the CD45 marker (4^{th} gate), where alive $CD45^+$ cells were identified with low viability staining (indicating membrane integrity and therefore alive cells) and high CD45 surface staining. $CD8^+$ and $CD4^+$ cells were then gated on alive $CD45^+$ cells. The right controls (Fluorescence Minus One – FMO) were used to identify the proper placement of the gates.

During this analysis a slight increase of the $CD8^+$ cell percentage, among the alive $CD45^+$ cells, was observed in tumors treated with FGK45 (Figure 19 B). While this difference was not statistically significant compared to the control treated tumors, a statistic difference between the FGK45 and the A2V monotherapy treated groups could be observed, where the later displayed a small decrease in the $CD8^+$ cell compartment. However, tumors treated with both A2V and FGK45 increased significantly the $CD8^+$ cells, compared with the control and the A2V monotherapy. Although not statistically different from the FGK45 monotherapy, the combination therapy displayed once more a trend for further increase in the percentage of $CD8^+$ cells. Even though no differences were found in the percentage of $CD4^+$ cells among the different treatments (Figure 19 C), the ratio between $CD8^+$ and $CD4^+$ cells was found increased in tumors treated with FGK45, either alone or in combination with A2V (Figure 19 D).

Then, each individual tumor growth curves were compared with its corresponding $CD8^+$ cell percentages in the combination therapy group. Following this analysis, a correlation between cases of stable disease (see Figure 15 C, bottom right panel, grey rectangle) - displayed as black dots in Figure 19 - and high percentages of $CD8^+$ cells (Figure 19 B) as well as high $CD8^+/CD4^+$ cell ratios (Figure 19 D) was detected. Although the number of these stable tumors is still low to draw conclusions, these data suggests that the high influx of $CD8^+$ cells into the tumor correlates with a better anti-tumor response in the combinatory therapeutic approach.

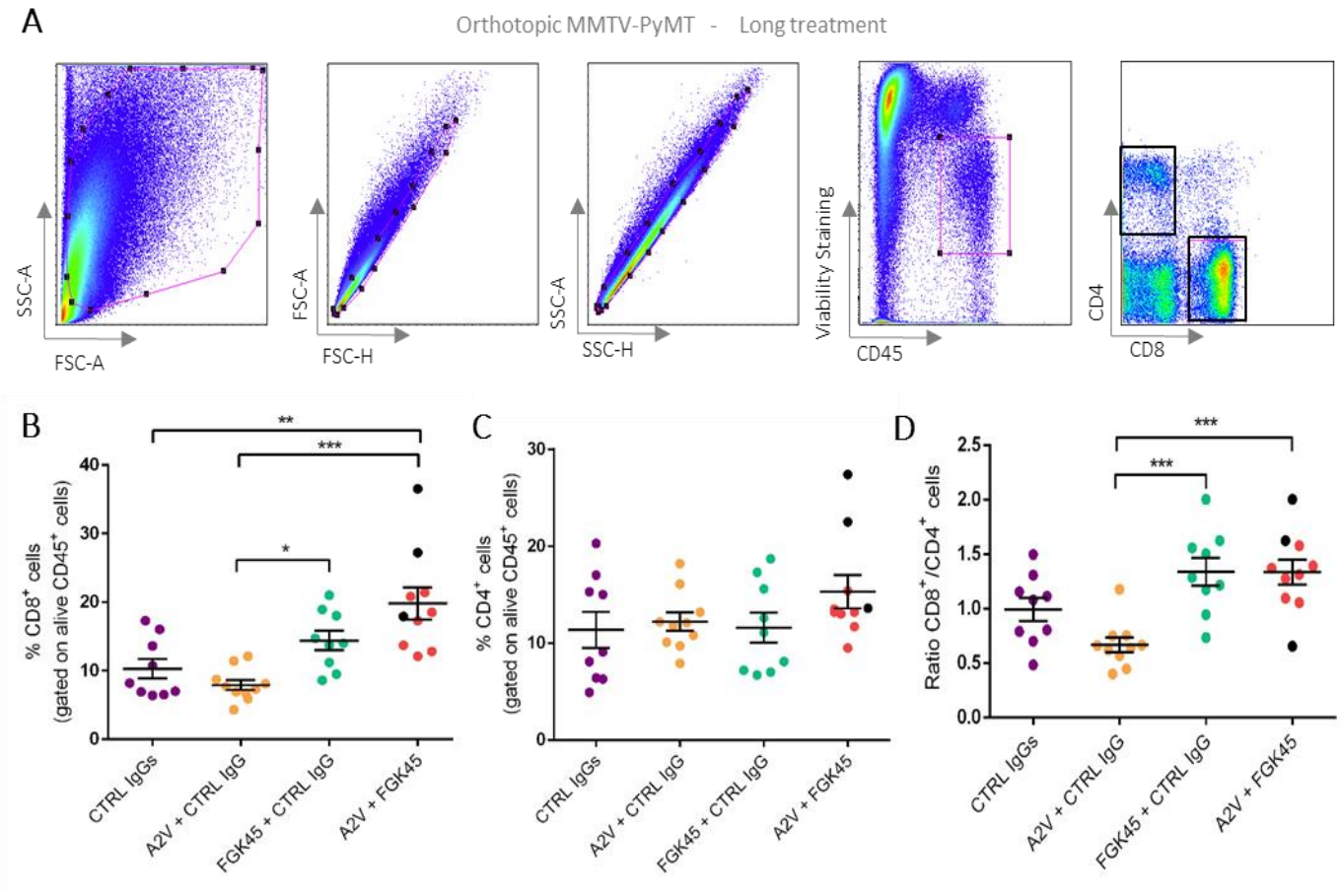

Figure 19. Combining A2V with FGK45 remarkably increases the percentage of $CD8^+$ cells in orthotopic MMTV-PyMT tumors treated after the long-term schedule. *(A) flow cytometry scatter plots demonstrating the gate strategy adopted (FSC – Forward Scatter; SSC – Side Scatter; A – Area; H – Height). Quantitative analysis of the percentage of $CD8^+$ cells (B) or $CD4^+$ cells (C), gated on alive $CD45^+$ cells, and the ratio of $CD8^+/CD4^+$ cells (D) (mean values ± SEM), in single cell suspensions of orthotopic MMTV-PyMT tumors treated for a long term schedule. For every graph each dot corresponds to one tumor/mouse and black dots in the combination therapy group indicate the cases of stable disease. Statistical analysis by ordinary one-way ANOVA with Tukey's multiple comparisons test (*, $p < 0.05$; **, $0.001<p< 0.01$; ***, $p < 0.001$).*

In conclusion, FGK45 treatment potentiates an anti-tumor immune response in the orthotopic MMTV-PyMT model, by increasing tumor infiltration of $CD8^+$ T lymphocytes. These changes in the normal lymphocyte compartment appear more profound after the combination of FGK45 with A2V, a synergistic effect likely due to the elimination of the immune suppressive tumor ECs, achieved with A2V treatment, which potentiates the immune effect of FGK45. Furthermore, the fact that FGK45 could increase the percentage of $CD8^+$ cells at the endpoint, in tumors treated for a long schedule, suggests that the only dose of FGK45 administered is effective even in later stages of tumor progression.

5. Discussion and Conclusions

Despite the promising activity of antiangiogenic drugs in pre-clinical tumor models, breast cancer patients treated with anti-angiogenic therapies show no apparent benefit from the therapy since, so far, all clinical studies of antiangiogenic therapies in breast cancer failed to improve OS (121). The majority of the current anti-angiogenic therapies in breast cancer are based on VEGF function inhibition. However, unlike other human cancers, there is no reported constitutive activation of the VEGF pathway in breast cancer (214). Therefore, breast cancer patients may benefit from therapeutic strategies targeting other angiogenic factors, such as the ANGs. Indeed high levels of ANG-2 correlate with poor prognosis in breast cancer patients (100). Nonetheless, the ANG-1 and ANG-2 target agent, AMG 386, displayed no clinical benefit in metastatic breast cancer patients in a phase II trial (126).

Nevertheless, high levels of both VEGF-A and ANG-2 correlate with worse prognosis in breast cancer patients, when compared with cancers expressing high levels of either alone (114). This information, as well as previous pre-clinical studies demonstrating the synergistic angiogenic inhibition effect achieved with dual ANG-2 and VEGF-A (95-97), led to the evaluation of the therapeutic efficacy of double ANG-2/VEGF-A blockade, using the A2V crossMab, in the aggressive MMTV-PyMT mouse model of breast cancer.

The findings of this study demonstrate that simultaneous blockade of ANG-2 and VEGF-A leads to powerful inhibition of tumor progression (50 to 70% inhibition) and increases the survival in this mouse model of breast carcinoma, as previously shown in other models (116, 215). Given that transgenic MMTV-PyMT mice die around 16 weeks of age due to the development of multiple aggressive carcinomas, the fact that some MMTV-PyMT mice treated with A2V were able to live up to 22 weeks of age is a remarkable achievement. Furthermore, A2V also led to increased necrosis in orthotopic MMTV-PyMT tumors, in agreement with studies reported by Hashizume *et al*., where increased apoptosis of tumor cells was observed after dual ANG-2 and VEGF-A blockade (96).

A2V tumor growth inhibitory effects were associated with the reduction of the overall tumor blood vessel density. Quantitative analysis of the relative tumor vascular area ($CD31^+$ % area) demonstrated a drastic reduction of blood vessels in tumors treated with A2V, where the remaining blood vessels display a short, small diameter and poorly branched morphology. Perfusion studies demonstrated that A2V is also capable of decreasing blood vessel functionality. Furthermore, after ANG-2/VEGF-A blockade, blood vessels were mainly located at the tumor periphery, leaving large avascular areas in the central core of the tumor, which suggests the occurrence of vascular regression.

Tumor revascularization upon VEGF target therapies have long been reported (29, 94), where the upregulation of ANG-2 has been one of the nominated mechanisms of

resistance to this therapies (95). In the present study, in agreement with those performed by Kienast *et al.* (116), a consistent fifty percent reduction of the blood vessel density was found in every tumor after A2V treatment, even in those treated for an extended period of time, with no reports of revascularization. Therefore, dual ANG-2/VEGF-A blockade impairs not only sprouting angiogenesis but also revascularization, displaying a potent anti-angiogenic effect in the MMTV-PyMT mouse model of breast cancer.

Although not demonstrated in this study, it can be speculated that this strong anti-angiogenic effect may be partially mediated by the ANG-2 blockade effect on TEMs: blocking ANG-2 can impede TIE-2 upregulation by TAM/myeloid cells and their association with tumor blood vessels (98, 108). Given that TAMs are known to potentiate tumor angiogenesis in breast cancer (83), impairing the pro-angiogenic functions of TEMs could contribute to the anti-angiogenic effect of A2V.

Consistent to angiogenesis inhibition and vessel regression, A2V also led to increased tumor hypoxia. It has been reported that increased tumor hypoxia drives therapeutic resistance and it's a strong stimuli for tumor angiogenesis (216, 217), however the findings of this study indicate otherwise. The tumor ability to escape hypoxia by vascular remodeling was drastically impaired in tumors treated with A2V, where tumor cells had no access to oxygen or nutrients, explaining the intense tumor cell death/necrosis in hypoxic areas.

Another finding of this study was the increased perivascular coverage of the remaining tumor blood vessels after A2V therapy. While the control treated tumors displayed blood vessels unevenly covered by perivascular cells, suggesting active angiogenesis, dual blockade of ANG-2/VEGF-A mediated by A2V increased mural cell coverage of the remaining tumor blood vessels, favoring vascular stability/normalization. Although not demonstrated here, it is possible that this effect is derived from the ANG-2 blockade, rather than VEGF-A blockade. Several studies support this theory (95, 98), including unreported experiments of this study using the ANG-2 neutralizing mAb, LCO6, where a similar effect could be observed. Therefore, A2V-mediated ANG-2 blockade may increase the ANG-1/TIE-2 signaling, due to increased ANG-1 bioavailability, promoting accumulation of adhesion molecules in cell–cell junctions and increasing pericyte coverage (107).

Given the blood vessel normalization effect mediated by A2V, as well as numerous studies recognizing the anti-metastatic effect of ANG-2 blockade (98, 116, 218, 219), it is reasonable to consider that A2V could also decrease tumor invasiveness and the frequency of metastatic dissemination. Besides, decreased blood vessel leakage accomplished by the maturation and stabilization of the remaining tumor blood vessels may increase the penetration of other drugs, such as chemotherapy (220). More importantly, the vascular normalization can create an immunosupportive microenvironment, which may improve

cancer immunotherapy (221). As stated previously, tumor blood vessels are typical abnormal, resulting in impaired blood vessel perfusion (222). This results in a hypoxic and acidic suppressive microenvironment that helps cancer cell evade the immune system, either by impairing the recruitment of cytotoxic lymphocytes, by upregulation of immune checkpoint molecules, such as PD-L1, by preferential recruitment of pro-tumoral Tregs or by impairing the function of resident immune effector cells (through the upregulation of TGF-β and IL-10) (223). While high doses of anti-angiogenic therapies lead to excessive vessel pruning and aggravation of this effect, low doses (or therapies targeting blood vessel normalization pathways, such as blockade of ANG-2) can lead to blood vessel normalization. This in turn can lead to lower increase in tumor hypoxia, enhancing the delivery of immune effector cells into tumors and creating a more immunosupportive microenvironment (221). Indeed, studies performed by Huang *et al.*, revealed that low doses of the DC101 anti-VEGFR2 Ab, but not high doses of the same Ab, lead to tumor vascular normalization in a breast cancer model (224). The authors observed that the vascular normalization was responsible for increased tumor infiltration of $CD8^+$ T cells and for the polarization of TAMs to an anti-tumor M1-like phenotype. This suggests that combining A2V with other therapies is a promising approach that should be further investigated.

In summary, targeting both ANG-2 and VEGF-A, through the action of A2V, induces durable tumor growth inhibition and vascular regression with normalization of the remaining tumor blood vessels. The strong anti-tumor effect of this molecule, characterized by Kienast et al. (116), supported its investigation in clinical trials, in patients with advanced or metastatic solid tumors (NCT01688206).

Taken the information above described, as well as the immunosuppressive role of ECs and tumor-derived VEGF-A in the tumor microenvironment (188), it was asked if a CD40 agonist (FGK45)-mediated immunotherapy could benefit from the combination therapy with A2V, in the mammary carcinoma mouse model, MMTV-PyMT.

It was observed that, while FGK45-based immunotherapy alone was not able to inhibit the growth of orthotopic MMTV-PyMT tumors, the combination therapy (A2V + FGK45) leads to a remarkable tumor growth inhibition, suggesting a potential benefit in this combined therapeutic approach. Moreover, the tumor growth inhibition effect of the combination therapy was even more pronounced than the one observed after the treatment with A2V alone, during later stages of tumor progression. In addition, combining A2V with FGK45 led to the establishment of cases of stable disease (3 out of 10 mice treated with the combination therapy), which is suggestive of a synergistic anti-tumor effect between these two mAbs.

In agreement with the aforementioned effect, a further increase in necrosis of orthotopic MMTV-PyMT tumors was also observed after the combination therapy,

compared to the monotherapies. This resulting intensive necrosis is an effect most likely mediated by the dual action of A2V and FGK45: it is reasonable to consider that tumor cell death mediated by A2V leads to increased presentation of tumor antigens to cytotoxic T cells by FGK45-activated APCs, enhancing adaptive anti-tumor immune responses. Furthermore, since breast cancer cells can also express CD40 (168), it is possible the occurrence of a direct apoptotic action of FGK45 on CD40 expressing MMTV-PyMT tumor cells, as previously reported (170). A possible T-cell independent anti-tumor activity of CD40-activated macrophages (166, 225) cannot also be excluded.

Since agonist CD40 mAbs were shown to decrease fibrosis (209), the percentage of the collagen positive tumor area was also assessed. However, differently from the reported data, a significant increase of the collagen$^+$ area in tumors treated with both A2V and FGK45 was found in this study. This contradictory effect may be due to tissue repair processes, mediated by the powerful increase in tumor necrosis.

Moreover, despite several studies indicating the pro-angiogenic effect of CD40 signaling in ECs (210-212), in this study comparable relative blood vessel areas were found between tumors treated with FGK45 and the control treatment. Besides, dual A2V + FGK45 therapy led to the same extent of angiogenesis inhibition as the A2V monotherapy, suggesting that FGK45 does not increase angiogenesis and does not impair the anti-angiogenic effect of the A2V.

Following, it was evaluated whether the potent anti-tumor effect mediated by this combination approach was associated with an increase in adaptive anti-tumors immune responses, mainly by evaluating the tumor infiltration of T lymphocytes. Using two different techniques, IFS and flow cytometry, an increased infiltration of CD8$^+$ cells in FGK45 treated tumors was detected, compared to the A2V monotherapy or control treated tumors. These results are in agreement with previous studies, where the administration of CD40 agonistic Abs was able to increase the number of tumor infiltrating CD8$^+$ T cells (226, 227). This increase can be explained by the enhanced differentiation and function of APCs through FGK45 engagement, which leads to recruitment and/or the activation/proliferation of effector T cells, supporting the mounting of an anti-tumor immune response. Studies performed by Fransen *et al.*, using the same CD40-agonistic mAb clone (FGK45), have disclosed that FGK45 activates local tumor-specific CD8 T cells, by inducing local but not systemic DC activation (228). However, in this study extravasation of CD8$^+$ cells into the tumors could be observed, suggesting that the FGK45-activated APCs may travel from the tumor site to secondary lymphatic organs, where they actively present the tumor antigens to Naïve CD8$^+$ T cells, leading to their activation and recruitment to the tumor. Therefore the increase of tumor infiltrating CD8$^+$ cells observed after the treatment with FGK45, may be due to both recruitment and/or activation of local effector T cells.

A trend for further increase of the $CD8^+$ cell numbers after dual FGK45 and A2V therapy was also observed, when compared to FGK45 monotherapy. This would be easily explained by the eliminating the tumor immunosuppressive ECs due to A2V therapy, and thereby the reduction of the negative regulation of adaptive immune responses. However, there was no statistic difference in the $CD8^+$ cell numbers between the FGK45 and the combination treated tumors. One possible reason explaining the stronger anti-tumor effect achieved by the combination therapy, would be that the tumor infiltrating $CD8^+$ cells present in this case are more activated or more antigen-specific compared to those in tumors treated with FGK45 alone. Further experiments using Ovalbumin-positive cancer models, such as the B16-OVA expressing melanoma cancer, would be the next logical step to assess a possible enhanced generation of antigen-specific $CD8^+$ T cells after the combination therapy, by checking their expression of OVA-Specific TCR using flow cytometry with double CD8 and OVA-Specific TCR cell surface staining. Evaluation of the $CD8^+$ cell *activated status* - by assessing their expression of perforin (both protein and mRNA levels, by ELISA or qPCR assays, respectively), IFN-γ and/or IL-2 (with intracellular cytokine staining in flow cytometry) -, or *proliferation status* – using the Bromodeoxyuridine (BrdU) Cell Proliferation Assay, a synthetic analog of the thymidine, which is incorporated into replicating DNA in dividing cells and can be subsequently detected by anti-BrdU antibodies -, are also necessary future studies.

The numbers of tumor infiltrating $CD4^+$ cells were similar between all the therapies, however the ratio between $CD8^+$ and $CD4^+$ cells, which correlates with good prognosis when increased (229), was significantly raised after the treatment with FGK45, either alone or in combination with A2V. Moreover, $CD8^+$ cells were more spread into the tumor tissue, rather than limited to the blood vessel surrounding areas at the invasive margin of the tumor, which is also a good prognostic factor in cancer patients (213).

Surprisingly, a slight decrease in the tumor infiltrating $CD8^+$ cells after A2V treatment could be observed. This effect was reproducible, as it was continuously observed in non-reported experiments of this study. Since $CD8^+$ cells rarely overlap with hypoxic areas, it is tempting to speculate that the decrease in the numbers of $CD8^+$ cells may be due to the increase of hypoxic areas in tumors treated with A2V. While in the A2V monotherapy increased hypoxia seems to be a limiting effect for $CD8^+$ cell proliferation, in the combination therapy this effect is most likely overpowered by the FGK45 effect.

An association between the cases of stable disease, achieved by the combination therapy, and increased tumor infiltration of $CD8^+$ cells was also detected in this study. Given that increased numbers of infiltrating $CD8^+$ T cells have been associated with better clinical outcomes in patients with breast cancer (179), the high influx of $CD8^+$ cells into these tumors was possibly responsible for the remarkable anti-tumor responses observed. These findings have important implications for the use of anti-CD40 therapies in breast

cancer patients. Given that therapeutic strategies relying solely on agonistic CD40 mAbs lead to clinical safety but not OS in patients with advanced solid tumors (176), the combination therapy with anti-angiogenic therapies would be a promising approach.

Taken together, combining A2V with FGK45 leads to a strong anti-tumor response in the orthotopic MMTV-PyMT tumor model, with addictive inhibitory effects compared to each therapy alone. An hypothetical mechanism for the synergist effect between A2V- and FGK45-based therapies is proposed in Figure 20, explained by the creation of an immunosupportive microenvironment followed by A2V therapy, given that this therapeutic approach leads to (a) vascular regression and elimination of the immunosuppressive tumor ECs and tumor derived VEGF-A, decreasing the negative immune regulation with consequent increase immune activation triggered by FGK45, and to (b) the normalization of the remaining tumor blood vessels, which is permissive to T cell tumor infiltration. Besides, A2V also leads to (c) augmented tumor cell death, increasing tumor antigen uptake by tumor resident APCs (DCs and Macrophages), which upon FGK45 therapy become activated and increase tumor antigen presentation to Naïve CD8+ T cells (in either secondary lymphatic organs or in the tumor) resulting in their activation and/or recruitment, with consequent increased immune-mediated cell death. However, further studies aiming to evaluate the activated/proliferating status of $CD8^{+}$ cells, as well as their specificity, are required to further understand the mechanisms behind this cooperative effect.

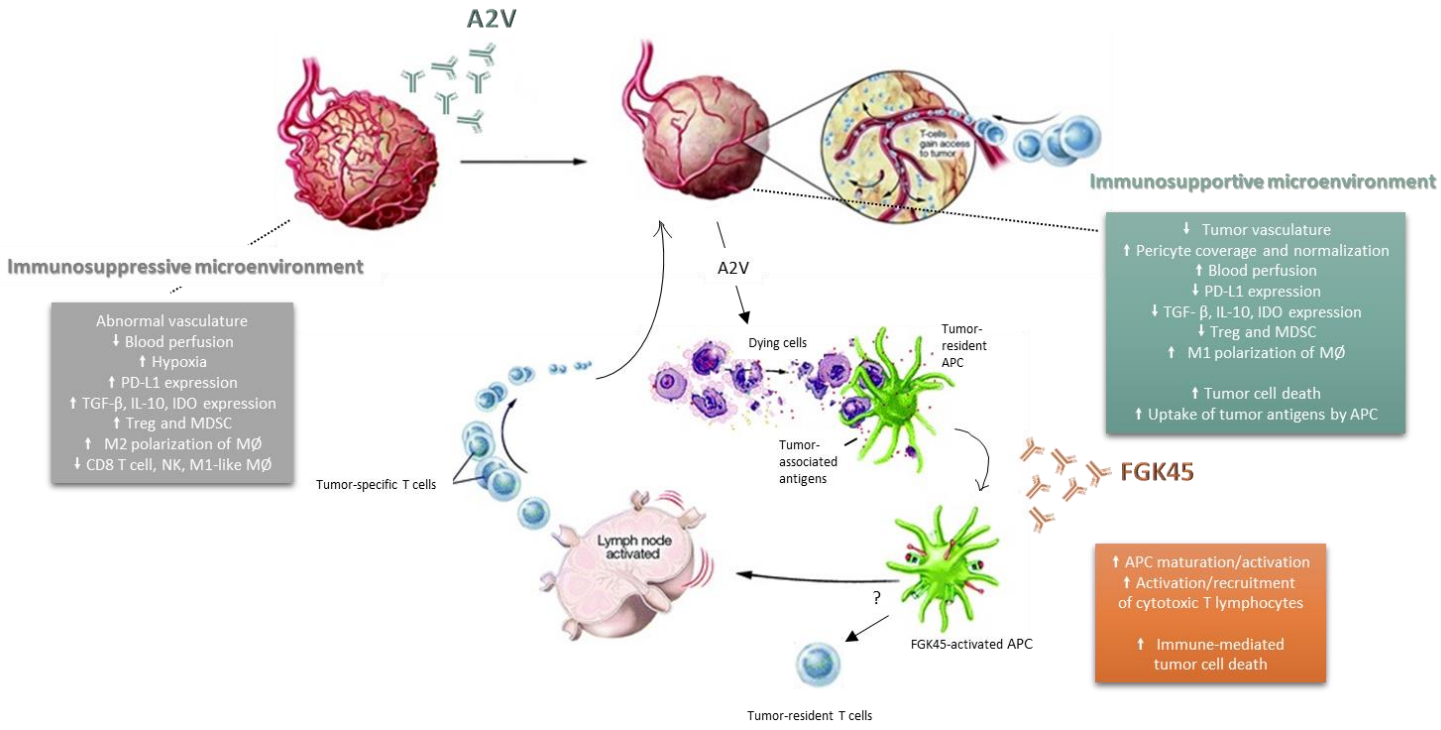

Figure 20. Synergistic effect between A2V-based antiangiogenic therapy and FGK45-mediated immunotherapy (Adapted from Kamrava, *et al.,* Mol. BioSyst., 2009 (230))

In conclusion, there is a clear benefit in combining A2V-mediated anti-angiogenic therapy with FGK45-mediated immunotherapy in the aggressive MMTV-PyMT pre-clinical model of breast cancer. However, MMTV-PyMT tumors resemble the Luminal B molecular subtype of human breast cancer, which accounts for 10-20% of all breast cancer cases (9). Therefore, it would be of interest to assess the anti-tumor effect of this therapy in other breast cancer mouse models, such as models of the Luminal A molecular breast cancer subtype, since they correspond to 50 to 60% of all cases, or models of the basal-like subtype, such as MMTV-Wnt1 transgenic mouse model (231), since they display the worst prognosis in human breast cancer patients (232). Besides, this combinatory approach might be improved if the cancer cells themselves are simultaneously targeted, using direct anti-cancer therapies such as chemotherapy or radiation therapy. Given that targeting different aspects of the tumor biology may produce better clinical benefit for cancer patients, especially with late-stage disease (230), this should also be assessed in a near future.

Taken everything into consideration, it is my opinion that the combinatory A2V- and FGK45-mediated therapy should be further addressed and potentially translated to the breast cancer clinical settings.

6. References

1. Hanahan D, Weinberg RA. The hallmarks of cancer. Cell. 2000;100(1):57-70.
2. Hanahan D, Weinberg RA. Hallmarks of cancer: the next generation. Cell. 2011;144(5):646-74.
3. Yamashita M, Ogawa T, Zhang X, Hanamura N, Kashikura Y, Takamura M, et al. Role of stromal myofibroblasts in invasive breast cancer: stromal expression of alpha-smooth muscle actin correlates with worse clinical outcome. Breast Cancer. 2012;19(2):170-6.
4. Higgins MJ BJ. Targeted therapies for breast cancer.: J Clin Invest. ; 2011. p. 3797-803.
5. Ercan C vDP, Vooijs M. Mammary development and breast cancer: the role of stem cells.: Curr Mol Med.; 2011. p. 270-85.
6. Ferlay J, Steliarova-Foucher E, Lortet-Tieulent J, Rosso S, Coebergh JW, Comber H, et al. Cancer incidence and mortality patterns in Europe: estimates for 40 countries in 2012. Eur J Cancer. 2013;49(6):1374-403.
7. Vargo-Gogola T, Rosen JM. Modelling breast cancer: one size does not fit all. Nat Rev Cancer. 2007;7(9):659-72.
8. Perou CM, Sørlie T, Eisen MB, van de Rijn M, Jeffrey SS, Rees CA, et al. Molecular portraits of human breast tumours. Nature. 2000;406(6797):747-52.
9. Eroles P, Bosch A, Pérez-Fidalgo JA, Lluch A. Molecular biology in breast cancer: intrinsic subtypes and signaling pathways. Cancer Treat Rev. 2012;38(6):698-707.
10. Perez EA. Paclitaxel in Breast Cancer. Oncologist. 1998;3(6):373-89.
11. Hassan MS, Ansari J, Spooner D, Hussain SA. Chemotherapy for breast cancer (Review). Oncol Rep. 2010;24(5):1121-31.
12. Rouzier R, Perou CM, Symmans WF, Ibrahim N, Cristofanilli M, Anderson K, et al. Breast cancer molecular subtypes respond differently to preoperative chemotherapy. Clin Cancer Res. 2005;11(16):5678-85.
13. Di Cosimo S. BJ. Management of breast cancer with targeted agents: importance of heterogeneity.: Nat Rev Clin Oncol.; 2010. p. 139-47.
14. Clarke MJ. WITHDRAWN: Tamoxifen for early breast cancer. Cochrane Database Syst Rev. 2008(4):CD000486.
15. Gradishar WJ. Adjuvant endocrine therapy for early breast cancer: the story so far. Cancer Invest. 2010;28(4):433-42.
16. Kaufman B, Mackey JR, Clemens MR, Bapsy PP, Vaid A, Wardley A, et al. Trastuzumab plus anastrozole versus anastrozole alone for the treatment of postmenopausal women with human epidermal growth factor receptor 2-positive, hormone receptor-positive metastatic breast cancer: results from the randomized phase III TAnDEM study. J Clin Oncol. 2009;27(33):5529-37.
17. Leyland-Jones B. Trastuzumab: hopes and realities. Lancet Oncol. 2002;3(3):137-44.
18. Romond EH, Perez EA, Bryant J, Suman VJ, Geyer CE, Davidson NE, et al. Trastuzumab plus adjuvant chemotherapy for operable HER2-positive breast cancer. N Engl J Med. 2005;353(16):1673-84.
19. Slamon DJ, Leyland-Jones B, Shak S, Fuchs H, Paton V, Bajamonde A, et al. Use of chemotherapy plus a monoclonal antibody against HER2 for metastatic breast cancer that overexpresses HER2. N Engl J Med. 2001;344(11):783-92.
20. Berns K, Horlings HM, Hennessy BT, Madiredjo M, Hijmans EM, Beelen K, et al. A functional genetic approach identifies the PI3K pathway as a major determinant of trastuzumab resistance in breast cancer. Cancer Cell. 2007;12(4):395-402.
21. Andre F, Campone M, O'Regan R, Manlius C, Massacesi C, Sahmoud T, et al. Phase I study of everolimus plus weekly paclitaxel and trastuzumab in patients with metastatic breast cancer pretreated with trastuzumab. J Clin Oncol. 2010;28(34):5110-5.

22. Anders C, Carey LA. Understanding and treating triple-negative breast cancer. Oncology (Williston Park). 2008;22(11):1233-9; discussion 9-40, 43.
23. Tutt A, Robson M, Garber JE, Domchek SM, Audeh MW, Weitzel JN, et al. Oral poly(ADP-ribose) polymerase inhibitor olaparib in patients with BRCA1 or BRCA2 mutations and advanced breast cancer: a proof-of-concept trial. Lancet. 2010;376(9737):235-44.
24. Baselga J. Treatment of HER2-overexpressing breast cancer. Ann Oncol. 2010;21 Suppl 7:vii36-40.
25. Siegel R, Ward E, Brawley O, Jemal A. Cancer statistics, 2011: the impact of eliminating socioeconomic and racial disparities on premature cancer deaths. CA Cancer J Clin. 2011;61(4):212-36.
26. Finak G, Bertos N, Pepin F, Sadekova S, Souleimanova M, Zhao H, et al. Stromal gene expression predicts clinical outcome in breast cancer. Nat Med. 2008;14(5):518-27.
27. Carmeliet P, Jain RK. Molecular mechanisms and clinical applications of angiogenesis. Nature. 2011;473(7347):298-307.
28. Hanahan D, Folkman J. Patterns and emerging mechanisms of the angiogenic switch during tumorigenesis. Cell. 1996;86(3):353-64.
29. Bergers G, Hanahan D. Modes of resistance to anti-angiogenic therapy. Nat Rev Cancer. 2008;8(8):592-603.
30. Folkman J, Kalluri R. Cancer without disease. Nature. 2004;427(6977):787.
31. Wicki A, Christofori G. The Angiogenic Switch in Tumorigenesis. In: Marmé D, Fusenig N, editors. Tumor Angiogenesis: Basic Mechanisms and Cancer Therapy. Germany: Springer-Verlag Berlin Heidelberg; 2008. p. 67 - 88.
32. Saharinen P, Eklund L, Pulkki K, Bono P, Alitalo K. VEGF and angiopoietin signaling in tumor angiogenesis and metastasis. Trends Mol Med. 2011;17(7):347-62.
33. Fraisl P, Mazzone M, Schmidt T, Carmeliet P. Regulation of angiogenesis by oxygen and metabolism. Dev Cell. 2009;16(2):167-79.
34. Phng LK, Gerhardt H. Angiogenesis: a team effort coordinated by notch. Dev Cell. 2009;16(2):196-208.
35. Jakobsson L, Franco CA, Bentley K, Collins RT, Ponsioen B, Aspalter IM, et al. Endothelial cells dynamically compete for the tip cell position during angiogenic sprouting. Nat Cell Biol. 2010;12(10):943-53.
36. Fukumura D, Jain RK. Imaging angiogenesis and the microenvironment. APMIS. 2008;116(7-8):695-715.
37. Heldin CH, Rubin K, Pietras K, Ostman A. High interstitial fluid pressure - an obstacle in cancer therapy. Nat Rev Cancer. 2004;4(10):806-13.
38. Ferrara N, Hillan KJ, Gerber HP, Novotny W. Discovery and development of bevacizumab, an anti-VEGF antibody for treating cancer. Nat Rev Drug Discov. 2004;3(5):391-400.
39. Carmeliet P, Ferreira V, Breier G, Pollefeyt S, Kieckens L, Gertsenstein M, et al. Abnormal blood vessel development and lethality in embryos lacking a single VEGF allele. Nature. 1996;380(6573):435-9.
40. Suri C, Jones PF, Patan S, Bartunkova S, Maisonpierre PC, Davis S, et al. Requisite role of angiopoietin-1, a ligand for the TIE2 receptor, during embryonic angiogenesis. Cell. 1996;87(7):1171-80.
41. Patan S. TIE1 and TIE2 receptor tyrosine kinases inversely regulate embryonic angiogenesis by the mechanism of intussusceptive microvascular growth. Microvasc Res. 1998;56(1):1-21.
42. Ferrara N, Henzel WJ. Pituitary follicular cells secrete a novel heparin-binding growth factor specific for vascular endothelial cells. Biochem Biophys Res Commun. 1989;161(2):851-8.
43. Ferrara N. VEGF-A: a critical regulator of blood vessel growth. Eur Cytokine Netw. 2009;20(4):158-63.

44. Houck KA, Ferrara N, Winer J, Cachianes G, Li B, Leung DW. The vascular endothelial growth factor family: identification of a fourth molecular species and characterization of alternative splicing of RNA. Mol Endocrinol. 1991;5(12):1806-14.
45. Ferrara N, Gerber HP, LeCouter J. The biology of VEGF and its receptors. Nat Med. 2003;9(6):669-76.
46. Pepper MS. Extracellular proteolysis and angiogenesis. Thromb Haemost. 2001;86(1):346-55.
47. Bergers G, Brekken R, McMahon G, Vu TH, Itoh T, Tamaki K, et al. Matrix metalloproteinase-9 triggers the angiogenic switch during carcinogenesis. Nat Cell Biol. 2000;2(10):737-44.
48. Gerber HP, McMurtrey A, Kowalski J, Yan M, Keyt BA, Dixit V, et al. Vascular endothelial growth factor regulates endothelial cell survival through the phosphatidylinositol 3'-kinase/Akt signal transduction pathway. Requirement for Flk-1/KDR activation. J Biol Chem. 1998;273(46):30336-43.
49. Shiojima I, Walsh K. Role of Akt signaling in vascular homeostasis and angiogenesis. Circ Res. 2002;90(12):1243-50.
50. Dvorak HF. Vascular permeability factor/vascular endothelial growth factor: a critical cytokine in tumor angiogenesis and a potential target for diagnosis and therapy. J Clin Oncol. 2002;20(21):4368-80.
51. Safran M, Kaelin WG. HIF hydroxylation and the mammalian oxygen-sensing pathway. J Clin Invest. 2003;111(6):779-83.
52. Okada F, Rak JW, Croix BS, Lieubeau B, Kaya M, Roncari L, et al. Impact of oncogenes in tumor angiogenesis: mutant K-ras up-regulation of vascular endothelial growth factor/vascular permeability factor is necessary, but not sufficient for tumorigenicity of human colorectal carcinoma cells. Proc Natl Acad Sci U S A. 1998;95(7):3609-14.
53. de Vries C, Escobedo JA, Ueno H, Houck K, Ferrara N, Williams LT. The fms-like tyrosine kinase, a receptor for vascular endothelial growth factor. Science. 1992;255(5047):989-91.
54. Millauer B, Wizigmann-Voos S, Schnürch H, Martinez R, Møller NP, Risau W, et al. High affinity VEGF binding and developmental expression suggest Flk-1 as a major regulator of vasculogenesis and angiogenesis. Cell. 1993;72(6):835-46.
55. Soker S, Takashima S, Miao HQ, Neufeld G, Klagsbrun M. Neuropilin-1 is expressed by endothelial and tumor cells as an isoform-specific receptor for vascular endothelial growth factor. Cell. 1998;92(6):735-45.
56. Karkkainen MJ, Mäkinen T, Alitalo K. Lymphatic endothelium: a new frontier of metastasis research. Nat Cell Biol. 2002;4(1):E2-5.
57. Ferrara N. Vascular endothelial growth factor: basic science and clinical progress. Endocr Rev. 2004;25(4):581-611.
58. Waltenberger J, Claesson-Welsh L, Siegbahn A, Shibuya M, Heldin CH. Different signal transduction properties of KDR and Flt1, two receptors for vascular endothelial growth factor. J Biol Chem. 1994;269(43):26988-95.
59. Kendall RL, Thomas KA. Inhibition of vascular endothelial cell growth factor activity by an endogenously encoded soluble receptor. Proc Natl Acad Sci U S A. 1993;90(22):10705-9.
60. Park JE, Chen HH, Winer J, Houck KA, Ferrara N. Placenta growth factor. Potentiation of vascular endothelial growth factor bioactivity, in vitro and in vivo, and high affinity binding to Flt-1 but not to Flk-1/KDR. J Biol Chem. 1994;269(41):25646-54.
61. Barleon B, Sozzani S, Zhou D, Weich HA, Mantovani A, Marmé D. Migration of human monocytes in response to vascular endothelial growth factor (VEGF) is mediated via the VEGF receptor flt-1. Blood. 1996;87(8):3336-43.

62. Hattori K, Heissig B, Wu Y, Dias S, Tejada R, Ferris B, et al. Placental growth factor reconstitutes hematopoiesis by recruiting VEGFR1(+) stem cells from bone-marrow microenvironment. Nat Med. 2002;8(8):841-9.
63. Hiratsuka S, Nakamura K, Iwai S, Murakami M, Itoh T, Kijima H, et al. MMP9 induction by vascular endothelial growth factor receptor-1 is involved in lung-specific metastasis. Cancer Cell. 2002;2(4):289-300.
64. Guo D, Jia Q, Song HY, Warren RS, Donner DB. Vascular endothelial cell growth factor promotes tyrosine phosphorylation of mediators of signal transduction that contain SH2 domains. Association with endothelial cell proliferation. J Biol Chem. 1995;270(12):6729-33.
65. Takahashi T, Ueno H, Shibuya M. VEGF activates protein kinase C-dependent, but Ras-independent Raf-MEK-MAP kinase pathway for DNA synthesis in primary endothelial cells. Oncogene. 1999;18(13):2221-30.
66. Gerber HP, Vu TH, Ryan AM, Kowalski J, Werb Z, Ferrara N. VEGF couples hypertrophic cartilage remodeling, ossification and angiogenesis during endochondral bone formation. Nat Med. 1999;5(6):623-8.
67. Ferrara N, Chen H, Davis-Smyth T, Gerber HP, Nguyen TN, Peers D, et al. Vascular endothelial growth factor is essential for corpus luteum angiogenesis. Nat Med. 1998;4(3):336-40.
68. Yoshiji H, Gomez DE, Shibuya M, Thorgeirsson UP. Expression of vascular endothelial growth factor, its receptor, and other angiogenic factors in human breast cancer. Cancer Res. 1996;56(9):2013-6.
69. Partanen J, Armstrong E, Mäkelä TP, Korhonen J, Sandberg M, Renkonen R, et al. A novel endothelial cell surface receptor tyrosine kinase with extracellular epidermal growth factor homology domains. Mol Cell Biol. 1992;12(4):1698-707.
70. Augustin HG, Koh GY, Thurston G, Alitalo K. Control of vascular morphogenesis and homeostasis through the angiopoietin-Tie system. Nat Rev Mol Cell Biol. 2009;10(3):165-77.
71. Davis S, Aldrich TH, Jones PF, Acheson A, Compton DL, Jain V, et al. Isolation of angiopoietin-1, a ligand for the TIE2 receptor, by secretion-trap expression cloning. Cell. 1996;87(7):1161-9.
72. Saharinen P, Eklund L, Miettinen J, Wirkkala R, Anisimov A, Winderlich M, et al. Angiopoietins assemble distinct Tie2 signalling complexes in endothelial cell-cell and cell-matrix contacts. Nat Cell Biol. 2008;10(5):527-37.
73. Maisonpierre PC, Suri C, Jones PF, Bartunkova S, Wiegand SJ, Radziejewski C, et al. Angiopoietin-2, a natural antagonist for Tie2 that disrupts in vivo angiogenesis. Science. 1997;277(5322):55-60.
74. Fiedler U, Krissl T, Koidl S, Weiss C, Koblizek T, Deutsch U, et al. Angiopoietin-1 and angiopoietin-2 share the same binding domains in the Tie-2 receptor involving the first Ig-like loop and the epidermal growth factor-like repeats. J Biol Chem. 2003;278(3):1721-7.
75. Huang H, Bhat A, Woodnutt G, Lappe R. Targeting the ANGPT-TIE2 pathway in malignancy. Nat Rev Cancer. 2010;10(8):575-85.
76. De Palma M, Naldini L. Angiopoietin-2 TIEs up macrophages in tumor angiogenesis. Clin Cancer Res. 2011;17(16):5226-32.
77. DeBusk LM, Hallahan DE, Lin PC. Akt is a major angiogenic mediator downstream of the Ang1/Tie2 signaling pathway. Exp Cell Res. 2004;298(1):167-77.
78. Daly C, Wong V, Burova E, Wei Y, Zabski S, Griffiths J, et al. Angiopoietin-1 modulates endothelial cell function and gene expression via the transcription factor FKHR (FOXO1). Genes Dev. 2004;18(9):1060-71.
79. Jeon BH, Khanday F, Deshpande S, Haile A, Ozaki M, Irani K. Tie-ing the antiinflammatory effect of angiopoietin-1 to inhibition of NF-kappaB. Circ Res. 2003;92(6):586-8.

80. De Palma M, Venneri MA, Galli R, Sergi Sergi L, Politi LS, Sampaolesi M, et al. Tie2 identifies a hematopoietic lineage of proangiogenic monocytes required for tumor vessel formation and a mesenchymal population of pericyte progenitors. Cancer Cell. 2005;8(3):211-26.
81. Coffelt SB, Tal AO, Scholz A, De Palma M, Patel S, Urbich C, et al. Angiopoietin-2 regulates gene expression in TIE2-expressing monocytes and augments their inherent proangiogenic functions. Cancer Res. 2010;70(13):5270-80.
82. Lin EY, Pollard JW. Tumor-associated macrophages press the angiogenic switch in breast cancer. Cancer Res. 2007;67(11):5064-6.
83. Lin EY, Li JF, Gnatovskiy L, Deng Y, Zhu L, Grzesik DA, et al. Macrophages regulate the angiogenic switch in a mouse model of breast cancer. Cancer Res. 2006;66(23):11238-46.
84. De Palma M, Lewis CE. Macrophage regulation of tumor responses to anticancer therapies. Cancer Cell. 2013;23(3):277-86.
85. Squadrito ML, De Palma M. Macrophage regulation of tumor angiogenesis: implications for cancer therapy. Mol Aspects Med. 2011;32(2):123-45.
86. Leek RD, Lewis CE, Whitehouse R, Greenall M, Clarke J, Harris AL. Association of macrophage infiltration with angiogenesis and prognosis in invasive breast carcinoma. Cancer Res. 1996;56(20):4625-9.
87. Folkman J. Tumor angiogenesis: therapeutic implications. N Engl J Med. 1971;285(21):1182-6.
88. Kim KJ, Li B, Winer J, Armanini M, Gillett N, Phillips HS, et al. Inhibition of vascular endothelial growth factor-induced angiogenesis suppresses tumour growth in vivo. Nature. 1993;362(6423):841-4.
89. FDA Approval for Bevacizumab http://www.cancer.gov/cancertopics/druginfo/fda-bevacizumab.
90. Sweeney P, Karashima T, Kim SJ, Kedar D, Mian B, Huang S, et al. Anti-vascular endothelial growth factor receptor 2 antibody reduces tumorigenicity and metastasis in orthotopic prostate cancer xenografts via induction of endothelial cell apoptosis and reduction of endothelial cell matrix metalloproteinase type 9 production. Clin Cancer Res. 2002;8(8):2714-24.
91. Spratlin J. Ramucirumab (IMC-1121B): Monoclonal antibody inhibition of vascular endothelial growth factor receptor-2. Curr Oncol Rep. 2011;13(2):97-102.
92. Morabito A, De Maio E, Di Maio M, Normanno N, Perrone F. Tyrosine kinase inhibitors of vascular endothelial growth factor receptors in clinical trials: current status and future directions. Oncologist. 2006;11(7):753-64.
93. Schmidinger M, Bellmunt J. Plethora of agents, plethora of targets, plethora of side effects in metastatic renal cell carcinoma. Cancer Treat Rev. 2010;36(5):416-24.
94. Casanovas O, Hicklin DJ, Bergers G, Hanahan D. Drug resistance by evasion of antiangiogenic targeting of VEGF signaling in late-stage pancreatic islet tumors. Cancer Cell. 2005;8(4):299-309.
95. Rigamonti N, Kadioglu E, Keklikoglou I, Wyser Rmili C, Leow CC, De Palma M. Role of angiopoietin-2 in adaptive tumor resistance to VEGF signaling blockade. Cell Rep. 2014;8(3):696-706.
96. Hashizume H, Falcón BL, Kuroda T, Baluk P, Coxon A, Yu D, et al. Complementary actions of inhibitors of angiopoietin-2 and VEGF on tumor angiogenesis and growth. Cancer Res. 2010;70(6):2213-23.
97. Brown JL, Cao ZA, Pinzon-Ortiz M, Kendrew J, Reimer C, Wen S, et al. A human monoclonal anti-ANG2 antibody leads to broad antitumor activity in combination with VEGF inhibitors and chemotherapy agents in preclinical models. Mol Cancer Ther. 2010;9(1):145-56.
98. Mazzieri R, Pucci F, Moi D, Zonari E, Ranghetti A, Berti A, et al. Targeting the ANG2/TIE2 axis inhibits tumor growth and metastasis by impairing angiogenesis and disabling rebounds of proangiogenic myeloid cells. Cancer Cell. 2011;19(4):512-26.

99. Hou HA, Chou WC, Lin LI, Tang JL, Tseng MH, Huang CF, et al. Expression of angiopoietins and vascular endothelial growth factors and their clinical significance in acute myeloid leukemia. Leuk Res. 2008;32(6):904-12.
100. Rykala J, Przybylowska K, Majsterek I, Pasz-Walczak G, Sygut A, Dziki A, et al. Angiogenesis markers quantification in breast cancer and their correlation with clinicopathological prognostic variables. Pathol Oncol Res. 2011;17(4):809-17.
101. Srirajaskanthan R, Dancey G, Hackshaw A, Luong T, Caplin ME, Meyer T. Circulating angiopoietin-2 is elevated in patients with neuroendocrine tumours and correlates with disease burden and prognosis. Endocr Relat Cancer. 2009;16(3):967-76.
102. Lind AJ, Wikström P, Granfors T, Egevad L, Stattin P, Bergh A. Angiopoietin 2 expression is related to histological grade, vascular density, metastases, and outcome in prostate cancer. Prostate. 2005;62(4):394-9.
103. Mitsuhashi N, Shimizu H, Ohtsuka M, Wakabayashi Y, Ito H, Kimura F, et al. Angiopoietins and Tie-2 expression in angiogenesis and proliferation of human hepatocellular carcinoma. Hepatology. 2003;37(5):1105-13.
104. Ogawa M, Yamamoto H, Nagano H, Miyake Y, Sugita Y, Hata T, et al. Hepatic expression of ANG2 RNA in metastatic colorectal cancer. Hepatology. 2004;39(2):528-39.
105. Wong MP, Chan SY, Fu KH, Leung SY, Cheung N, Yuen ST, et al. The angiopoietins, tie2 and vascular endothelial growth factor are differentially expressed in the transformation of normal lung to non-small cell lung carcinomas. Lung Cancer. 2000;29(1):11-22.
106. Hata K, Nakayama K, Fujiwaki R, Katabuchi H, Okamura H, Miyazaki K. Expression of the angopoietin-1, angopoietin-2, Tie2, and vascular endothelial growth factor gene in epithelial ovarian cancer. Gynecol Oncol. 2004;93(1):215-22.
107. Falcón BL, Hashizume H, Koumoutsakos P, Chou J, Bready JV, Coxon A, et al. Contrasting actions of selective inhibitors of angiopoietin-1 and angiopoietin-2 on the normalization of tumor blood vessels. Am J Pathol. 2009;175(5):2159-70.
108. Huang H, Lai JY, Do J, Liu D, Li L, Del Rosario J, et al. Specifically targeting angiopoietin-2 inhibits angiogenesis, Tie2-expressing monocyte infiltration, and tumor growth. Clin Cancer Res. 2011;17(5):1001-11.
109. Lewis CE, Ferrara N. Multiple effects of angiopoietin-2 blockade on tumors. Cancer Cell. 2011;19(4):431-3.
110. Rosen L, Mendelson D, Gordon M, Goldman J, Allen J, Curti B, et al. Phase Ib safety trial of CVX-060, an intravenous humanized monoclonal CovX body inhibiting angiopoietin 2 (Ang-2), with sunitinib. J Clin Oncol. 2012;30.
111. Herbst RS, Hong D, Chap L, Kurzrock R, Jackson E, Silverman JM, et al. Safety, pharmacokinetics, and antitumor activity of AMG 386, a selective angiopoietin inhibitor, in adult patients with advanced solid tumors. J Clin Oncol. 2009;27(21):3557-65.
112. Mita AC, Takimoto CH, Mita M, Tolcher A, Sankhala K, Sarantopoulos J, et al. Phase 1 study of AMG 386, a selective angiopoietin 1/2-neutralizing peptibody, in combination with chemotherapy in adults with advanced solid tumors. Clin Cancer Res. 2010;16(11):3044-56.
113. Karlan BY, Oza AM, Richardson GE, Provencher DM, Hansen VL, Buck M, et al. Randomized, double-blind, placebo-controlled phase II study of AMG 386 combined with weekly paclitaxel in patients with recurrent ovarian cancer. J Clin Oncol. 2012;30(4):362-71.
114. Tsutsui S, Inoue H, Yasuda K, Suzuki K, Takeuchi H, Nishizaki T, et al. Angiopoietin 2 expression in invasive ductal carcinoma of the breast: its relationship to the VEGF expression and microvessel density. Breast Cancer Res Treat. 2006;98(3):261-6.
115. Koh YJ, Kim HZ, Hwang SI, Lee JE, Oh N, Jung K, et al. Double antiangiogenic protein, DAAP, targeting VEGF-A and angiopoietins in tumor angiogenesis, metastasis, and vascular leakage. Cancer Cell. 2010;18(2):171-84.

116. Kienast Y, Klein C, Scheuer W, Raemsch R, Lorenzon E, Bernicke D, et al. Ang-2-VEGF-A CrossMab, a novel bispecific human IgG1 antibody blocking VEGF-A and Ang-2 functions simultaneously, mediates potent antitumor, antiangiogenic, and antimetastatic efficacy. Clin Cancer Res. 2013;19(24):6730-40.
117. Thomas M, Kienast Y, Scheuer W, Bähner M, Kaluza K, Gassner C, et al. A novel angiopoietin-2 selective fully human antibody with potent anti-tumoral and anti-angiogenic efficacy and superior side effect profile compared to Pan-Angiopoietin-1/-2 inhibitors. PLoS One. 2013;8(2):e54923.
118. Liang WC, Wu X, Peale FV, Lee CV, Meng YG, Gutierrez J, et al. Cross-species vascular endothelial growth factor (VEGF)-blocking antibodies completely inhibit the growth of human tumor xenografts and measure the contribution of stromal VEGF. J Biol Chem. 2006;281(2):951-61.
119. Mazzone M, Dettori D, Leite de Oliveira R, Loges S, Schmidt T, Jonckx B, et al. Heterozygous deficiency of PHD2 restores tumor oxygenation and inhibits metastasis via endothelial normalization. Cell. 2009;136(5):839-51.
120. Miller K, Wang M, Gralow J, Dickler M, Cobleigh M, Perez EA, et al. Paclitaxel plus bevacizumab versus paclitaxel alone for metastatic breast cancer. N Engl J Med. 2007;357(26):2666-76.
121. Fakhrejahani E, Toi M. Antiangiogenesis therapy for breast cancer: an update and perspectives from clinical trials. Jpn J Clin Oncol. 2014;44(3):197-207.
122. O'Shaughnessy JA, Brufsky AM. RiBBON 1 and RiBBON 2: phase III trials of bevacizumab with standard chemotherapy for metastatic breast cancer. Clin Breast Cancer. 2008;8(4):370-3.
123. Miles DW, Chan A, Dirix LY, Cortés J, Pivot X, Tomczak P, et al. Phase III study of bevacizumab plus docetaxel compared with placebo plus docetaxel for the first-line treatment of human epidermal growth factor receptor 2-negative metastatic breast cancer. J Clin Oncol. 2010;28(20):3239-47.
124. Miller K, Burstein H, Elias H, Rugo M, Cobleigh M, Pegram M, et al. Phase II study of SU11248, a multitargeted receptor tyrosine kinase inhibitor (TKI), in patients (pts) with previously treated metastatic breast cancer (MBC). Journal of Clinical Oncology. 2005;23(16).
125. Baselga J, Roché H, Costa F. SOLTI-0701: A multinational double-blind, randomized phase 2b study evaluating the efficacy and safety of sorafenib compared to placebo when administered in combination with capecitabine in patients with locally advanced or metastatic breast cancer (BC). 2009;69(24).
126. Diéras V, Wildiers H, Jassem J, Dirix LY, Guastalla JP, Bono P, et al. Trebananib (AMG 386) plus weekly paclitaxel with or without bevacizumab as first-line therapy for HER2-negative locally recurrent or metastatic breast cancer: A phase 2 randomized study. Breast. 2015.
127. Burnet FM. Cancer—A Biological Approach. Br Med J. 1957;1(5023):841–7.
128. Burnet FM. The concept of immunological surveillance. Prog Exp Tumor Res. 1970;13:1-27.
129. Shankaran V, Ikeda H, Bruce AT, White JM, Swanson PE, Old LJ, et al. IFNgamma and lymphocytes prevent primary tumour development and shape tumour immunogenicity. Nature. 2001;410(6832):1107-11.
130. Dunn GP, Bruce AT, Ikeda H, Old LJ, Schreiber RD. Cancer immunoediting: from immunosurveillance to tumor escape. Nat Immunol. 2002;3(11):991-8.
131. Dunn GP, Old LJ, Schreiber RD. The three Es of cancer immunoediting. Annu Rev Immunol. 2004;22:329-60.
132. Vesely MD, Kershaw MH, Schreiber RD, Smyth MJ. Natural innate and adaptive immunity to cancer. Annu Rev Immunol. 2011;29:235-71.
133. Schreiber RD, Old LJ, Smyth MJ. Cancer immunoediting: integrating immunity's roles in cancer suppression and promotion. Science. 2011;331(6024):1565-70.
134. Schumacher TN, Schreiber RD. Neoantigens in cancer immunotherapy. Science. 2015;348(6230):69-74.

135. Graziano DF, Finn OJ. Tumor antigens and tumor antigen discovery. Cancer Treat Res. 2005;123:89-111.
136. Renkvist N, Castelli C, Robbins P, Parmiani G. A listing of human tumor antigens recognized by T cells. Cancer Immunol Immunother. 2001;50(1):3-15.
137. Rock KL, Shen L. Cross-presentation: underlying mechanisms and role in immune surveillance. Immunol Rev. 2005;207:166-83.
138. Khong HT, Restifo NP. Natural selection of tumor variants in the generation of "tumor escape" phenotypes. Nat Immunol. 2002;3(11):999-1005.
139. Pardoll DM. The blockade of immune checkpoints in cancer immunotherapy. Nat Rev Cancer. 2012;12(4):252-64.
140. Greenwald RJ, Freeman GJ, Sharpe AH. The B7 family revisited. Annu Rev Immunol. 2005;23:515-48.
141. Sharma P, Allison JP. The future of immune checkpoint therapy. Science. 2015;348(6230):56-61.
142. Rudd CE, Taylor A, Schneider H. CD28 and CTLA-4 coreceptor expression and signal transduction. Immunol Rev. 2009;229(1):12-26.
143. Parry RV, Chemnitz JM, Frauwirth KA, Lanfranco AR, Braunstein I, Kobayashi SV, et al. CTLA-4 and PD-1 receptors inhibit T-cell activation by distinct mechanisms. Mol Cell Biol. 2005;25(21):9543-53.
144. Ishida Y, Agata Y, Shibahara K, Honjo T. Induced expression of PD-1, a novel member of the immunoglobulin gene superfamily, upon programmed cell death. EMBO J. 1992;11(11):3887-95.
145. Linsley, P, Greene, J, Brady, W, et al. Human B7-1 (CD80) and B7-2 (CD86) bind with similar avidities but distinct kinetics to CD28 and CTLA-4 receptors. Immunity. 1994;1(9).
146. Okazaki T, Honjo T. PD-1 and PD-1 ligands: from discovery to clinical application. Int Immunol. 2007;19(7):813-24.
147. Iwai Y, Ishida M, Tanaka Y, Okazaki T, Honjo T, Minato N. Involvement of PD-L1 on tumor cells in the escape from host immune system and tumor immunotherapy by PD-L1 blockade. Proc Natl Acad Sci U S A. 2002;99(19):12293-7.
148. Dong H, Strome SE, Salomao DR, Tamura H, Hirano F, Flies DB, et al. Tumor-associated B7-H1 promotes T-cell apoptosis: a potential mechanism of immune evasion. Nat Med. 2002;8(8):793-800.
149. Rabinovich GA, Gabrilovich D, Sotomayor EM. Immunosuppressive strategies that are mediated by tumor cells. Annu Rev Immunol. 2007;25:267-96.
150. Teicher BA. Transforming growth factor-beta and the immune response to malignant disease. Clin Cancer Res. 2007;13(21):6247-51.
151. Muller A, Prendergast G. Indoleamine 2,3-dioxygenase in immune suppression and cancer. Curr Cancer Drug Targets. 2007;7:31-40.
152. Zou W. Regulatory T cells, tumour immunity and immunotherapy. Nat Rev Immunol. 2006;6:295-307.
153. Nagaraj S, Gabrilovich DI. Myeloid-derived suppressor cells. Adv Exp Med Biol. 2007;601:213-23.
154. Kusmartsev S, Nagaraj S, Gabrilovich DI. Tumor-associated CD8+ T cell tolerance induced by bone marrow-derived immature myeloid cells. J Immunol. 2005;175(7):4583-92.
155. Sinha P, Clements V, Bunt S, Albelda S, Ostrand-Rosenberg S. Crosstalk between myeloid-derived suppressor cells and macrophages subverts tumor immunity toward a type 2 response. J Immunol. 2007;179:977-83.
156. Hodi FS, O'Day SJ, McDermott DF, Weber RW, Sosman JA, Haanen JB, et al. Improved survival with ipilimumab in patients with metastatic melanoma. N Engl J Med. 2010;363(8):711-23.
157. Hamid O, Robert C, Daud A, Hodi FS, Hwu WJ, Kefford R, et al. Safety and tumor responses with lambrolizumab (anti-PD-1) in melanoma. N Engl J Med. 2013;369(2):134-44.

158. Robert C, Long GV, Brady B, Dutriaux C, Maio M, Mortier L, et al. Nivolumab in previously untreated melanoma without BRAF mutation. N Engl J Med. 2015;372(4):320-30.
159. Vonderheide RH. Prospect of targeting the CD40 pathway for cancer therapy. Clin Cancer Res. 2007;13(4):1083-8.
160. Vogel LA, Noelle RJ. CD40 and its crucial role as a member of the TNFR family. Semin Immunol. 1998;10(6):435-42.
161. Grewal IS, Flavell RA. CD40 and CD154 in cell-mediated immunity. Annu Rev Immunol. 1998;16:111-35.
162. van Kooten C, Banchereau J. CD40-CD40 ligand. J Leukoc Biol. 2000;67(1):2-17.
163. Quezada SA, Jarvinen LZ, Lind EF, Noelle RJ. CD40/CD154 interactions at the interface of tolerance and immunity. Annu Rev Immunol. 2004;22:307-28.
164. Smith C, Wilson N, Waithman J, Villadangos J, Carbone F, Heath W, et al. Cognate CD4(+) T cell licensing of dendritic cells in CD8(+) T cell immunity. Nat Immunol. 2004;5(11):1143-8.
165. Bennett S, Carbone F, Karamalis F, Flavell R, Miller J, Heath W. Help for cy totoxic-T-cell responses is mediated by CD40 signalling. Nature. 1998;393(478 - 480.).
166. Lum HD, Buhtoiarov IN, Schmidt BE, Berke G, Paulnock DM, Sondel PM, et al. In vivo CD40 ligation can induce T-cell-independent antitumor effects that involve macrophages. J Leukoc Biol. 2006;79(6):1181-92.
167. Eliopoulos AG, Young LS. The role of the CD40 pathway in the pathogenesis and treatment of cancer. Curr Opin Pharmacol. 2004;4(4):360-7.
168. Wingett DG, Vestal RE, Forcier K, Hadjokas N, Nielson CP. CD40 is functionally expressed on human breast carcinomas: variable inducibility by cytokines and enhancement of Fas-mediated apoptosis. Breast Cancer Res Treat. 1998;50(1):27-36.
169. Eliopoulos AG, Davies C, Knox PG, Gallagher NJ, Afford SC, Adams DH, et al. CD40 induces apoptosis in carcinoma cells through activation of cytotoxic ligands of the tumor necrosis factor superfamily. Mol Cell Biol. 2000;20(15):5503-15.
170. Tong AW, Papayoti MH, Netto G, Armstrong DT, Ordonez G, Lawson JM, et al. Growth-inhibitory effects of CD40 ligand (CD154) and its endogenous expression in human breast cancer. Clin Cancer Res. 2001;7(3):691-703.
171. Vonderheide RH, Glennie MJ. Agonistic CD40 antibodies and cancer therapy. Clin Cancer Res. 2013;19(5):1035-43.
172. Vonderheide RH, Flaherty KT, Khalil M, Stumacher MS, Bajor DL, Hutnick NA, et al. Clinical activity and immune modulation in cancer patients treated with CP-870,893, a novel CD40 agonist monoclonal antibody. J Clin Oncol. 2007;25(7):876-83.
173. Khubchandani S, Czuczman MS, Hernandez-Ilizaliturri FJ. Dacetuzumab, a humanized mAb against CD40 for the treatment of hematological malignancies. Curr Opin Investig Drugs. 2009;10(6):579-87.
174. Bensinger W, Maziarz RT, Jagannath S, Spencer A, Durrant S, Becker PS, et al. A phase 1 study of lucatumumab, a fully human anti-CD40 antagonist monoclonal antibody administered intravenously to patients with relapsed or refractory multiple myeloma. Br J Haematol. 2012;159(1):58-66.
175. Beatty GL, Chiorean EG, Fishman MP, Saboury B, Teitelbaum UR, Sun W, et al. CD40 agonists alter tumor stroma and show efficacy against pancreatic carcinoma in mice and humans. Science. 2011;331(6024):1612-6.
176. Vonderheide RH, Burg JM, Mick R, Trosko JA, Li D, Shaik MN, et al. Phase I study of the CD40 agonist antibody CP-870,893 combined with carboplatin and paclitaxel in patients with advanced solid tumors. Oncoimmunology. 2013;2(1):e23033.
177. Hallett WH, Ames E, Alvarez M, Barao I, Taylor PA, Blazar BR, et al. Combination therapy using IL-2 and anti-CD25 results in augmented natural killer cell-mediated antitumor responses. Biol Blood Marrow Transplant. 2008;14(10):1088-99.

178. Ries CH, Cannarile MA, Hoves S, Benz J, Wartha K, Runza V, et al. Targeting tumor-associated macrophages with anti-CSF-1R antibody reveals a strategy for cancer therapy. Cancer Cell. 2014;25(6):846-59.
179. Mahmoud SM, Paish EC, Powe DG, Macmillan RD, Grainge MJ, Lee AH, et al. Tumor-infiltrating CD8+ lymphocytes predict clinical outcome in breast cancer. J Clin Oncol. 2011;29(15):1949-55.
180. Bohling S, Allison K. Immunosuppressive regulatory T cells are associated with aggressive breast cancer phenotypes: a potential therapeutic target. . Mod Pathol 2008;21:1527–32.
181. DeNardo DG, Brennan DJ, Rexhepaj E, Ruffell B, Shiao SL, Madden SF, et al. Leukocyte complexity predicts breast cancer survival and functionally regulates response to chemotherapy. Cancer Discov. 2011;1(1):54-67.
182. Verbrugge I, Hagekyriakou J, Sharp LL, Galli M, West A, McLaughlin NM, et al. Radiotherapy increases the permissiveness of established mammary tumors to rejection by immunomodulatory antibodies. Cancer Res. 2012;72(13):3163-74.
183. Brahmer JR, Drake CG, Wollner I, Powderly JD, Picus J, Sharfman WH, et al. Phase I study of single-agent anti-programmed death-1 (MDX-1106) in refractory solid tumors: safety, clinical activity, pharmacodynamics, and immunologic correlates. J Clin Oncol. 2010;28(19):3167-75.
184. Vonderheide RH, LoRusso PM, Khalil M, Gartner EM, Khaira D, Soulieres D, et al. Tremelimumab in combination with exemestane in patients with advanced breast cancer and treatment-associated modulation of inducible costimulator expression on patient T cells. Clin Cancer Res. 2010;16(13):3485-94.
185. Weiss VL, Lee TH, Song H, Kouo TS, Black CM, Sgouros G, et al. Trafficking of high avidity HER-2/neu-specific T cells into HER-2/neu-expressing tumors after depletion of effector/memory-like regulatory T cells. PLoS One. 2012;7(2):e31962.
186. Strachan DC, Ruffell B, Oei Y, Bissell MJ, Coussens LM, Pryer N, et al. CSF1R inhibition delays cervical and mammary tumor growth in murine models by attenuating the turnover of tumor-associated macrophages and enhancing infiltration by CD8(+) T cells. Oncoimmunology. 2013;2(12):e26968.
187. Rech AJ, Mick R, Recio A, DeMichele A, Tweed CK, Fox KR, et al. Phase I study of anti-CD25 mab daclizumab to deplete regulatory T cells prior to telomerase/survivin peptide vaccination in patients (pts) with metastatic breast cancer (MBC). Journal of Clinical Oncology. 2010;28(15).
188. Motz GT, Coukos G. The parallel lives of angiogenesis and immunosuppression: cancer and other tales. Nat Rev Immunol. 2011;11(10):702-11.
189. Muller WA. Mechanisms of leukocyte transendothelial migration. Annu Rev Pathol. 2011;6:323-44.
190. Griffioen AW, Damen CA, Blijham GH, Groenewegen G. Tumor angiogenesis is accompanied by a decreased inflammatory response of tumorassociated endothelium. Blood. 1996;88:667–73.
191. Griffioen AW, Damen CA, Martinotti S, Blijham GH, Groenewegen G. Endothelial intercellular adhesion molecule-1 expression is suppressed in human malignancies: the role of angiogenic factors. Cancer Res. 1996;56(5):1111-17.
192. Shetty S, Weston CJ, Oo YH, Westerlund N, Stamataki Z, Youster J, et al. Common lymphatic endothelial and vascular endothelial receptor-1 mediates the transmigration of regulatory T cells across human hepatic sinusoidal endothelium. J Immunol. 2011;186(7):4147-55.
193. Mazanet MM, Hughes CC. B7-H1 is expressed by human endothelial cells and suppresses T cell cytokine synthesis. J Immunol. 2002;169(7):3581-8.
194. Munn DH, Shafizadeh E, Attwood JT, Bondarev I, Pashine A, Mellor AL. Inhibition of T cell proliferation by macrophage tryptophan catabolism. J Exp Med. 1999;189(9):1363-72.

195. Ma L, Mauro C, Cornish GH, Chai JG, Coe D, Fu H, et al. Ig gene-like molecule CD31 plays a nonredundant role in the regulation of T-cell immunity and tolerance. Proc Natl Acad Sci U S A. 2010;107(45):19461-6.
196. Pirtskhalaishvili G, Nelson JB. Endothelium-derived factors as paracrine mediators of prostate cancer progression. Prostate. 2000;44(1):77-87.
197. Lin E, Jones J, Li P, Zhu L, Whitney K, Muller W, et al. Progression to malignancy in the polyoma middle T oncoprotein mouse breast cancer model provides a reliable model for human diseases. Am J Pathol. 2003;163(5):2113–26.
198. Fluck MM, Schaffhausen BS. Lessons in Signaling and Tumorigenesis from Polyomavirus Middle T Antigen. MICROBIOLOGY AND MOLECULAR BIOLOGY REVIEWS. 2009;73(3):542–63.
199. GUY CT, CARDIFF RD, MULLER WJ. Induction of Mammary Tumors by Expression of Polyomavirus Middle T Oncogene: A Transgenic Mouse Model for Metastatic Disease. MOLECULAR AND CELLULAR BIOLOGY. 1992;12(3):954-61.
200. Maglione JE, Moghanaki D, Young LJ, Manner CK, Ellies LG, Joseph SO, et al. Transgenic Polyoma middle-T mice model premalignant mammary disease. Cancer Res. 2001;61(22):8298-305.
201. Fantozzi A, Christofori G. Mouse models of breast cancer metastasis. Breast Cancer Res. 2006;8(4):212.
202. Schindelin J, Arganda-Carreras I, Frise E, Kaynig V, Longair M, Pietzsch T, et al. Fiji: an open-source platform for biological-image analysis. Nat Methods. 2012;9(7):676-82.
203. **Burri O**, **Guiet R**. VSI READER ACTIONBAR http://biop.epfl.ch/TOOL_VSI_Reader.html [19.05.2015].
204. Nanka O, Peumans WJ, Van Damme EJ, Pfüller U, Valásek P, Halata Z, et al. Lectin histochemistry of microvascular endothelium in chick and quail musculature. Anat Embryol (Berl). 2001;204(5):407-11.
205. Krohn KA, Link JM, Mason RP. Molecular imaging of hypoxia. J Nucl Med. 2008;49 Suppl 2:129S-48S.
206. De Vos K. Cell Counter http://rsb.info.nih.gov/ij/plugins/cell-counter.html [20.05.2015].
207. Boyd NF, Dite GS, Stone J, Gunasekara A, English DR, McCredie MR, et al. Heritability of mammographic density, a risk factor for breast cancer. N Engl J Med. 2002;347(12):886-94.
208. Hasebe T, Sasaki S, Imoto S, Mukai K, Yokose T, Ochiai A. Prognostic significance of fibrotic focus in invasive ductal carcinoma of the breast: a prospective observational study. Mod Pathol. 2002;15(5):502-16.
209. Long KB, Beatty GL. Harnessing the antitumor potential of macrophages for cancer immunotherapy. Oncoimmunology. 2013;2(12):e26860.
210. Melter M, Reinders ME, Sho M, Pal S, Geehan C, Denton MD, et al. Ligation of CD40 induces the expression of vascular endothelial growth factor by endothelial cells and monocytes and promotes angiogenesis in vivo. Blood. 2000;96(12):3801-8.
211. Reinders ME, Sho M, Robertson SW, Geehan CS, Briscoe DM. Proangiogenic function of CD40 ligand-CD40 interactions. J Immunol. 2003;171(3):1534-41.
212. Flaxenburg JA, Melter M, Lapchak PH, Briscoe DM, Pal S. The CD40-induced signaling pathway in endothelial cells resulting in the overexpression of vascular endothelial growth factor involves Ras and phosphatidylinositol 3-kinase. J Immunol. 2004;172(12):7503-9.
213. Fridman WH, Pagès F, Sautès-Fridman C, Galon J. The immune contexture in human tumours: impact on clinical outcome. Nat Rev Cancer. 2012;12(4):298-306.
214. Nielsen DL, Andersson M, Andersen JL, Kamby C. Antiangiogenic therapy for breast cancer. Breast Cancer Res. 2010;12(5):209.
215. Daly C, Eichten A, Castanaro C, Pasnikowski E, Adler A, Lalani AS, et al. Angiopoietin-2 functions as a Tie2 agonist in tumor models, where it limits the effects of VEGF inhibition. Cancer Res. 2013;73(1):108-18.

216. De Bock K, Mazzone M, Carmeliet P. Antiangiogenic therapy, hypoxia, and metastasis: risky liaisons, or not? Nat Rev Clin Oncol. 2011;8(7):393-404.
217. Dewhirst MW, Cao Y, Moeller B. Cycling hypoxia and free radicals regulate angiogenesis and radiotherapy response. Nat Rev Cancer. 2008;8(6):425-37.
218. Holopainen T, Saharinen P, D'Amico G, Lampinen A, Eklund L, Sormunen R, et al. Effects of angiopoietin-2-blocking antibody on endothelial cell-cell junctions and lung metastasis. J Natl Cancer Inst. 2012;104(6):461-75.
219. Minami T, Jiang S, Schadler K, Suehiro J, Osawa T, Oike Y, et al. The calcineurin-NFAT-angiopoietin-2 signaling axis in lung endothelium is critical for the establishment of lung metastases. Cell Rep. 2013;4(4):709-23.
220. Jain RK. Normalizing tumor vasculature with anti-angiogenic therapy: a new paradigm for combination therapy. Nat Med. 2001;7(9):987-9.
221. Huang Y, Goel S, Duda DG, Fukumura D, Jain RK. Vascular normalization as an emerging strategy to enhance cancer immunotherapy. Cancer Res. 2013;73(10):2943-8.
222. Jain RK. Determinants of tumor blood flow: a review. Cancer Res. 1988;48(10):2641-58.
223. Jain RK. Antiangiogenesis strategies revisited: from starving tumors to alleviating hypoxia. Cancer Cell. 2014;26(5):605-22.
224. Huang Y, Yuan J, Righi E, Kamoun WS, Ancukiewicz M, Nezivar J, et al. Vascular normalizing doses of antiangiogenic treatment reprogram the immunosuppressive tumor microenvironment and enhance immunotherapy. Proc Natl Acad Sci U S A. 2012;109(43):17561-6.
225. Rakhmilevich AL, Buhtoiarov IN, Malkovsky M, Sondel PM. CD40 ligation in vivo can induce T cell independent antitumor effects even against immunogenic tumors. Cancer Immunol Immunother. 2008;57(8):1151-60.
226. French RR, Chan HT, Tutt AL, Glennie MJ. CD40 antibody evokes a cytotoxic T-cell response that eradicates lymphoma and bypasses T-cell help. Nat Med. 1999;5(5):548-53.
227. Murphy WJ, Welniak L, Back T, Hixon J, Subleski J, Seki N, et al. Synergistic anti-tumor responses after administration of agonistic antibodies to CD40 and IL-2: coordination of dendritic and CD8+ cell responses. J Immunol. 2003;170(5):2727-33.
228. Fransen MF, Sluijter M, Morreau H, Arens R, Melief CJ. Local activation of CD8 T cells and systemic tumor eradication without toxicity via slow release and local delivery of agonistic CD40 antibody. Clin Cancer Res. 2011;17(8):2270-80.
229. Gooden MJ, de Bock GH, Leffers N, Daemen T, Nijman HW. The prognostic influence of tumour-infiltrating lymphocytes in cancer: a systematic review with meta-analysis. Br J Cancer. 2011;105(1):93-103.
230. Kamrava M, Bernstein MB, Camphausen K, Hodge JW. Combining radiation, immunotherapy, and antiangiogenesis agents in the management of cancer: the Three Musketeers or just another quixotic combination? Mol Biosyst. 2009;5(11):1262-70.
231. Chakrabarti R, Wei Y, Hwang J, Hang X, Andres Blanco M, Choudhury A, et al. ΔNp63 promotes stem cell activity in mammary gland development and basal-like breast cancer by enhancing Fzd7 expression and Wnt signalling. Nat Cell Biol. 2014;16(10):1004-15, 1-13.
232. Dent R, Hanna WM, Trudeau M, Rawlinson E, Sun P, Narod SA. Pattern of metastatic spread in triple-negative breast cancer. Breast Cancer Res Treat. 2009;115(2):423-8.